

**PREDICTION AND ANALYTICS OF
OPERATING PARAMETERS ON
THERMOELECTRIC GENERATOR
ENERGY GENERATION**

Ang Zi Yang Adrian

**A thesis submitted to the University of Newcastle for the degree of
Doctor of Philosophy**



School of Electrical, Electronic and Computer Engineering
Faculty of Science, Agriculture and Engineering

June 2017

Abstract

The efficient use of energy at all stages along the energy supply chain and the utilization of renewable energies are very important elements of a sustainable energy supply system, specially at the conversion from thermal to electrical energy. Converting the low-grade waste heat into electrical power would be useful and effective for several primary and secondary applications. One of the viable means to convert the low-grade waste heat into electrical energy is the use of thermoelectric power conversion.

The performance of thermoelectric generators, subjected to thermal effects, can vary considerably depending on the operating conditions, therefore it is necessary to measure and have a better understanding of the characteristics and performance of the thermoelectric generator. It is important to understand the thermoelectric generator's dynamic behavior and interaction with its operating environmental parameters. Based on this knowledge, it is then significant to develop an effective mathematical model that can provide the user with the most probable outcome of the output voltage. This will contribute to its reliability and calculation to increase the overall efficiency of the system.

This thesis provides the transient solution to the three-dimensional heat transfer equation with internal heat generation. It goes on to describes the transfer and generation of heat across the thermoelectric generator with dynamic exchange of heat. This solution is then included in a model in which the thermal masses and the operating environmental parameters of the thermoelectric generator are factored in. The resulting model is created in MATLAB. The comparison with experimental results from a thermoelectric generator system confirms the accuracy of the artificial neural network model.

This thesis also presents two practical applications, the prediction of the input parameters with a given output voltage, and sensitivity analysis designed for the model. This is to enable users to customize the thermoelectric generator for their requirements. This allows for better usage of resources eventually.

*Dedicating this thesis to my mother,
The late Rebecca Ang Kar Cheng*

Acknowledgements

I would like to express special appreciation and thanks to my supervisors Dr Wai Lok Woo and Professor Ehsan Mesbahi, who have both been a tremendous mentor to me. I would like to thank them for their encouragements, constructive ideas and allowing me to grow as a researcher. I would like to thank my annual progression panel, Dr Khalid Abidi and Dr Logan for giving me good advice at each milestone in my studies and my examiners, Dr Eugene Wong and Dr Edmund Liew for their feedbacks on my research work. I would also like to thank Joan and Eddie who helped proof-read this thesis.

A special thanks to my family. Words cannot express how grateful I am to my them for all the sacrifices that they've made on my behalf. Your prayers for me was what sustained me thus far. I would also like to thank all my friends who supported me in writing and motivating me to strive towards my goal.

Finally, I would like to express appreciation to my beloved wife, Raphaela, who spent sleepless nights with me and has always been my support in the moments when there was no answers to my queries. To you too, Kathryn, my beloved new born daughter.

List of Publications

Conferences

Z. Y. A. Ang and E.Mesbahi, "TEG Review Paper," presented at the International Symposium on Engineering and Natural Science, Macau, 2013

Z. Y. A. Ang, W.L.Woo, and E.Mesbahi," Influence of Environmental Parameters on the Prediction of Thermoelectric Generator Energy Generation,' in *IEEE 2016 International Conference on Power and Renewable Energy*, Shanghai, 21-23 October 2016, pp.100-106. (Publication awarded "Most Excellent Paper Award")

Z. Y. A. Ang, W.L.Woo, and E.Mesbahi," Prediction and Analysis of Energy Generation from Thermoelectric Energy Generator With Operating Environmental Parameters," in *2017 International Conference on Green Energy and Application*, Singapore, 2017, pp. 1-5, 25-27 March 2017. (Publication awarded "Best Presentation Award")

Journals

Z. Y. A. Ang, W.L.Woo, and E.Mesbahi,"Artificial Neural Network Based Prediction of Energy Generation from Thermoelectric Generator with Environmental Parameters," *Journal of Clean Energy Technologies*, pp.1-5, 7-9 January 2017.

Z. Y. A. Ang, W. L. Woo, and E. Mesbahi, "Prediction and Analysis of Energy Generation from Thermoelectric Energy Generator In Its Operating Environment," *Renewable Energy Focus*, pp. 1-5, 2017. (Pending)

Nomenclature

TEG	Thermoelectric Power Generator
TE	Thermoelectric
ZT	Figure of Merit
GUI	Graphical User Interface
SC	Seebeck Coefficient
EMF	Electromotive Force
Bi ₂ Te ₃	Bismuth Telluride
PbTe	Lead Telluride
SiGe	Silicon Germanium
WSN	Wireless Sensor Network
DC	Direct Current
RTG	Radioisotope Thermoelectric Generator
NASA	National Aeronautics and Space Administration
ANN	Artificial Neural Network
3D	Three Dimensional
CFD	Computational Fluid Dynamics
TDMA	TriDiagonal Matrix Algorithm
1D	One Dimensional
2D	Two Dimensional
MSE	Mean Squared Error

SA	Sensitivity Analysis
RI	Relative Importance

List of Symbols

T	Absolute temperature
σ	Electrical conductivity
k	Thermal conductivity
V	Voltage difference
I	Electrical current
W	Watts
R_m	Maximum resistance
q_{Peltier}	Rate of peltier effect heat transfer
SB	Seebeck
S_p	Seebeck coefficient of P-Type thermocouple element
S_n	Seebeck coefficient of N-Type thermocouple element
T_{hot}	Heat source on hot side
T_{hsur}	Surface temperature on hot side
T_{csur}	Surface temperature on cold side
ΔT_{max}	Maximum temperature gradient
I_{max}	Maximum input current
V_{max}	Maximum voltage
E_{max}	Maximum electromotive force
p	Scalar input
w	Scalar weight

b	Bias
N	Net input
F	Transfer function
A	Scalar neuron output
L_h	Thickness of ceramic substrate on hot side
L_c	Thickness of ceramic substrate on cold side
L_t	Height of PN junction thermocouple
L_f	Length of heat sink fin
k_h	Thermal conductivity of hot side ceramic substrate
K_t	Thermal conductivity of PN thermocouple
K_c	Thermal conductivity of cold side ceramic substrate
K_{hs}	Thermal conductivity of heat sink
T_1	Surface temperature on the underside of hot side ceramic substrate
T_2	Surface temperature on the underside of the cold side ceramic substrate
T_{amb}	Ambient temperature
q''	Convective heat flux
T_∞	Fluid temperature
H	Convective heat transfer coefficient
T_s	Surface temperature
V	Computational volume
\hat{n}	Outward-pointing unit normal of the boundary
S	Rate of temperature change due to heat sources

A	Area
P	General nodal point in a cell
N	North nodal point
E	East nodal point
S	South nodal point
W	West nodal point
T	Top nodal point
B	Bottom nodal point
PN	PN thermocouple
w	Width of thermocouple
k_{air}	Thermal conductivity of air
$C_{p,\text{air}}$	Specific heat of air
ρ_{air}	Density of air
U_w	Velocity of air
R_n	Reynolds number
P_n	Prandtl number
ΔT_{int}	Temperature difference between internal side of hot and cold side ceramic substrate
ΔT_{ext}	Temperature difference between external side of hot and cold side ceramic substrate
H_b	Height of heat sink base
D_f	Diameter of heat sink fin
N_x	Quantity of fins per dimension

A_b	Area of heat sink base
U_{app}	Wind velocity approaching heat sink fin
S_l	Distance between centre of two consecutive fins
ν_{air}	Kinematic viscosity of air
h_f	Heat transfer coefficient for heat sink fin
h_b	Heat transfer coefficient for heat sink base
η_f	Efficiency of fins
R_b	Thermal resistance of heat sink base
R_f	Thermal resistance of heat sink fin
K_f	Average heat sink thermal conductivity
ΔT_{exthsa}	Temperature difference between internal side of hot and external side of the cold side ceramic substrate
T_{ambh}	Hot Side Ambient Temperature
T_{ambc}	Cold Side Ambient Temperature
V_{wh}	Hot Side Wind Velocity
V_{wc}	Cold Side Wind Velocity
W_c	Width of Ceramic Substrate
K_{csh}	Thermal Conductivity of Hot Side Ceramic Substrate
K_{csc}	Thermal Conductivity of Cold Side Ceramic Substrate
L_{pn}	Length of PN junction
K_{pn}	Thermal Conductivity of PN Junction
L_{fin}	Length of Heat Sink Fins
A_{teg}	Area of Thermoelectric Generator

T_{sur}	Surface Temperature
T_{ambh}	Hot Side Ambient Temperature
n_h	Number of hidden layer node in each ANN network
n_i	Number of hidden input layer nodes
n_o	Number of hidden output layer nodes
n_p	Number of training samples in the dataset used
V_{ss}	Output voltage obtained from manufacturer specification sheet using temperature differential obtained from hot and cold side TEG ceramic substrate surface
V_{ep}	Output voltage obtained from manufacturer specification sheet using temperature differential obtained from PN junction with environmental parameters
V_{ephs}	Output voltage obtained from manufacturer specification sheet using temperature differential obtained from PN junction with environmental parameters and a heat sink
H	Hessian matrix
J	Jacobian Matrix
$F(\omega)$	Bayesian regularization
E_ω	Sum of squared network weights for Bayesian regularization
E_D	Sum of network errors for Bayesian regularization
$P(A B)$	Posterior probabilities of A conditional on B for Bayes theorem
$P(B A)$	Posterior probabilities of B conditional on A for Bayes theorem
D	Weight distribution for Bayesian regularization method
λ_k	Scaling factor to approximate the Hessian matrix
σ_k	Scaling factor to approximate the Hessian matrix

β_k	Factor calculation and direction of new search for Scaled conjugate
Y_i	Neural network predicted values
X_i	Neural network actual output values

Table of Content

Abstract.....	i
Acknowledgements	iii
List of Publications	iv
Nomenclature	v
List of Symbols	vii
Chapter 1 Introduction	1
1.1 Motivation.....	1
1.2 Aim.....	3
1.3 Scope of Work	3
1.4 Contributions of the Thesis	4
1.5 Organization of the Thesis	5
Chapter 2 Literature Review	6
2.1 Overview of Thermoelectric Phenomenon.....	6
2.2 Renewable Energy Comparison.....	7
2.2.1 Solar Energy vs Thermoelectric Energy.....	7
2.2.2 Wind Energy vs Thermoelectric Energy	8
2.3 Principles of Thermoelectric Energy Conversion.....	8
2.3.1 Thermoelectric Figure of Merit.....	10
2.3.2 The Seebeck Effect.....	11
2.3.3 Peltier Effect.....	12
2.4 Conventional Mathematical Model for Thermoelectric Generator	13
2.5 Thermoelectric Material	15
2.6 Commercialization	16
2.7 Thermoelectric Applications	17
2.7.1 Buildings	19
2.7.2 Automobile	21
2.7.3 Aerospace	22
2.7.4 Domestic Application.....	23

2.8 Past Research Area	24
2.8.1 Experimental Method	25
2.8.2 Material Properties	26
2.8.3 Summary of Research Areas	27
2.9 Challenges	28
2.10 Overview of Artificial Neural Network	28
2.10.1 Application of the Artificial Neural Network.....	29
2.10.2 Neurons	29
2.10.3 Transfer Functions	30
2.10.4 Artificial Neural Network Processing Units	31
2.10.5 Network Architectures.....	31
2.10.6 Artificial Neural Network Training	33
2.11 Summary	34
Chapter 3 Research Methodology for Novel Thermoelectric Performance Model	35
3.1 Thermal Modeling of Thermoelectric Generator	35
3.1.1 Limitations on Mathematical Model.....	39
3.2 Heat Transfer Equation	40
3.2.1 Finite Volume Method for Three-Dimensional Diffusion Case	40
3.2.2 Numerical Implementations Without Heat Sink.....	43
3.2.3 Boundary conditions.....	44
3.2.4 Initial Conditions.....	45
3.3 Modeling of Heat Sink	46
3.3.1 Numerical Implementation with Heat Sink.....	49
3.4 Tri Diagonal Matrix Method	51
3.5 Summary	53
Chapter 4 Research Methodology for Artificial Neural Network Model	54
4.1 Artificial Neural Network Model	54
4.1.1 Proposed Method of Artificial Neural Network Model.....	57
4.1.2 Coupled Neural Networks.....	61
4.1.3 Training Algorithms.....	65
4.1.4 Sensitivity Analysis.....	69

4.2 Graphical User Interface	71
4.3 Summary	74
Chapter 5 Results Analysis and Discussions.....	75
5.1 Data Set Generation and Validation	75
5.2 Training of the Artificial Neural Network.....	80
5.3 Sensitivity Analysis Output	86
5.4 Results and Discussion.....	89
5.4.1 Operating Environmental Parameters	90
5.4.2 TEG Construction Parameters.....	94
5.5 Summary	100
Chapter 6 Conclusion and Future Work.....	102
6.1 Future Work	104
6.1.1 Standardization of Thermoelectric Generator Material Specification Library	104
6.1.2 Calculation for Anisotropic Thermoelement.....	105
6.1.3 Unsupervised Learning	106
Appendix A.....	107
Appendix B.....	109
Appendix C.....	122
Appendix D	128
References	130

List of Figures

FIGURE 2.1 STRUCTURE OF THE THERMOELECTRIC GENERATOR	9
FIGURE 2.2 THERMOELECTRIC EFFECT	12
FIGURE 2.3 PROJECTIONS OF SALES OF POWER GENERATOR AND WASTE HEAT MATERIAL	17
FIGURE 2.4 MARKET FORECASTS FOR THERMOELECTRIC ENERGY HARVESTERS (US\$ MILLION) ..	18
FIGURE 2.5 PAIRS OF PROTOTYPE THERMOELECTRIC WINDOW.....	19
FIGURE 2.6 OUTPUT POWER FROM A PROTOTYPE THERMOELECTRIC WINDOW.....	20
FIGURE 2.7 THERMOELECTRIC ENERGY HARVESTERS FOR THE USE OF WIRELESS SENSOR NETWORK	20
FIGURE 2.8 ARRANGEMENTS OF THERMOELECTRIC MODULES AND HEAT EXCHANGER IN THE AUTOMOBILE EXHAUST THERMOELECTRIC GENERATOR	21
FIGURE 2.9 RADIOISOTOPE THERMOELECTRIC GENERATOR	23
FIGURE 2.10 SINGLE-INPUT NEURON.....	30
FIGURE 2.11 TYPES OF TRANSFER FUNCTIONS.....	30
FIGURE 2.12 LAYERS OF L NEURONS	32
FIGURE 2.13 THREE-LAYER NETWORK.....	32
FIGURE 3.1 SCHEMATIC DIVISION OF THE PHYSICAL STRUCTURE OF A TEG	35
FIGURE 3.2 VARIOUS MODES OF HEAT TRANSFER ACROSS THE THERMOELECTRIC POWER GENERATOR.....	36
FIGURE 3.3 CONDUCTION HEAT TRANSFER WITH DIFFUSION OF ENERGY DUE TO MOLECULAR ACTIVITY.....	37
FIGURE 3.4 HEAT TRANSFER BY CONDUCTION ACROSS MATERIAL	37
FIGURE 3.5 BOUNDARY LAYER DEVELOPMENT IN CONVECTION HEAT TRANSFER.....	38
FIGURE 3.6 A CELL IN THREE DIMENSIONS AND NEIGHBORING NODES.....	41
FIGURE 3.7 A CELL IN THREE DIMENSIONS AND NEIGHBORING NODES.....	43
FIGURE 3.8 GEOMETRIC ARRANGEMENT OF A HEAT SINK	46
FIGURE 3.9 LINE BY LINE APPLICATION OF THE TDMA METHOD.....	52
FIGURE 3.10 TDMA METHOD IN A 3D VOLUME OF TEG	53
FIGURE 4.1 GENERALISATION OF ARTIFICIAL NEURAL NETWORK	55
FIGURE 4.2 THREE-LAYERED ARTIFICIAL NEURAL NETWORK	57
FIGURE 4.3 OPERATION OF AN ARTIFICIAL NEURON IN A LAYER	61
FIGURE 4.4 SCHEMATIC OF A COUPLED NEURAL NETWORK	62

FIGURE 4.5 COUPLED NEURAL NETWORK	65
FIGURE 4.6 MAIN GUI.....	71
FIGURE 4.7 TRAINING GUI	72
FIGURE 4.8 TRAINING OF ANN MODEL.....	72
FIGURE 4.9 TESTING GUI.....	73
FIGURE 4.10 INPUT VALUE RANGE CONSTRAINT	74
FIGURE 5.1 EXPERIMENTAL SETUP OF TEG WITH LED HEAT SOURCE	76
FIGURE 5.2 EXPERIMENT SETUP SCHEMATIC OVERVIEW.	77
FIGURE 5.3 GRAPH COMPARISONS BETWEEN MEASURED, TECHNICAL SHEET DATA AND MATHEMATICAL MODEL FOR TEG WITHOUT HEAT SINK.	78
FIGURE 5.4 ERROR DISTRIBUTIONS IN THE FIRST NETWORK.....	80
FIGURE 5.5 COMPARISON OF THE ACTUAL ERROR OF THE FIRST NETWORK AND THE ESTIMATED UNCERTAINTY PREDICTED BY THE SECOND NETWORK	81
FIGURE 5.6 PERFORMANCE PLOT	82
FIGURE 5.7 ERROR HISTOGRAM PLOT.....	83
FIGURE 5.8 REGRESSION PLOT	84
FIGURE 5.9 TRAINING STATE PLOTS.....	85
FIGURE 5.10 SENSITIVITY ANALYSIS	86
FIGURE 5.11 HOT SIDE AMBIENT TEMPERATURE EFFECTS ON OUTPUT VOLTAGE.....	90
FIGURE 5.12 COLD SIDE AMBIENT TEMPERATURE EFFECTS ON OUTPUT VOLTAGE.....	91
FIGURE 5.13 HOT SIDE WIND VELOCITY EFFECT ON OUTPUT VOLTAGE.....	92
FIGURE 5.14 COLD SIDE WIND VELOCITY EFFECT ON OUTPUT VOLTAGE	93
FIGURE 5.15 THICKNESS OF THE CERAMIC SUBSTRATE EFFECT ON OUTPUT VOLTAGE	94
FIGURE 5.16 THERMAL CONDUCTIVITY OF THE CERAMIC SUBSTRATE ON HOT SIDE EFFECT ON OUTPUT VOLTAGE	95
FIGURE 5.17 THERMAL CONDUCTIVITY OF THE CERAMIC SUBSTRATE ON COLD SIDE EFFECT ON OUTPUT VOLTAGE	96
FIGURE 5.18 HEIGHT OF TE EFFECT ON OUTPUT VOLTAGE	97
FIGURE 5.19 THERMAL CONDUCTIVITY OF TE EFFECT ON OUTPUT VOLTAGE	98
FIGURE 5.20 INPUT HEAT ON HOT SIDE SURFACE EFFECT ON OUTPUT VOLTAGE	99
FIGURE 5.21 LENGTH OF HEAT SINK FIN EFFECT ON OUTPUT VOLTAGE	100

List of Tables

TABLE 4.1. INPUTS PARAMETERS FOR ANN MODEL.....	58
TABLE 4.2. OUTPUT PARAMETER FROM ANN MODEL	60
TABLE 5.3 PARAMETER RANGE FOR DATA SET GENERATION	79
TABLE 5.4. RANKING ON THE SENSITIVITIES OF THE INPUT VARIABLES ON THE OUTPUT VOLTAGES ACROSS THE THREE SCENARIOS.	87
TABLE 5.5. DEFAULT PARAMETERS USED FOR VALIDATION	89

Chapter 1 Introduction

1.1 Motivation

The demand for energy worldwide has exploded due to unbridled economic development and industrialization, and is now showing signs of receding or plateauing. Most of the efforts to conserve energy have by far, not been able to compensate for economic growth or at least, to keep the consumption of limited fossil reserves on a constant level. While the general awareness about the value of our energy supply has to increase, a new consciousness of consumption has to gain impact in the international market.

The role of science and engineering to develop and identify technologies to increase the production of energy through increasing efficiency of renewable sources on a broad basis, incorporates an immense responsibility for the environment and energy security for the next generation. Apart from technical excellence, economic and environmental factor should be part of the engineering process. Decentralized power facilities based on renewable sources have been constructed and these will play a significant role in the future. But there is also a need to explore the potential of improving the efficiency of the wide range of other energy generating applications. Innovative and unconventional ideas should be turned into well-established solutions. Besides the power consumption optimization of the device, interdisciplinary research should be explored by a system-wide methodology to find intelligent global solutions that are beneficial to the scientific community.

The scientific community is actively working to advance the new energy technologies and strategies to meet future energy demand while reducing dependency on the conventional forms of energy that drive our economy [1]. Many theoretical and experimental studies have also been conducted to evaluate the feasibility of systems that convert waste heat into electrical power. Investigations on the characteristics of thermoelectric power generation (TEG) often highlight the importance in green energy generation through its application in waste heat recovery [2]. The often-cited alternative forms of conventional renewable energy are wind, solar and thermal energy conversion. Developing such a mix of alternatives is a reasonable approach to bring about a desired stable energy future [3].

Most of the thermal energy in the environment are from unwanted heat generated by thousands of industrial and power generation processes [4], including higher heat operating turbines, boilers or other co-generative processes. If the amount of wasted heat expelled is not significant enough to be used in a conventional way, the heat will be exhausted into the environment. One promising option for recovering the energy lost through waste heat is the use of TEG.

TEG incorporates the direct energy conversion from the temperature gradients to electric energy. The fundamental theory behind this conversion has been known for almost two centuries. Despite the promotion of the use of TEG as a source of alternative energy, it can only be used on a few highly specialized applications due to its low conversion efficiency. Over the past decade, the research community has been focusing on improving the material properties of the TEG, hoping that a breakthrough in the material of the TEG will boost the conversion efficiency. However, given the current maturity of the science and engineering knowledge, there does not seem to be any significant breakthrough over the past few years that is worth mentioning.

The motivation of this research is not only to make use of the available waste heat sources but to also create a novel model based on neural networks that are learnt in a supervised way to predict and anticipate the output energy generated by a TEG. Due to the limitation of information stated in the manufacturer's specification sheet, it is not possible to have access to all the variables that determine the behavior of the TEG. Once many of the measurable variables are identified, there might still be some hidden variables that will influence the dynamics of the TEG with the parameters in its surrounding operating environment. The degree of ambiguity may vary widely across the whole range of input values. Hence to evaluate the accuracy of the model, a method incorporating two coupled neural network, has been used to obtain the degree of reliability of each output results. The first network will compute an average predicted value for each set of inputs that includes the operating environmental parameters and construction of the TEG, while the second network will evaluate the reliability of the output, which is learned from the error values of the first network.

Apart from predicting the output voltage of the TEG, this model will perform a sensitivity analyses on the 12 inputs and rank the input parameters from the most influential to the least influential on the output voltage generated by the TEG. This will benefit users when deciding on the best parameters to adjust for greater efficiency from the TEG during designing phase for an

application. The model will also aid in the prediction of selected input parameters when given an output voltage stated by user through reverse artificial neural network (ANN). This model will be applicable to almost any industrial process in which unwanted heat is produced, hence providing potential users with better understanding of their application.

1.2 Aim

The main aim of this research is to design a novel and robust model:

- a) that can reliably reflect the output voltage generated by a TEG under *various operating environmental parameters*.
- b) to provide users with *selected environmental and TEG construction parameters* that will help to produce the output voltage stated by users.
- c) that will identify and arrange the input parameters in a *sequence which define their importance* to influence the output voltage of the TEG through sensitivity analysis (SA).

1.3 Scope of Work

An experimental approach is taken to assess the functionality and robustness of the model. Samples were prepared to emulate real world conditions. The samples used in this study include TECTEG MFR TEG1-1263-4.3 TEG [5], a 11-volt light emitting diode to provide the thermal energy required for a temperature gradient across the TEG and an aluminum heat sink to help dissipate the heat on the cold side of the TEG. The samples are set up in an air-conditioned laboratory to maintain its ambient temperature and wind velocity. These samples emulate real world problems in terms of the operating environmental parameters that are critical to field scenarios. They are closely monitored and logged with a R-Type thermoelement at various points of the TEG, and a digital voltmeter.

As this research seeks to exploit the operating environmental parameters of the TEG to boost the temperature gradient which directly relates to the increase in output voltage, numerical and experimental investigation of the influence of the environmental parameters of the test sample were carried out. This was done to determine the distinctive or dominant influences of these

environmental parameters.

Following this initial investigation, a system based on neural networks that learn in a supervised way would be developed. This would include a computational scheme with the ability to evaluate the degree of reliability of predictive models. Lastly, identifying the environmental parameters that have a great influence over the output voltage generated, will allow users to manipulate the parameter to achieve their output voltage requirements.

Validation of the significance of the environmental parameters of the operating environment is presented through graphical means.

1.4 Contributions of the Thesis

This thesis contributes three novel solutions for the generation of energy using a conventional TEG. The proposed methods conquer the constraints related to the current energy generation methods using a TEG. The following outlines the contributions of this thesis:

- i. A holistic and novel approach that includes the environmental parameters and construction of the TEG is proposed, to predict an accurate output voltage generated by a TEG. The proposed model will provide users with the output voltage generated by the TEG in conjunction with its environmental parameters and construction which can be both beneficial as well as detrimental to the performance of the TEG. In addition, imposing the environmental and construction parameters to the model is necessary to give a unique and realistic representation of the TEG.
- ii. When dealing with a real-world problem, some degree of uncertainty cannot be avoided. Therefore, a novel computational scheme with the ability to improve on the accuracy and evaluate the degree of reliability of the predicted TEG output voltage based on coupled neural networks that learn in a supervised way will be applied.
- iii. With a total of 12 inputs, comprising of environmental parameters and construction of the TEG, an understanding of the influence of the 12 individual inputs will allow users to save time and cost to manipulate the inputs in order to achieve the required output voltage for

application. This thesis proposes a novel ranking method for the 12 inputs according to their influence in the model, from the highest and the lowest. With this knowledge, users will be able to obtain their required output voltage by changing the parameter that has the highest influence over the model. This will in turn help to reduce the need to manipulate various input parameters hence saving on the cost of adjusting multiple parameters of the TEG.

1.5 Organization of the Thesis

Chapter two gives an introduction on the thermoelectric (TE) phenomenon from discovery to its current implementation, and outlines the principles of TE such as the Figure of Merit (ZT), Seebeck Effect, Peltier Effect, material properties and energy conversion. Commercialization of the TEG and its applications in various sector such as building, automobile, aerospace and domestic applications will also be discussed. Past research carried by academics were also reviewed and discussed and this chapter will conclude with an overview on the challenges ahead for the TEG.

Chapter three and four will discuss in detail the approach and methodology of this research for both TE performance model as well as ANN. This will include the three main heat transfer modes that contribute to the temperature gradient across the TEG, namely conduction, convection and radiation. The effects of environmental parameters that influence the temperature on the construction of the TEG will be discussed too. The experimental setup in a typical air conditioned laboratory environment, used to compare against the dataset collected through the mathematical model formulated, will be discussed. Special attention will also be drawn to the instructional process to derive the output voltages using the graphical user interface (GUI) designed for the model.

Chapter five will present the analysis of the results generated from the model. Several scenarios on the application of TEG will be presented. Comparison between the output voltage derived from the manufacturer's specification sheet and the novel mathematical model created through this research work will also be analyzed.

Chapter six will conclude the current research work and provide a summary. Future works that can be carried out on the TEG will be recommended and discussed in this chapter.

Chapter 2 Literature Review

2.1 Overview of Thermoelectric Phenomenon

The TE phenomenon began in the early 1800s with the discovery of the TE effect by Thomas Seebeck and it was not until the mid 1900s, when semiconductor materials research became prevalent. TE materials by then have become more important. But there are still no well-established and widespread applications of TE for power generation due to the fact that there have been no significant advances in its efficiency, with the energy conversion efficiency rate hovering at approximately 3%, after the mid 1960s when the number of breakthroughs in the field decelerated [6]. Hence, study and development of TE remained predominately academic from there. Dismal energy conversion efficiencies of the materials and the general lack of interest for direct energy conversion methods discouraged further investigations into applications that we could benefit from TE technology.

Since the 1970s, TEG has been known as an alternative source of energy that is used on wider applications such as on space missions, military usage, medical apparatus, etc, where the application's lifespan and reliability is of primary and utmost concern [7]. These trends are followed by a significant improvement in the geometry and fabrication process of the TEG through extensive engineering efforts. Together with the advent of improved technology, the TEG started to attract significant attention from various industry stakeholders. TEG soon become well-known for being a 'green' and flexible source of electricity and for its application on a wide range of power requirements.

In recent years, this interest has been further driven by the discovery of new materials, which have a higher ZT value, In tandem with an increasing awareness of energy and environmental conservation issues. These led to the interest of the application of TE materials, such as the use of waste heat as an energy source, where the low efficiency of the conversion system is no longer an overriding issue in TEG.

The use of low grade heat from the surrounding environment of the TEG totally revolutionizes its economic competitions as it comes free. It has been demonstrated that using the current available material technology of the TE module, a TEG if operated over a 3 years period will produce electrical power at a cost which matches the major utilities [8]. In time to come, with

the advancement of technology, the 3 years period will eventually be shorten proportionally with the rising cost of energy worldwide due to the scarcity of fossil fuel [9].

2.2 Renewable Energy Comparison

There are several kinds of renewable energy that are currently available. However, each of them is based on quite different energy harvesting concept and science and each has its unique advantages. Analysis and comparison of the various kinds of technology will provide us with the most efficient and beneficial technology given a specific set of conditions.

While the field of TE continues developing, academics are still debating on its usage on a wide scale implementation. The main concern is still the energy conversion efficiency of the TEG as compared to photovoltaic (PV) which is in the range of 5% to 10% and up to 46% respectively [10].

2.2.1 Solar Energy vs Thermoelectric Energy

The TEG require heat as an energy source that can generate power so long as there is a heat source providing heat energy to the TEG. Solar modules on the other hand convert light energy into usable electricity that need direct sunlight to generate maximum rated power. In order to further boost the efficiency of the solar module, it uses solar tracking to receive direct sunlight which increases the cost of the photovoltaic system.

The generation of energy using thermoelectric can be carried out throughout the day when there is a temperature difference whereas for the solar module, energy will be generated as long as sunlight is available. However, it is not easy to reach an appreciable amount of temperature difference for the TEG for energy generation.

Costs of solar modules have been rapidly dropping, making them good candidates for energy generation in appropriate climates. For the space required, TEGs are good modules when compared with solar panels. TEGs are better than a single solar module in terms of weight. There is a huge difference when weight of both modules is compared. To match the power output of a single solar module there should be four TEGs connected together which increases the cost of the total number of TEGs. This becomes a disadvantage of TEGs when compared with solar panels.

However, weight and size (area) are still advantages of TEG modules for the appropriate application, environment and power requirement.

2.2.2 Wind Energy vs Thermoelectric Energy

Despite the low negative impacts and unlimited supply of resources, wind turbine still does possess some unwanted attributes. They are noise, shadow flickering, low efficiency and aesthetics are some of the main arguments from the critics of wind power. Therefore the installation of wind turbine in the small island of Singapore with dense built up areas can at times be limited and challenging [11].

Typically, the wind conditions in Singapore are not favorable for the utilization of wind turbines due to its geographical attributes that are not as desirable as those in Europe and United States. The wind speed compiled by the weather station in Singapore shows that she has an average wind speed of approximately 2m/s to 3m/s and when measured at strategically located sites, speed of up to 8m/s can be obtained [12] but most of the wind turbines will function most efficiently in areas with an average wind speed of above 5m/s. They are also not well suited for suburban areas as turbulent air leaves the turbine constantly chasing the wind and rather than extracting power from it.

The only same advantage that the wind turbine has when compared to the TEG is that they can produce energy day and night so long as there is wind.

2.3 Principles of Thermoelectric Energy Conversion

The TEG is a device that can directly convert thermal energy into electrical energy and vice versa. The energy conversion requires the temperature on both side of the solid state to produce an electromotive force that will create the voltage potential. When the TE material is at a stable temperature, all phonons are equal in magnitude and opposite in direction only to canceling one another out. When charge carriers diffuse, a temperature differential is introduced, forming a temperature gradient, until equilibrium is reached between the diffusion potential and the electrostatic potential. This would result in a buildup of charge carriers known as the Seebeck

effect.

Typically, a TEG consists of alternating P and N type semiconductors connected electrically in series and thermally in parallel. This allows the holes and electrons to flow in an opposite direction forming an electric current for power generation. A set of ceramic substrate layer that holds the P and N type semiconductors, serve as an electrical isolation and mechanical substrate for the TE device

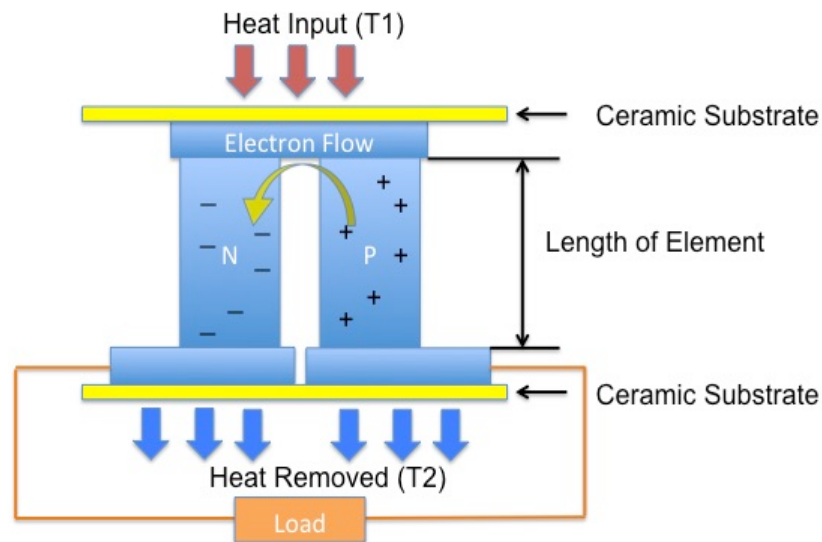


Figure 2.1 Structure of the thermoelectric generator

The TEGs are commercially produced in different sizes for various applications, ranging from a few millimeters to several centimeters as seen in Figure 2.1. The cross-sectional area of each element also greatly influences the internal resistance and the current-voltage of the generator. Multiple devices can be electrically connected in series or in parallel to achieve higher output voltage and currents, hence providing the required power level.

Even though it seems unlikely in the near future that TEGs will have a role to play in the large-scale energy production market, they do have some unique benefits that are worth highlighting over current technologies. The solid-state technology offers several advantages when compared to the other power generation technologies. The advantages are as shown below:

- i. extremely reliable, typically exceeding 100,000 hours of steady-state operation and silent in operation since they have no mechanical moving parts and require considerably less maintenance [13].
- ii. simple, compact and safe [14].
- iii. capable of operating at elevated temperatures [14].
- iv. suited for small scale and remote applications [15].

The biggest advantage of the TEG is scalability. Typical power generation engines experience significant drops in efficiency when they are reduced in size or power level, whereas for the TEG, regardless of the power level, they consistently maintained their efficiency. This leads to a crossover point where the TEGs are more efficient compared to conventional power generation engines. An increase in the ZT value will therefore increase the range of its applications, where these alternative generators will be much more efficient and makes more economical sense to use [16].

2.3.1 Thermoelectric Figure of Merit

The ZT value is a critical dimensionless metric used to evaluate the performance of a given TE material. A small increase can lead to a significant improvement in the performance of the TE and the value varies with temperature gradient. Therefore the goal is to find materials with a large ZT value in the temperature gradient range that suits the application. A good TE material should have the following characteristics:

- i. a high electrical conductivity that will minimize the rise in temperature from resistance to electric current flowing through it;
- ii. a large Seebeck coefficient (S) for maximum conversion of heat to electrical power or electrical power to cooling performance;
- iii. a low thermal conductivity to prevent thermal conductance through the material.

These three properties when combined into a single metric will measure the overall performance of the TE device known as the ZT . Therefore, the ZT value can be expressed as follows:

$$ZT = S^2\sigma T/k \tag{2.1}$$

where T is the absolute temperature, S (also known as thermopower), σ is electrical conductivity and κ is the thermal conductivity.

To have a higher ZT value, a large value for $S^2\sigma$ and a large reduction in κ are needed. Although there is no theoretical upper limit for the ZT value, it is still a challenge faced by researchers to achieve a higher limit, as there will always be a conflict between the three-transport properties, S , σ and k . Thus researchers have constantly been trying to find a compromise between the three properties to improve the ZT value.

2.3.2 The Seebeck Effect

The Seebeck (SB) effect was discovered in 1821 by Thomas J. Seebeck. The Seebeck effect asserts that a potential temperature gradient will be created across a conducting material when one side of the material is hotter than the other.

When exposed to a higher temperature, the charge carriers in the material will diffuse at a faster rate from the hot side to the cold side, due to the higher thermal velocities caused by the high temperature. In situations where thermal gradient across the material is maintained, the flowing charge carrier is accumulated on the cold side of the object. This separation of charge creates a potential difference between the two sides of the material which counters this charge imbalance.

In cases where the material is part of a circuit, this voltage induces a current which can be used to power up a load. The potential difference created per degree of temperature gradient across the material is its Seebeck coefficient, S , which is material dependent.

If a temperature difference is created between two different conductors, “a” and “b” having junctions at M and N, a voltage difference (V) will be created between M and N appearing between the two green segments. Placed under open circuit conditions, the Seebeck coefficient is defined as

$$S_{ab} = \frac{dV}{dT} \quad (2.2)$$

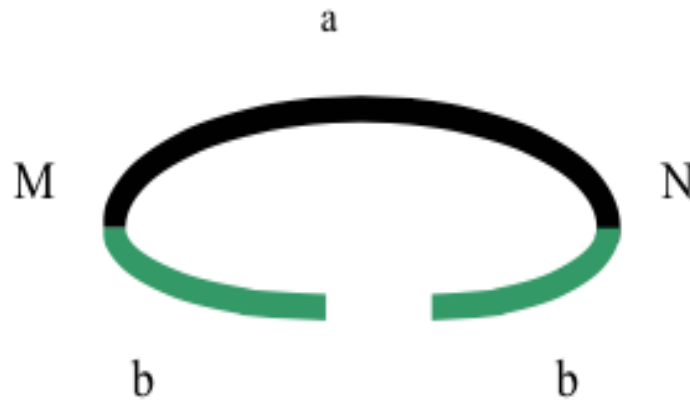


Figure 2.2 Thermoelectric effect

For small temperature differences, the relationship is linear. S is positive if the electromotive force (EMF) causes a current to flow in a clockwise direction around the circuit and is measured in V/K or more often in the range of micro V/K.

2.3.3 Peltier Effect

The Peltier effect, which was discovered in 1834, is the reverse of the Seebeck phenomenon. Thermal energy is absorbed or emitted when translating charge carriers, associated with an electric current, transition from relatively high voltage in the N type thermoelement to the lower voltage of the P type thermoelement. The excited carriers in the N type thermoelement must transit from high-energy state to low energy state in the P type element. In order for the transition to take place, they must discharge energy. In the reverse case of moving from P type to N type, they must absorb the energy. The rate at which the Peltier heat is liberated or rejected at the junction is given by:

$$q_{Peltier} = I(S_p - S_n)T \quad (2.3)$$

where I is the electrical current. It is also important to note that the heat emitted or absorbed due to the Peltier effect occurs at the contact boundary between two materials different from the Seebeck coefficients. The Peltier heat is also reversible depending on the direction of the carrier

flow, or electrical current. TE refrigeration cycles are driven by Peltier effect and it is also important to note that Peltier effect is present during TEG operation as well.

2.4 Conventional Mathematical Model for Thermoelectric Generator

Most of the physical phenomena discussed above are associated with the operation of the TEG. Under steady state conditions, the contribution of the phenomena to energy flow through a unit volume is expressed as follows [17]:

$$TI \frac{dS}{dx} + \tau I \frac{dT}{dx} - \rho I^2 - \frac{d}{dx} \left(k \frac{dT}{dx} \right) = 0 \quad (2.4)$$

where τ is the Thomson coefficient, ρ is the electrical resistivity of the material. Neglecting the contribution of the Thomson effect, the equation that governs the hot side is,

$$Q_H = K_{TEG}(T_{hsur} - T_{csur}) + S_{TEG}(T_{hsur})I + \frac{1}{2}I^2R_{TEG} \quad (2.5)$$

where K_{TEG} is the total thermal conductance of the number of TE couples, S_{TEG} is the total seebeck coefficient and R_{TEG} is the total resistance. Similarly, the heat that flows from the cold side is

$$Q_C = K_{TEG}(T_{hsur} - T_{csur}) + S_{TEG}(T_{csur})I + \frac{1}{2}I^2R_{TEG} \quad (2.6)$$

Therefore, the total voltage produced by the TEG is

$$V_{TEG} = S_{TEG}(T_{hsur} - T_{csur}) - IR_{TEG} \quad (2.7)$$

In practice, it is impossible to measure the exact temperature of both the hot and cold surface as the surface temperature will fluctuate according to the surrounding environmental elements such as wind and ambient temperature.

To allow better prediction of the surface temperature, some researchers suggested the use of finite element method. The governing equations to describe behavior of TE material are govern

by the coupled equations of heat transfer and continuity of current density phenomena as follow [18],

$$\rho c \frac{dT}{dt} + \vec{\nabla} \cdot \vec{q} = Q \quad (2.8)$$

$$\vec{\nabla} \cdot \left(\varepsilon \frac{d\vec{E}}{dt} \right) + \vec{\nabla} \cdot \vec{J} = Q \quad (2.9)$$

where \vec{E} is the electric field, \vec{q} is the heat flux, \vec{J} is the electrical current density and ε is the electric permittivity.

(2.8) and (2.9) are then transformed into finite element equations by approximating the primitive physical unknowns, temperature T and electrical potential ϕ , into interpolation functions and value of nodal known on an element by

$$T = [N]\{T_e\} \quad (2.10)$$

$$\phi = [N]\{\phi_e\} \quad (2.11)$$

where T_e is vector of nodal temperature, ϕ_e is vector of nodal electrical potential and N is element shape functions. Based on Galerkin weighting scheme, the differential equations become algebraic finite element equations [19],

$$\begin{bmatrix} C_T & 0 \\ 0 & C_E \end{bmatrix} \begin{Bmatrix} \frac{dT}{dt} \\ \frac{d\phi}{dt} \end{Bmatrix} + \begin{bmatrix} K_T & 0 \\ K_{ET} & K_E \end{bmatrix} \begin{Bmatrix} T^e \\ \phi^e \end{Bmatrix} = \begin{Bmatrix} Q \\ I \end{Bmatrix} \quad (2.12)$$

The global matrix equation is assembled from the individual finite element equations. The solution yields temperatures, T_e , and electric potentials, ϕ_e , at unconstrained nodes, or reactions in the form of heat flow rate and electric current at nodes with imposed temperature and electric potential respectively.

In this research, not only will finite element method be incorporated into the conventional

method of measuring the total voltage produced by the TEG, the influence of convection, conduction and radiation from the surrounding environmental elements will be taken into consideration too to ensure that users will be able to better predict the output voltage of the TEG when working in an environment.

2.5 Thermoelectric Material

In the past 15 years, there has been an exponential growth in the TE research field according to the Web of Science database [20]. The number of publications have increased tremendously to the current 28,000 publications in the scholastic database. Early TE material research in the 1950s and 1960s mentioned that bismuth telluride (Bi_2Te_3), lead telluride (PbTe) and Silicon-germanium (SiGe) alloys as materials with the best ZT . With the advent of nanostructured TE and complex bulk materials, and renewed interest in thermoelectricity in the 1990s, a number of publications have reported an increase in the peak ZT value over the current value of 1 [21]. TE materials can be classified into three categories. They are ceramics, polymers and semiconductors [22].

The ceramic material having a ZT value of approximately 1 is an important material for TE energy conversion, to retrieve high temperature waste heat from incinerators or combustion engines [23]. In comparison with TE alloys, metal oxide has advantages in better chemical stability, oxidation resistance, less toxicity and lower cost.

The conductive polymer composite families containing insulating polymer matrices and conducting fibers have been studied for its advantages of mechanical flexibility, low cost synthesis, inexpensive, lightweight and more environmentally friendly alternatives [24], despite its low ZT of approximately 0.1.

Semiconductors are a more promising batch for the constructions of the thermocouple as they have a larger 'S'. The proper way to reduce thermal conductivity of the TE material without affecting the other parameters and thus increasing the ZT value is to use semiconductors as they have a high atomic weight, such as Bi_2Te_3 . The higher atomic weight will help to reduce the speed of sound within the material and hence decrease the thermal conductivity. Semiconductors are also deemed reliable when operating in an ambient temperature environment.

2.6 Commercialization

The commercialization of TE materials involves the validation of a TE performance at the system level in a commercial configuration. It is considered beyond the material research that has been looked into since the past few decades. Currently, the most common and reliable commercialized TE material is the Bi_2Te_3 . There are also other new forms of materials introduced into the market as exclusive research is being conducted.

However, due to the limitation of equipment and standards for the measurement of the ZT value, many of the materials, claiming to have a high ZT value, are not reproducible or the experiment can only be done within a standard lab environment, which is conventionally not feasible for manufacturing purposes. For the fabrication of the TE module, a reliable, repeatable, economical and durable fabrication method will thus be needed to connect the large number of TE couples in arrays, bundled with the capability of withstanding mechanical shocks, adverse physical conditions as well as harsh environmental conditions that they will be operating under [25].

To achieve a TE system that is stable and reliable, a set of standardization tools needs to be developed. The cost, performance, usage and final disposal of the system has to be standardized [26]. Although the TE application has many uses in various segments of our day-to-day life, we are still far from achieving commercialization, as the ZT value is the criterion to the success to the commercialization of TE system.

Figure 2.3 shows the projection of sales of power generation and waste heat recovery material as a function of the ZT value, assuming materials are available with an average ZT value of 2 by 2018 and are mass produced by 2023 [27]. The graph shows that market size is a strong function of the ZT value, for device level values up to approximately 2.

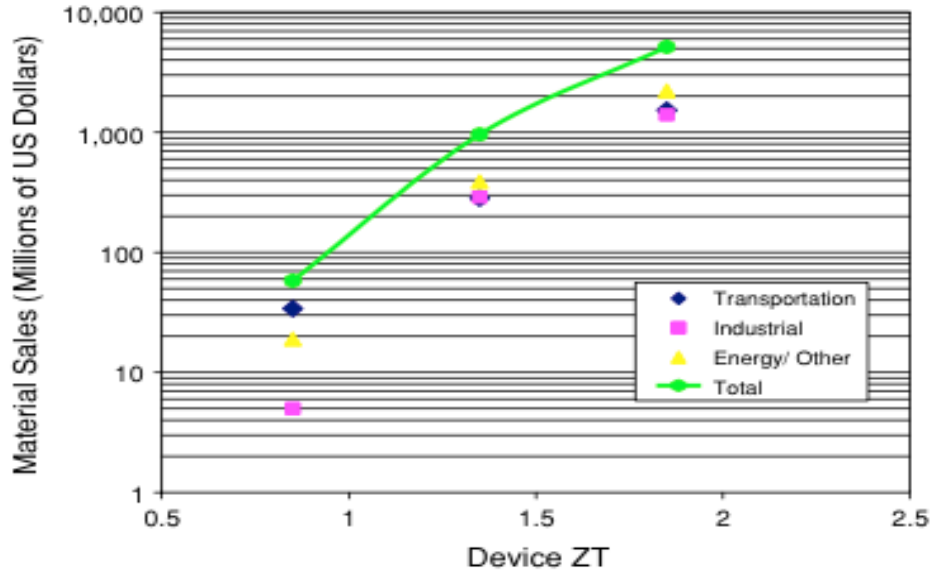


Figure 2.3 Projections of sales of power generator and waste heat material [27]

Commercialization is a key factor in TE research and development. In most of the proceedings published since 2000, that touched on the development of TE, the authors unanimously referenced the commercial need for better TE materials. [26]. However, this commercialization process is going to take a long time if the aim of achieving high ZT value is the “light that we are looking for at the end of the tunnel”. Instead we should be looking into other means to enhance the efficiency of TE applications using conventional TE material.

2.7 Thermoelectric Applications

Half of the power nominally available worldwide is wasted as low enthalpy heat during its conversion [28], Hence alternative approaches such as harnessing this waste heat from the surrounding environment to generate power has been actively explored in recent years, This in an attempt to improve the competitiveness of the TEG without a prerequisite of increasing the ZT value.

Not all industrial waste heat is of the same quality. The quality of heat varies from one industrial application to the other in terms of its temperature, applications and accessibility. The harnessing of waste heat energy to produce electrical power is essentially free. Therefore, instead

of efficiency, the economic factor is the overriding consideration when implementing the use of waste heat in an application [29].

Many manufacturing industries offer several opportunities for energy recovery. Aluminum, glass, metal casting and steel all have process furnaces discharging large amount of high temperature waste heat which some industries used this heat to preheat raw materials. In a recent report by IDTechEX, an independent market research company, it was reported that the market on the application of TE energy harvesters will reach over \$950 million by 2024 [30]. Figure 2.4 shows that the military and aerospace sector dominates most of the TE energy harvester market shares with wireless sensor network (WSN) catching up aggressively in the next few years.

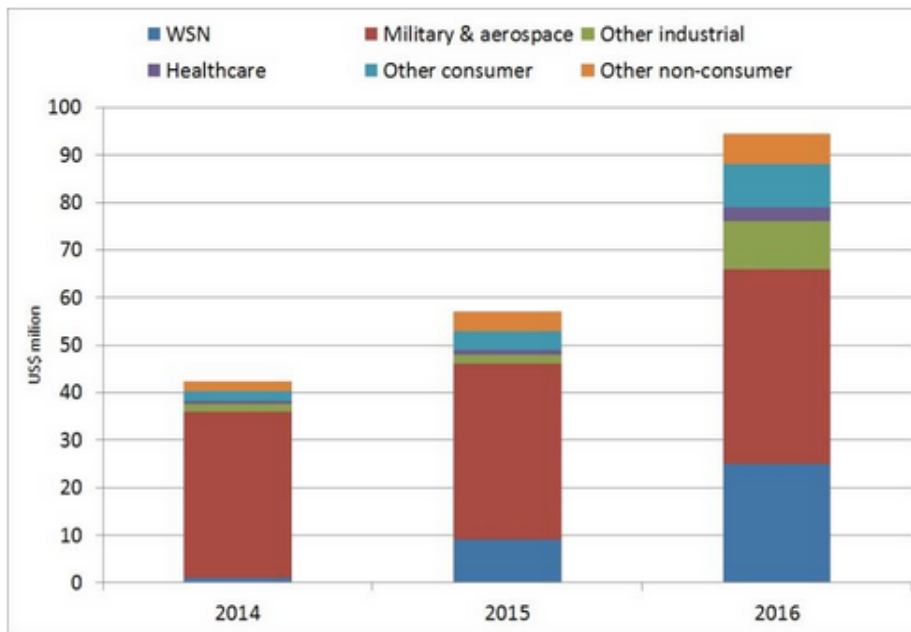


Figure 2.4 Market forecasts for thermoelectric energy harvesters (US\$ million) [30]

TE application can be classified into two main categories according to methods, namely host application and parasitic application. In host application, all the energy in the heat source is used for the energy conversion, while for parasitic applications; only partial heat is converted to electricity without affecting the main function of the operation. The heat source varies from low-grade waste heat, at 325K to 350K, to high-grade waste heat at 850K to 1100K. Apart from applications described above, TE devices have also been explored in various sectors, such as building, automobile, aerospace and domestic purposes.

2.7.1 Buildings

Inayat et al [31] successfully demonstrated the use of a large plexiglas prototype panel integrated with 72 pairs of nano-manufactured TE pillars (Figure 2.5). This helps to generate electrical energy (Figure 2.6), using high occurring temperature between outdoor high temperatures attributed by the sun and relatively cold indoor ambient room temperature. The checked board layout version of non-optimized TE material deposition produced TE power. It is measured to be more than 10nW on a transparent plexiglas slide of thickness 5mm cured from individual strips of 5mm width, for an outdoor ambient temperature gradient. This amount of energy generated may not be a huge power source but can instead be a supplemental source. Therefore, the temperature gradient using air conditioners in the indoor environment need not have to be in operation round the clock. Instead the TE windows will generate power as long as there is a temperature gradient for the powering and charging of small appliances [32].

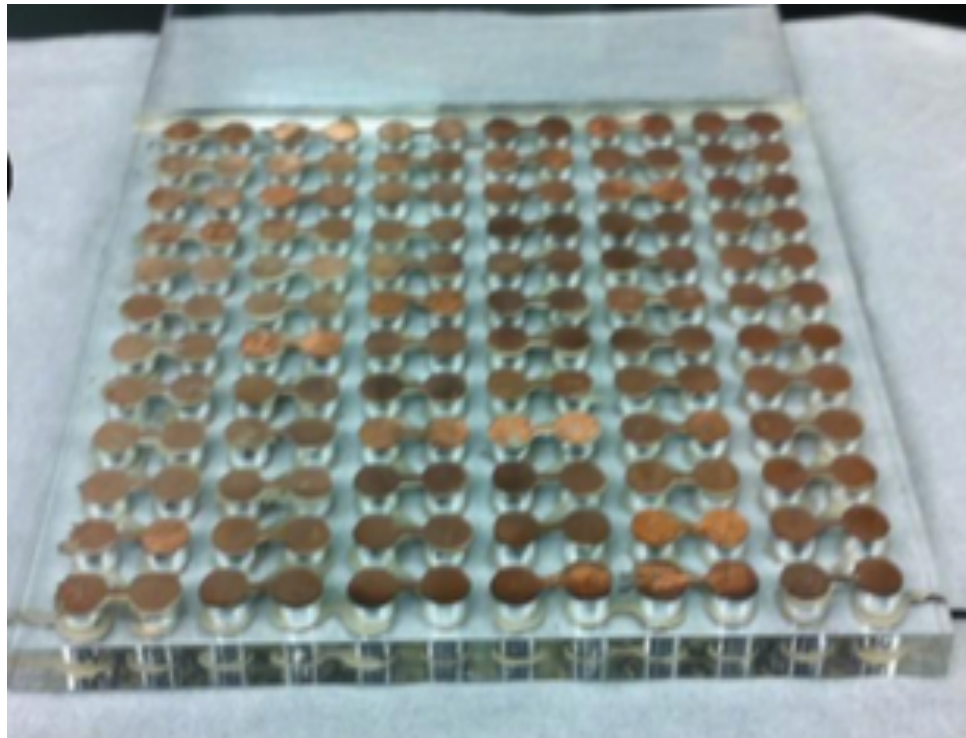


Figure 2.5 Pairs of prototype thermoelectric window [32]

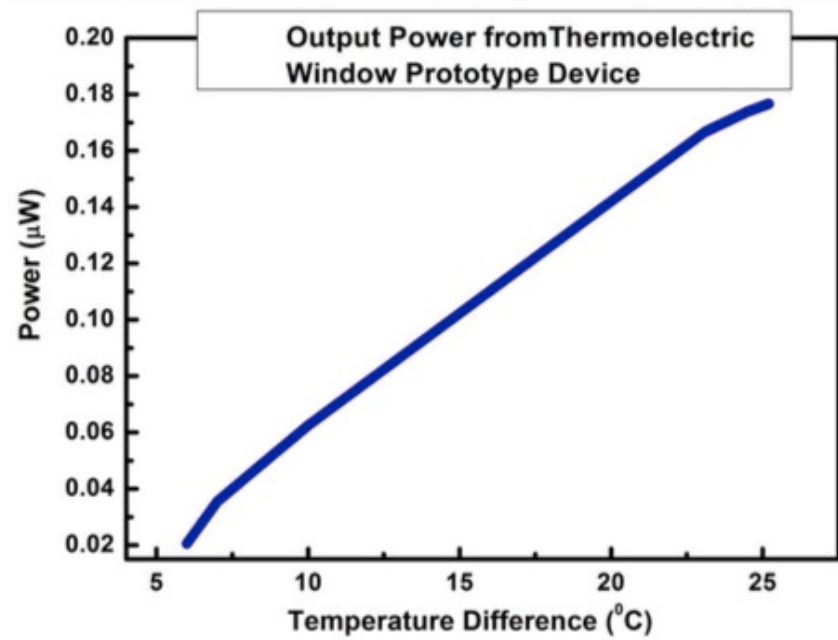


Figure 2.6 Output power from a prototype thermoelectric window [32]

Wensi Wang et al. [33] designed a TE energy harvester, using the heat generated from a typical wall mount heater with a surface temperature of 333.15K to power the WSN for building energy management applications. The low voltage output from the TE harvester was amplified using a DC/DC converter, boosting of a 0.5V output voltage to a 3.3V output voltage. Figure 2.7 below shows the application of TE energy harvester in the application.

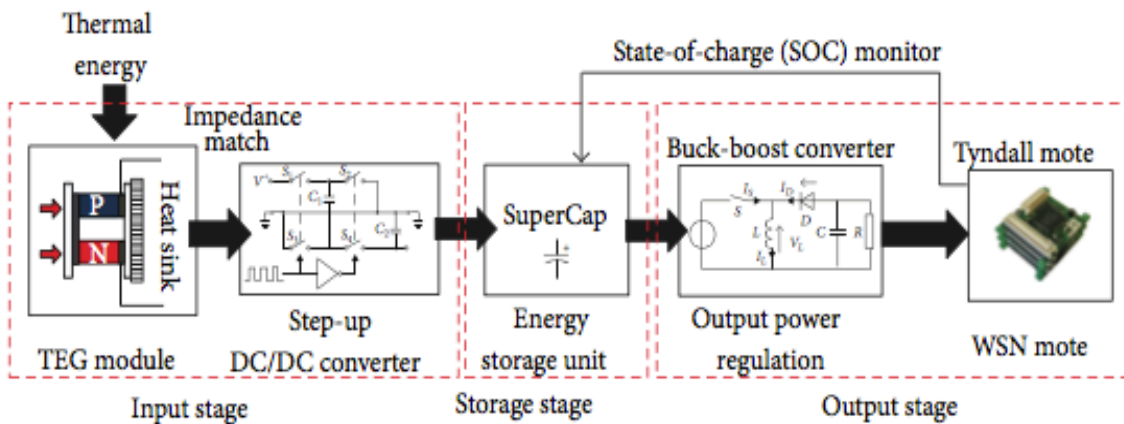


Figure 2.7 Thermoelectric energy harvesters for the use of wireless sensor network [33]

2.7.2 Automobile

Takanose and Tamakoshi [34] installed an automobile exhaust TEG in a passenger car and tested it under vigorous driving conditions. The generator output ranged from 10W to 20W for speed of 40 km/h – 60 km/h on an uphill road. Bass et al. [35] also presented experimental studies on the use of TEG to recover energy from the exhaust of a diesel fueled truck. The above-mentioned experiments demonstrated maximum electric power output of 1000W and this power output increased together with the engine loading. Richter et al. [36] also tested the power generation of the automobile exhaust TEG, as shown in Figure 2.8, and highlighted the importance of identifying the influencing factors in a vehicle system (i.e. pressure and flow rate measurement of the exhaust and coolant systems were observed) as they are also important for optimizing the design of TEG in an automobile exhaust. Richter et al. concluded that this would not only enable fuel efficiency to be assessed, but also losses incurred due to the additional pumping strain placed on the coolant system and the backpressure of the vehicle exhaust.

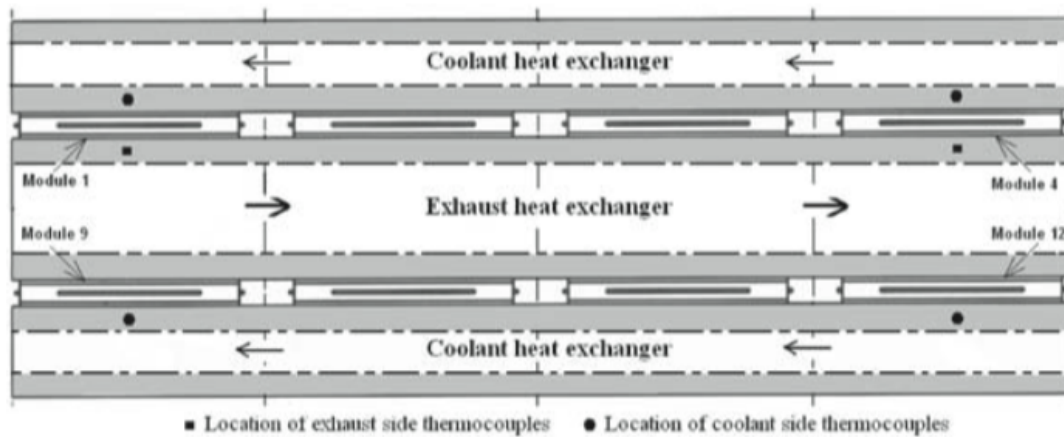


Figure 2.8 Arrangements of thermoelectric modules and heat exchanger in the automobile exhaust thermoelectric generator [36]

Thacher Karri et al. [37] used the same automobile exhaust TEG model investigated by Richter et al.. However, he used quantum well based TE material and investigated the potential benefits in the power and fuel savings of two practical applications, a sports utility vehicle and a stationary, compressed natural gas fueled engine generator. The results showed that for the sports

utility vehicle, the quantum well based TEG generated between 100W to 450W. This should result in fuel saving of about 2% to 2.3%. However, the savings decreased by about 30% primarily due to rolling resistance parasitic loss. In contrast in the compressed natural gas case, the total parasitic loss was low, relative to the TEG stack power. As this was a stationary application, there isn't a space constraint which has allowed an increase in the system size. The optimized quantum well based TEG stack generated about 5.3kW - 5.8kW resulting in a fuel saving of about 3%. Karri concluded that despite the higher stack power and lower parasitic loss, the low relative fuel gains was still primarily due to the high efficiency of the electrical generator.

Saqr et al. [38] presented the use of TEG via waste heat recovery in the automobile to displace alternators and provide additional charging to a vehicle battery pack. They concluded that the TEG efficiency is closely linked with the geometry and material of the heat exchanger, the location where the TEG is installed. It has been noted that when the TEG is installed at sites closer to the engine and away from the exhaust pipe, there will be a significantly greater temperature difference as well as in the coolant system of the TEG, to create the temperature differential.

2.7.3 Aerospace

Space exploration missions require safe and reliable long lasting power systems to provide electricity for the operation of the spacecraft and the sophisticated equipment onboard. A flight proven capable source of power is the Radioisotope Thermoelectric Generator (RTGs) units, also known as space batteries or nuclear batteries, as shown in Figure 2.9. They worked by converting heat from the natural decay of the radioisotope materials into electricity. RTGs have been used in 27-space missions since 1961 [39] for National Aeronautics and Space Administration (NASA). With the use of the RTG, the expenditure duration of the Solar System lasted for more than five decades and counting.

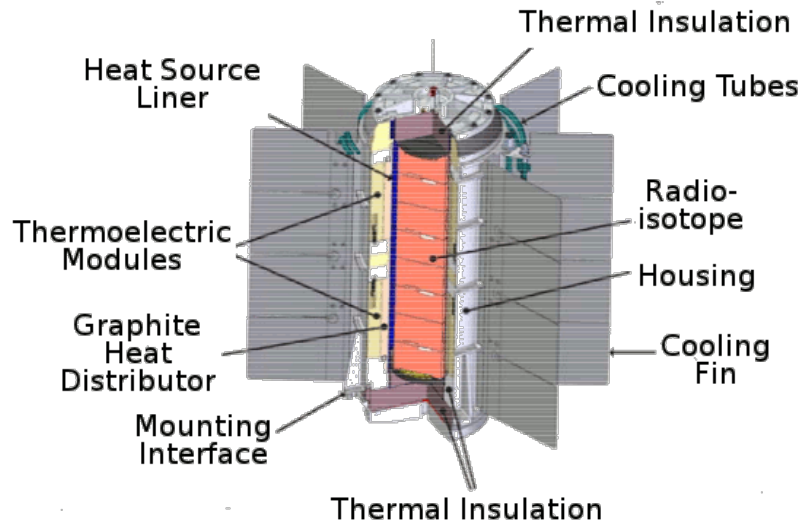


Figure 2.9 Radioisotope thermoelectric generator [40]

NASA's Voyager 1 spacecraft, launched in 1977 and powered by three units of RTG, has entered interstellar space in 2013 and has travelled further than any craft in history. Each RTG onboard Voyager 1 was designed to operate in the vacuum of space and has a flexible modular design capable of meeting the various needs of each individual space mission. The RTG is made up of an isotopic heat source, a TE converter, a gas pressure venting system, temperature transducers, connectors, a heat rejecting cylindrical container and its bracket. The heat source radioisotope fuel is Plutonium in the form of oxide and the energy released is converted to heat, which in turn is used to power the RTG. When exposed to deep space environments, each RTG contains a total of 4.8kg of plutonium dioxide that provides approximately 2KW of thermal power and 110W of electrical power. The power source of spacecraft is estimated to be able to be self-sustainable through at least year 2020, which would mark 43 years of continuous operation. The current power level is 315W, down from 470W at the launch of Voyager 1 [40].

2.7.4 Domestic Application

Nuwayhid et al [41] explored improving the efficiency of the TEG stove by producing extra electrical power from the heat that is not used. However, it requires a cooling fan to cool the heat sink by blowing ambient air on the heat sink extrusions. This posed a disadvantage, since the

cooling fan that is required to cool down the heat sink extrusion consumes energy and also discharging the unmanageable heat output.

In recent years, similar home use stoves have been studied. Killander [42] reported on the development of a stove mounted TEG for use in remote areas in Northern Sweden. The TEG, which is designed to use the heat of existing wood-fired stoves, are typically used in areas beyond the electric grid range. This will allow occupants to have electric lights and watch television during long winter nights. Using a gasoline powered motor electricity generator will produce too much noise and the power output will always exceed electricity requirements. Moreover, using gasoline is an expensive option that comes with a high maintenance cost. The stove at its optimum performance was in the morning with a power output of 10W when the ambient temperature was low and the stove frequently fueled. During the daytime, the power output range from 4-7W.

There are many more examples of using a TEG for power generation in various sectors and they are discussed by Riffat et al [13].

2.8 Past Research Area

Performance of the TEG has been a topic of constant study by end users and academics. In the literature of TEG, there are both analytical and experimental approaches with varying degree of results when comparing to the data provided by the manufacturer specification sheets. Many similarities were also found in the analytical, experimental and methodologies between work done by various research groups. There are two main areas that the publications found on TEG can be categorized. There are many forms of research done on the experimental methods and the material properties of TEG.

Experimental methods are basically done to recreate the performance curves presented by the manufacturers in their specification sheet hence evaluating on their integrity. Most of the test are done under various environmental conditions as the actual test environment used by manufacturers are usually unknown to users. Most common scenarios would be carrying out the experiment in a vacuum environment or an environment with a set of operating parameters. In this research, we will focus on the later but factoring in the actual surrounding operating environmental parameters. Material properties of TEG module are usually the next unknown hence causing disagreement between the performance curve of the measured data and data provided by

manufacturer's specification sheet of the TEG.

2.8.1 Experimental Method

Performing the experiment in a vacuum environment will provide good agreement with the data provided in the manufacturer specification sheet. However, it comes at a cost of inaccurately representing the realistic operating environment where heat transfer through convection, conduction and radiation are part of the equation [43]. Having a set of test parameters to mimic the experiment conducted by manufacturer, Takazawa et al [44] and Anatychnuk and Havrylyuk pay great attention to ensure the uniform distribution of compression and heat applied to the hot surface of the module. This is because performance of the TEG will depend on the uniformity of the temperature across the TEG. Temperature on the hot side of the TEG is particularly important as inhomogeneous temperature and poor thermal contact between heater and TEG will lead to unequal heating which will affect the generated power [45].

Test benches were designed to measure the performance of commercial TEG modules. Vizquez et al designed a test bench that sandwich the TEG module between a main block, which is the source of heat and insulated to prevent heat loss, together with an aluminum water cooled block to dissipate the heat transferred. This created a temperature gradient across the TEG module. Two scenarios were performed using the test bench. There was the variation of the cold junction temperature while the hot junction temperature is maintained. Next, maintaining the cold junction temperature was done while the input heat source to the main block was varied. The results generated through both scenarios showed a degree of accuracy but the thermal losses at the heat source and the thermal bypass has been neglected in this experiment [46]. Faraji and Akbarzadeh designed a compact, standalone and portable test system that measures the main parameters of a TEG over a wide range of temperature difference together with the compression pressure on the hot and cold side of the TEG. This derived both S and Z. When comparing the experimental values obtained with the manufacturer's specification sheet data, there is a good agreement [47]. Both experiments serve as a good guide for the design of a TEG prior to implementation on applications.

Seebeck coefficient studies have been done by Hsu et al. and the experimental results shows that there is approximately a 30% difference in its value when compared to the manufacturer's specification sheet. Two effects have been identified as the cause of these

discrepancies. They are the increase in thermal resistance between the junctions of the modules due to lower clamping force and inaccurate temperature readings by the thermocouples placed on the ceramic plate of the module during operation [48].

2.8.2 Material Properties

The detail material properties of the TEG are often not provided in the manufacturer's specification sheets hence Sandoz-Rosado and Stevens developed a test standard to characterize the performance of TEGs. The heat transfer rate on the TEG is the most difficult to accurately conduct in this experiment. Both Sandoz-Rosado and Stevens need to analytically predict the performance of TEG modules with known intrinsic material properties. The analytical model accounted for parasitic losses that occurred in the unoccupied voids between the ceramic plates of the TEG. From this experiment, it was concluded that the values obtained from the analytical and experimental results when compared to the manufacturers specification sheet were inaccurate [49].

To minimize parasitic heat loss through heat transfer and to mimic the same type of laboratory experiment by the manufacturer, Huang et al. developed an automated means of determining the material properties of a TEG [50]. Analytical prediction of the performance curves agreed well with the data provided by the manufacturer although they did not fit perfectly. The discrepancy was attributed to the correlation that was only valid to unique TEG modules. This sometimes happens even when using the same model due to manufacturing variability.

Subject to large temperature difference, the material properties of a TEG plays a critical role in the amount of energy generated. Muto et al. performed a research that take into consideration the radiation and heating in their analysis. The material properties were evaluated as functions of temperature. These material properties derived were further simplified to become "effective material properties" that were evaluated as integrals over the operating temperature.

Lineykin and Ben-Yakoov, using reverse engineering method, developed an analytical model to determine the material properties of TEG. The three parameters used to compute the TEG module properties S , K and maximum resistance, R_m , are the maximum temperature gradient (ΔT_{max}) across the TEG module, maximum input DC current (I_{max}) and maximum voltage (V_{max}). Computer software was used to analytically predict the performance curves. When compared with the data provided in the manufacturer specification sheet, the results indicated good agreement

[51]. However, when the same method was used by Luo in his research, the results obtained showed a different result. Compared with four manufacturer specification sheet performance curve, the data generated by Luo showed a difference of approximately 13% [52].

Another difference is the non-standardization of information provided by manufacturers. Hence Tan and Fok proposed a standard to compare the performance of modules from different companies using the same three maximum parameters used by Lineykin and Ben-Yakoov and Luo. There is also discrepancy found in the data generated when compared to data presented in the manufacturing specification sheet. It was concluded by Tan and Fok that this was caused by the inherent temperature dependence of the material properties of the TEG [53].

Alternative computer controlled method was also looked into by Ahiska et al. where they are able to use the maximum parameters of the TEG without having to use the data provided by Manufacturer. Using a series of automated test on a computer controlled test bench, the values of I_{max} , V_{max} and the maximum electromotive force (E_{max}) were used for the equations. Using this set of data, the performance curves were analytically predicted. They showed good agreement with those on the manufacturer specification sheet [54]. This concept has been repeated and further improved by Ciylan and Yilmaz [55] in their research work.

2.8.3 Summary of Research Areas

There are various experimental methods and techniques developed to evaluate the performance of the TEG. Many a time, experiments conducted do not indicate the brand, model, construction, material and environmental parameters that the TEG is operating. Hence what is lacking in the TEG research community is a generic method of predicting the output power of any TEG bought commercially off the shelf, taking into consideration the application's operating environmental conditions. With the knowledge of how the surrounding environmental parameters and construction of the TEG can affect the output power of the TEG, users will be able to optimize the use of TEG on applications. This can improve efficiency, making it more cost effective.

2.9 Challenges

Pursuing a high ZT value through the application of various phonon engineering and electron engineering schemes has been the focal point for many researchers in the TE community. For practical applications, a high ZT value for low-grade waste heat is not sufficient as it is not enough to result in high efficiency. In addition, efficiency is not the only concern. High output power density is just as important as the efficiency when the surrounding heat source is large, or when the cost to produce the heat source is not a big factor in the application.

The preliminary design of an application using TEG bought off the shelf will usually involve the referencing of performance curves and data stated in specification sheets provided by manufacturers.

Values and graphs reported in the specification sheets are usually obtained from a lab test environment. This often neglects the countless permutations of the real-world operation environment that the TEG might be operating in. Hence, the values obtained in real life applications, may usually reflect much lower than indicated in the specification sheet and do not correlate with the values and graphs stated on the specification sheets provided by manufacturers. Therefore, they do not meet the design requirements or power output stipulated by the application. These will therefore affect the precision and output product, as well as the cost of the application when using the TEG.

2.10 Overview of Artificial Neural Network

Artificial neural network, has become a modelling tool frequently used in applications in different disciplines and for analyzing complex problems that cannot be easily modeled mathematically. In particular, the ANN usage has been used widely in engineering applications such as heat transfer analysis, performance prediction and dynamic prediction [56, 57]. It has also been applied in many fields as a function approximation tool including time series prediction, regression analysis, interpolation and extrapolation. It can also be in the form of a classification tool including fault detection and pattern recognition as a data processing tool including filtering and clustering [58].

ANN is known to be an adaptive system where all parameters are changed and deployed for solving problems. The changing of the parameter values is known as the training phase and the

neural network is developed step-by-step with the optimization of criterion called the learning rule. Upon feeding the input data into the ANN, an error value is calculated using the difference between the actual and desired output. Depending on the architecture of the network, this error value will be fed back again into the ANN for adjustment of the parameters on the basis of the learning rule used. This looping will be done until the predicted output values become equal to the actual output or an acceptable error value is achieved.

2.10.1 Application of the Artificial Neural Network

ANN has also been successfully used in the analysis of heat transfer data as well as heat transfer coefficient [59-61]. Sablani [62] in his research, developed a non-iterative procedure of an ANN to determine the fluid to particle heat transfer coefficient, while Islamoglu [63] applied a new approach of an ANN model for predicting the rate of heat transfer of a heat exchanger. This is the wire-on-tube type.

The advantages of using ANN instead of other methods rest in its capability in modeling a complex problems with many variables [64]. It can handle noisy data and can be implemented to any application. Once a network is trained, parameters are fixed and any case can be executed within a few seconds without the need for re-programming and re-modeling [58].

In this research, a multilayer feedforward ANN model has been developed. This is the most common model used for mechanical engineering applications and is being trained using propagation, genetic algorithm or simulated annealing technique. It consists of an input and output layer, with at least one layer of processing units called the hidden layer between them.

2.10.2 Neurons

Although the neurons form a communication conduit and are connected together, they are not equal and each can be assigned with an individual weight. These weights provide the neural network the ability to recognize certain patterns. To allow the different patterns to be recognized by the network, the weights should be adjusted [65]. This is a very important operation during training of the neural network, the weights between each of the individual neurons are adjusted until a desired output is achieved.

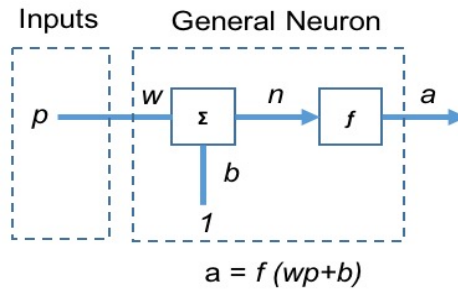


Figure 2.10 Single-input neuron

A single-input neuron is shown in Figure 2.10 where the scalar input, p , is multiplied by the scalar weight, w , to form wp . Next, where it is summed together with an input that is multiplied by a bias b . The net input, n , goes into a transfer function, f , which will therefore produce a scalar neuron output a . Both w and b are adjustable scalar parameters of the neurons [66]. Typically, the transfer function is chosen by the designer of the ANN and both parameters can be adjusted to some training rules so that the neuron input and output relationship can meet specific goals.

2.10.3 Transfer Functions

The transfer function acts as an entity to transform the output range between -1 to 1 or 0 to 1 as shown in Figure 2.11.

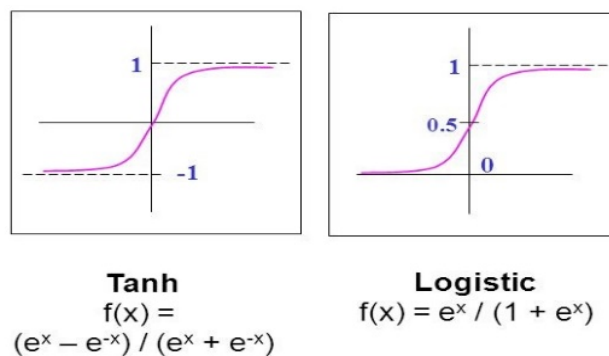


Figure 2.11 Types of transfer functions [67]

Hyperbolic tangent transfer function in terms of ANN is mathematically equivalent to \tanh (n). The results will usually have very small numerical differences. This function is a good tradeoff for ANN where speed is more important than the exact shape of the transfer function [67].

The log-sigmoid transfer function is a transfer function that takes the input. This will usually range in any value between plus and minus infinity, and compress the output into the range from 0 – 1. Because this function is differentiable, the log-sigmoid transfer function is commonly used in multilayer networks that are trained using the backpropagation algorithm.

2.10.4 Artificial Neural Network Processing Units

There are multiple smaller and simple processing units in an ANN for the iteration purpose, they are connected to each other through weighted connections as they send signals to each other through these connections. Each small unit performs a relatively simple task which involves receiving some inputs from the neighborhood or some outward source and transferring the computation of some output signal to the other units of the ANN. After the actual task of processing starts, the weights are adjusted according to the information and data. ANN are parallel in nature as many smaller units of network can perform processing simultaneously and contain three main types of units:

- i. Input units responsible for receiving the data from outside of the network.
- ii. Output units which are the end points of the network.
- iii. Hidden units which contain input and output signal during the processing of ANN and these units can be changed during the processing of network.

2.10.5 Network Architectures

In a typical ANN, one neuron with many inputs might not be sufficient. More neurons operating in parallel are required and this is known as the “layer”.

A single layer with a network of L neurons is shown in Figure 2.12. Each of the input is connected to each of the neurons and that the weight matrix has L rows. The layer includes the weight matrix, the summers, the bias vector b , the transfer function boxes and the output vector a . Each element of the input vector p is connected to each individual neuron through the weight

matrix W . Each neuron has a summer, bias, a transfer function and an output. Output vector, a , is formed when all the above comes together [68].

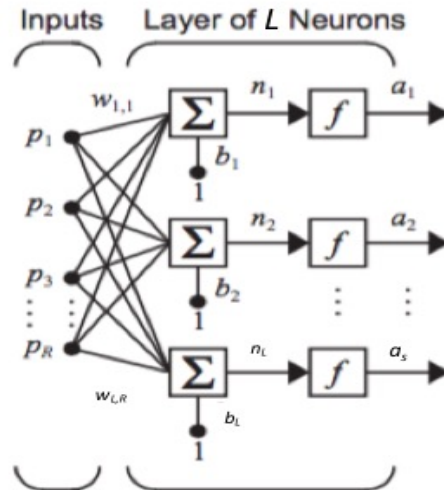


Figure 2.12 Layers of L neurons [68]

The number of inputs to a layer is usually different from the number of neurons where P is not equal to L . All neurons in the layers need not have to use the same transfer function.

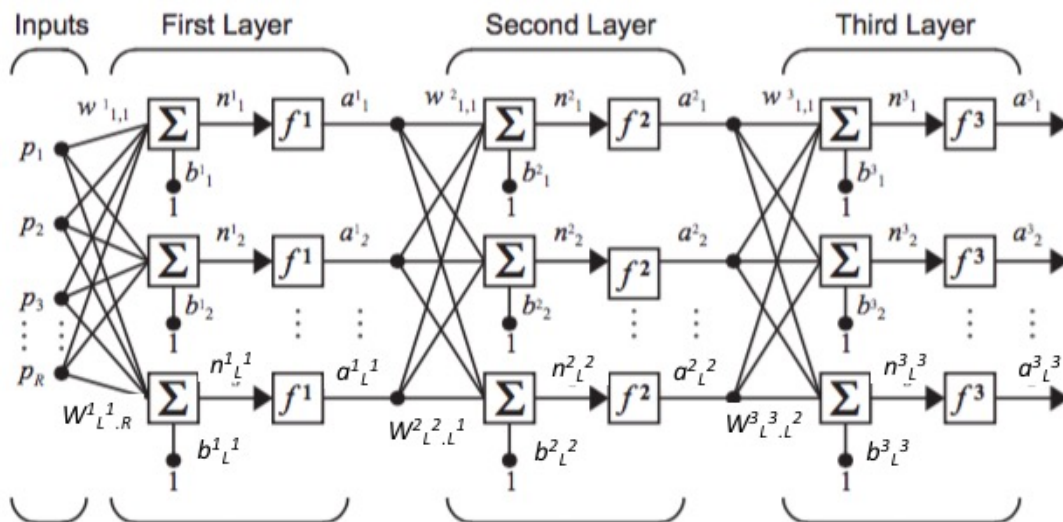


Figure 2.13 Three-layer network [68]

Apart from a single layer of neurons, there are multiple layers of neurons too. This is a network that comprises of several layers where each layer will have its own weight matrix w , its own bias b , a net input vector, n , and an output vector a . Additional notation will be used to distinguish between these layers as shown in figure 2.13. The three-layer network shows L^1 neurons in the first layer and L^2 neurons in the second layer. Note that different layers will have different numbers of neurons as discussed above. A layer whose output is the network output is known as the output layer and the other layers are known as the hidden layers.

Multi-layers are usually more powerful than single layer networks. An example is the use of a two-layer network having a sigmoid first layer and a linear second layer can be trained to approximate most functions arbitrarily well. This can only be done with a multi-layer network.

2.10.6 Artificial Neural Network Training

An ANN is to be designed and developed in a way to ensure the conversion of input data into desired output data by using either some relaxation method or some direct method. There are many different methods which can be applied to enhance the strength of ANN connections. The weights can be set in an explicit way by feeding learning rule for the training which can adjust the weights of the network based on this learning rule. Solutions based on learning rules can be divided into following categories:

Unsupervised Learning

This is the type of learning in which output units are designed to identify pattern clusters in input data. There is no output sample data available in this type and only input data values are available. These systems are supposed to discover important statistics patterns in the input data available. Also, there is no cluster-related information available in this type as compared to supervised learning, and the system has to decide itself about the clusters. Many different learning rules in both unsupervised and supervised learning methods represent variants of the Hebbian Learning Method [69].

Supervised Learning

This is the type of learning in which both input and output data are available for the training of the ANN. This data can be either provided by some external source or by the network itself [70].

Reinforcement Learning

As compared to other two types of learning, reinforcement learning performs some actions on the environment of the system and then gets some feedback. After getting some response, the system grades this feedback based on environment conditions as good or as bad feedback and then adjusts its parameters on the basis of this feedback. This parameter adjustment process is repeated many times until some constant state is achieved and there remains no need for further adjustments of parameters [71].

2.11 Summary

The progress for heat transfer has been driven by the need to understand the performance of a thermal system which requires the application of fundamental laws (mass, momentum and energy conservation) for heat transfer problems. These problems are usually augmented with complex parameters such as the geometry, velocity of wind flow and the construction of the heat transfer mechanism [72].

This research will spearhead a paradigm shift on the present research area of TEG, which has predominantly focused on increasing the ZT value through the discovery of new materials. The ANN model has been developed to better predict a TEG performance over a wide range of operating conditions, which includes surrounding environmental operating conditions such as ambient temperature, wind velocity, density of air, kinematic viscosity of air, as well as the design and material use for the construction of the TEG. This is particularly useful in the case of complex flow situation occurring in day-to-day TEG applications. It allows researchers to increase their knowledge of and insights on fundamental phenomena.

Chapter 3 Research Methodology for Novel Thermoelectric Performance Model

3.1 Thermal Modeling of Thermoelectric Generator

The estimation of the output voltage generated by a TEG is based on the surface temperature measured on the two substrates that sandwich the thermocouple. The output voltage generated will be dictated by the temperature gradient across the TEG, as referenced to the voltage-temperature graphs stated in the manufacturer’s technical sheet provided. The set of values reported on the manufacturer technical sheet in the form of a graph is usually obtained in a laboratory environment, with little or no interference from the surrounding environment that the TEG is operating. This will usually provide the user with an inaccurate output voltage generated by the TEG.

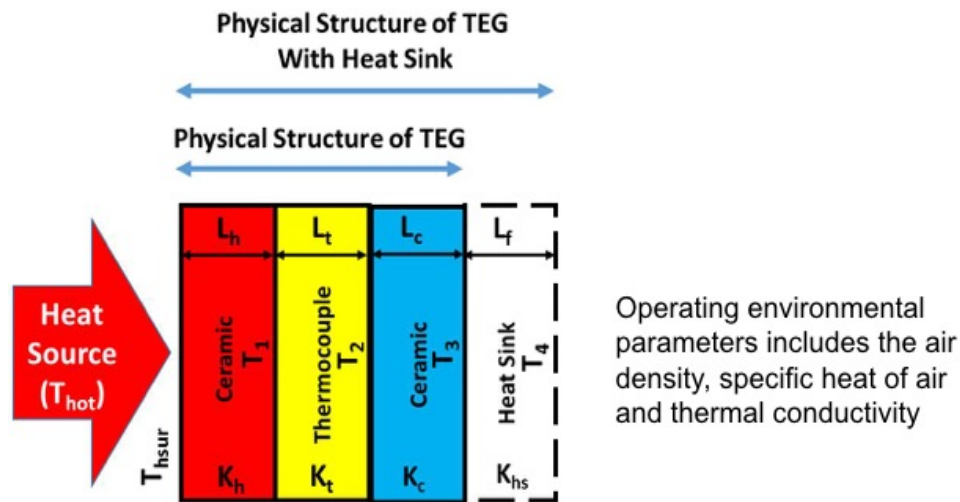


Figure 3.1 Schematic division of the physical structure of a TEG

In this model, a finite volume method for solving the three-dimensional heat transfer equation will be used. This will allow better prediction with an understanding on the distribution of the surface temperature on the TEG substrates, It also takes into account the properties of air,

as well as those of the TEG materials through the physics that govern the behavior of the TEG using heat transfer principles and influences caused by various parameters of the TEG. The TEG used in this research will be segregated into various regions as shown in Figure 3.1, where the thickness of the various layer, thermal conductivity of the material used and areas are defined by L , K and A respectively. They play a role in the temperature gradient across the TEG which will correlate to the output voltage generated by the TEG. A simple schematic in Figure 3.2 is used to represent the different modes.

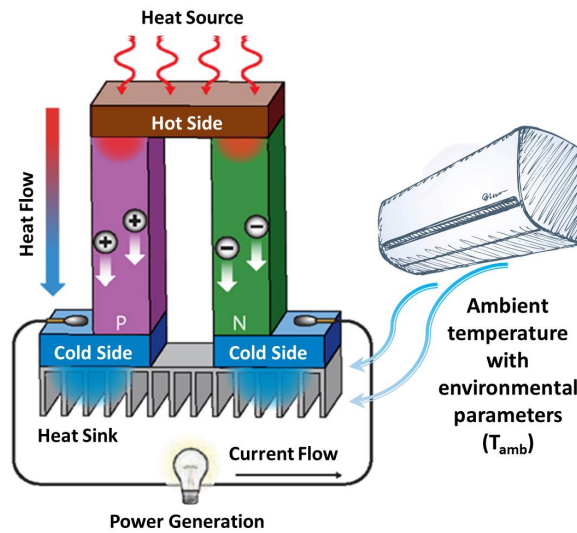


Figure 3.2 Various modes of heat transfer across the thermoelectric power generator

The thermal conductivity of the substrates that sandwich the thermocouple and also that of the thermocouple will be taken into consideration through conduction which forms the basis for many other numerical analyses. As a diffusion mechanism, this transfer of heat energy through conduction can be explained by using a gas that occupy the space between two surfaces that are maintained at a different temperature as shown in Figure 3.3. This is where the temperature at any point of the TEG substrate can be associated with the energy of gas molecules in proximity to the point.

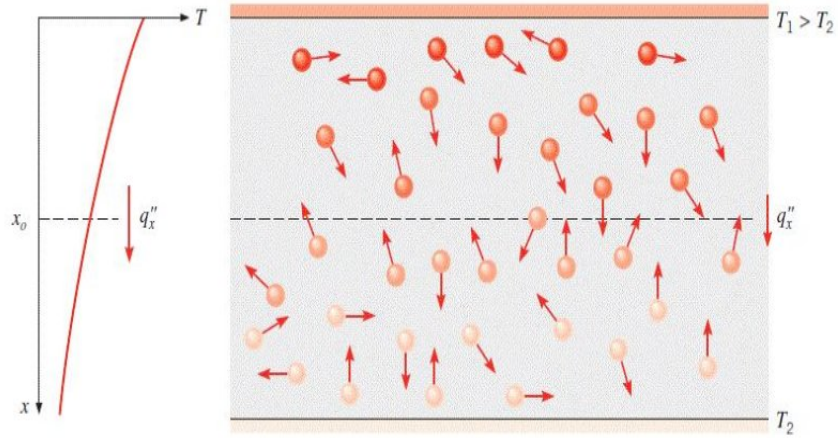


Figure 3.3 Conduction heat transfer with diffusion of energy due to molecular activity. [73]

This energy is created through the random translational motion, internal and rotational vibrational movement of the molecules within the material used for the TEG. The higher the temperature on the TEG substrate surface, the higher molecular energies will be. This will increase with the constant colliding of molecules within confine space. Heat energy will always flow from the hot side ceramic substrate surface to the cold side ceramic substrate surface or the heat sink attached as shown in Figure 3.4.

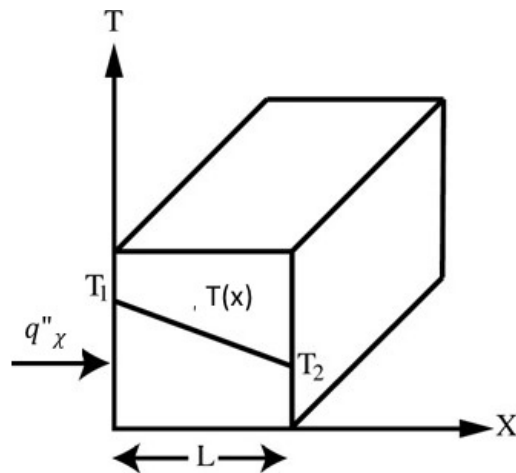


Figure 3.4 Heat transfer by conduction across material

The cooling of the TEG will also be attributed to air flowing at cold side of the TEG through convection. It is the transfer of energy due to random molecular motion, where heat energy is also transferred through the motion of the fluid in the surrounding environment. In the context of this research, is known as wind velocity. This is because the wind velocity, which comprises of many molecules, will move as aggregates. Such movement of the wind velocity contributes to the transfer of heat distribution on the surface of the ceramic substrate. Therefore, the total heat transfer can be described as the superposition of energy transported by the random motion of molecules and by the bulk motion of the wind velocity.

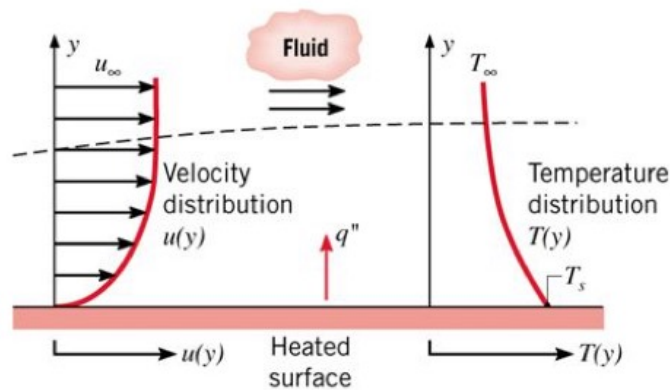


Figure 3.5 Boundary layer development in convection heat transfer [73]

Figure 3.5 shows the wind velocity over the heated surface of the TEG ceramic substrate. There is a development in a region within the wind through which the velocity varies from zero at the surface to a finite value, u_{∞} , associated with a flow. This region is known as the boundary layer velocity profile.

Convection can be classified according to the nature of the flow. When the flow is caused by an external means such as a mechanical fan or a pump, it is known as forced convection. On the other hand, in natural convection, the force is induced by natural buoyancy forces. This is caused by the difference in surrounding environmental parameters. In this research, a natural convection scenario will be adopted for all experiments and analysis.

The magnitude of convective heat transfer is influenced by wind velocity flowing past both the hot and cold ceramic substrate. Higher wind velocity will therefore increase convective heat

transfer on the TEG. The convective heat transfer can also be improved by expanding the surface area of the ceramic substrate on both the hot and cold side of the TEG.

The equation for the heat transfer process, regardless of being natural or forced convection, is stated as,

$$q'' = h(T_s - T_\infty) \quad (3.1)$$

where q'' , the convective heat flux measured in W/m^2 , is proportional to the difference between the surface temperature T_s and the fluid temperatures T_∞ . This expression is known as Newton's law of cooling, and the proportionality constant h is known as the convection heat transfer coefficient, a parameter that is being considered as one of the essential ones required when choosing the material for a heat exchanger [74].

Temperature gradients measured across the thermocouple with conduction and convection in this manner can be related to a more realistic output voltage as compared to those which are measured in a vacuumed laboratory environment.

To increase the temperature gradient across the TEG, a metal heat sink can be attached onto the TEG ceramic substrate surface on the cold side to help with the dissipation of heat from the hot side ceramic substrate. This increment in the temperature gradient across the TEG will be translated proportionally to an increase in the output voltage, based on the graphs provided in the manufacturer's specifications sheet. In addition to those mentioned previously, the parameters that determine the output voltage in this scenario with the heat sink attached are the thermal conductivity of the heat sink, its geometrical arrangement, as well as the air flow characteristics across the metal heat sink used.

3.1.1 Limitations on Mathematical Model

Mathematical models are not reality. The real world is often much more complex than a set of mathematical models and so that is the limitation. This mathematical model encompassing various surrounding environmental parameters does have its own fair share of limitations when predicting the distribution of the surface temperature using finite element method. Although majority of the

surrounding environmental parameters, wind velocity, the viscosity, density, specific heat, thermal conductivity and prandtl number of air at various ambient temperature are factored in the mathematical model to derive the output voltage from the TEG but due to the lack of some available data, it will be difficult to build a complete model. However, this mathematical model can reasonably predict the behavior of the TEG surface temperature and is able to help validate the results obtained from the physical processes.

3.2 Heat Transfer Equation

This section will discuss the development of the numerical method based on finite volume by considering the simplest transport process of pure diffusion in the steady state. The steady-state heat transfer equation, with heat sources for both scenarios, with and without a heatsink, in a three-dimensional (3D) situation is given by

$$\nabla(k\nabla T) + S = 0 \quad (3.2)$$

The control volume integration, is one of the important steps for finite volume method that distinguishes it apart from the rest of the computational fluid dynamic (CFD) techniques. This is as shown in (3.3) over computational volume V with the use of Gauss' theorem,

$$\int (\nabla(k\nabla T) + S) dV = \int \hat{n} \cdot (k\nabla T) dA + \int S dV = 0 \quad (3.3)$$

where \hat{n} denotes the outward-pointing unit normal of the boundary and the respective integral is over the area surrounding V .

All finite volume methods start from this integral form of the heat equation and this equation will be applied to this research. The discussion of the three-dimensional (3D) heat transfer case [75] will be discussed in the following chapter.

3.2.1 Finite Volume Method for Three-Dimensional Diffusion Case

This section will discuss the finite volume method for 3D diffusion case with a three-dimensional

grid used to subdivide the domain. Figure 3.6 is an example of the control volume of the TEG ceramic substrate on both the hot and cold side and the thermocouple.

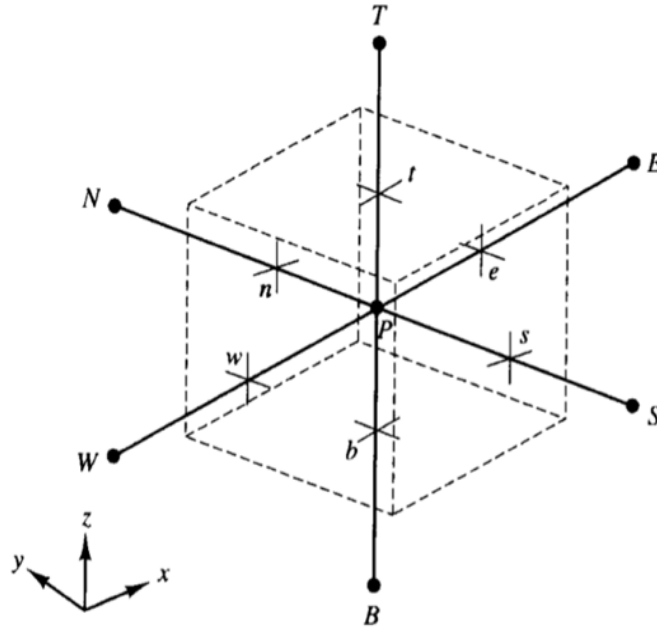


Figure 3.6 A cell in three dimensions and neighboring nodes [73]

The three dimensional (3D) steady-state heat transfer Equation is,

$$\frac{\partial}{\partial x} \left(k \frac{\partial T}{\partial x} \right) + \frac{\partial}{\partial y} \left(k \frac{\partial T}{\partial y} \right) + \frac{\partial}{\partial z} \left(k \frac{\partial T}{\partial z} \right) + S = 0 \quad (3.4)$$

where T is the temperature, k the thermal conductivity, and S the rate of temperature changes due to heat sources with and without the use of heat sinks. All quantities are in general functions of location inside the material, e.g. $k=k(x, y, z)$.

The material volume is discretized in several smaller control volumes (of volume $\Delta V = \Delta x \Delta y \Delta z$), as shown in Figure 3.6. A general nodal point P is accompanied by the six neighbouring nodal points identified as W, E, S, N, B and T where they are west, east, south, north, bottom and top respectively. The respective cell faces of the control volume are referred by the corresponding lowercase letters 'w', 'e', 's', 'n', 'b', and 't' and have area that is denoted likewise, i.e. the area of the

east face is A_e .

Integration of (3.4) over the control volume along the same lines gives,

$$\left[K_e A_e \left(\frac{\partial T}{\partial x} \right)_e - K_w A_w \left(\frac{\partial T}{\partial x} \right)_w \right] + \left[K_n A_n \left(\frac{\partial T}{\partial y} \right)_n - K_s A_s \left(\frac{\partial T}{\partial y} \right)_s \right] + \left[K_t A_t \left(\frac{\partial T}{\partial z} \right)_t - K_b A_b \left(\frac{\partial T}{\partial z} \right)_b \right] + \bar{S} \Delta V = 0 \quad (3.5)$$

the discretized form of (3.5) is obtained:

$$\left[K_e \frac{(\phi_E - \phi_P) A_e}{\delta x_{PE}} - K_w \frac{(\phi_P - \phi_W) A_w}{\delta x_{WP}} \right] + \left[K_n \frac{(\phi_N - \phi_P) A_n}{\delta y_{PN}} - K_s \frac{(\phi_P - \phi_S) A_s}{\delta y_{SP}} \right] + \left[K_t \frac{(\phi_T - \phi_P) A_t}{\delta z_{PT}} - K_b \frac{(\phi_P - \phi_B) A_b}{\delta z_{BP}} \right] + (S_U + S_p \phi_P) = 0 \quad (3.6)$$

forwarding difference operators for the derivatives and the linear interpolation for the thermal conductivities. Following that, the collecting terms with the same temperature will arrive at the following end point arrived at:

$$a_P T_P = a_W T_W + a_E T_E + a_S T_S + a_N T_N + a_B T_B + a_T T_T + S_U \quad (3.7)$$

where

$$a_W = \frac{K_w A_w}{\delta x_{PW}} \text{ and } a_E = \frac{K_e A_e}{\delta x_{PE}},$$

$$a_S = \frac{K_s A_s}{\delta y_{SP}} \text{ and } a_N = \frac{K_n A_n}{\delta y_{PN}},$$

$$a_B = \frac{K_b A_b}{\delta z_{BP}} \text{ and } a_T = \frac{K_t A_t}{\delta z_{PT}},$$

and

$$a_P = a_W + a_E + a_S + a_N + a_B + a_T - S_p.$$

The source function of point P is again linearized as $\bar{S} \Delta V = S_U + S_p T_P$, and this is used in the boundary conditions, fixed-temperature or fixed-flux. Note that the temperature of each point is related to the temperature of the six nearest neighboring points to it.

3.2.2 Numerical Implementations Without Heat Sink

In the numerical solution of the heat transfer equation in a TEG, assumptions have been made for some of the parameters. Assuming that the ceramic plates are both square with the same length, L , and width, W , together with corresponding area, A , and a width along the z -axis, w , the PN thermocouple region extends to the same area and has a width w_{PN} .

The whole TEG system has a volume of $A(2w+w_{PN})$ and it has three regions of different thermal conductivities. To discretize it, the number of nodal points is chosen along the x -axis, n_x , and along the z -axis, n_z . The number of points in y -axis is equal to those in x -axis, $n_y=n_x$.

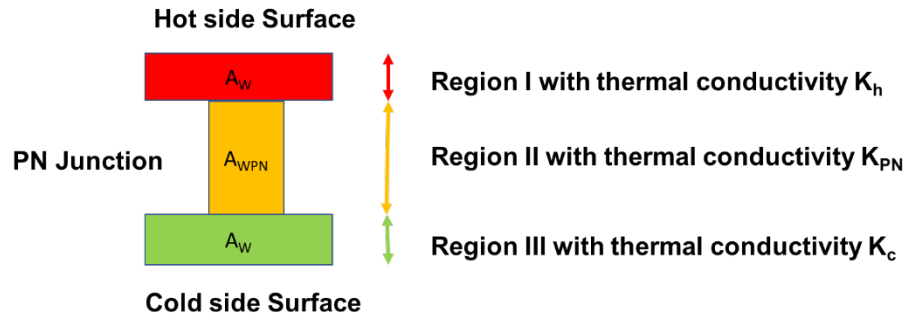


Figure 3.7 Segmentation of TEG

The three regions shown in Figure 3.7 are as described below:

- i. Region I: This is the hot side ceramic substrate, with volume A_w and thermal conductivity K_h , that is discretized by $(n_x) \times (n_y) \times (n_{z1})$ points where n_{z1} is proportional to $w/(2w+w_{PN})$.
- ii. Region II: This is the middle PN region, with volume A_{wPN} and thermal conductivity K_{PN} , that is discretized by $(n_x) \times (n_y) \times (n_{z2})$ points, where $n_{z2}=n_z-2n_{z1}$.
- iii. Region III: This is the cold side ceramic substrate, with volume A_w and thermal conductivity K_c , that is discretized by $(n_x) \times (n_y) \times (n_{z1})$ points as in Region I.

3.2.3 Boundary conditions

The main difference between the three regions, besides the volume they occupy, is their thermal conductivity, which in total is given by

$$K = \begin{cases} K_h, 0 \leq z < w \\ K_{PN}, w < z < w + w_{PN} \\ K_c, w + w_{PN} < z \leq H \end{cases} \quad (3.8)$$

and in transition regions (such as $z=w$) the harmonic mean is taken. The hot side surface is held at constant temperature

$$T(x, y, z = 0) = T_h \quad (3.9)$$

where the lateral edges are insulated. No flux enters or leaves from there, as shown,

$$q(x = 0, y, z) = q(x = L, y, z) = q(x, y = 0, z) = q(x, y = L, z) = 0 \quad (3.10)$$

As the ceramic substrate surface on the cold side cools convectively using wind velocity from the operating environment of the TEG, the heat flux leaving the plate is,

$$q(x, y, z = H) = h_c(T(x, y, z = H) - T_c) \quad (3.11)$$

given that the heat transfer coefficient for two-dimensional is an incompressible, laminar flow over a flat wall. This is shown as [76]

$$h_c = 0.664Rn^{1/2}Pr^{1/3}\frac{K_{air}}{L} \quad (3.12)$$

where Rn , Pr , K_{air} are the Reynolds number, Prandtl number and thermal conductivity of air respectively. For the case of turbulent flow the heat transfer coefficient can be given by [77]

$$h_{cT} = 0.930Rn^{-1/2}Pr^{-2/3}C_{p,air}\rho_{air}U_w \quad (3.13)$$

where $C_{p,air}$, ρ_{air} , U_w are the specific heat, density and velocity of air flowing below the bottom plate.

All air properties such as density, thermal conductivity, specific heat and Prandtl number are spline-interpolated to the desired temperature T_c [78].

3.2.4 Initial Conditions

The initial surface temperature of the TEG is commonly taken as an average constant value across both the hot and cold surface of the TEG,

$$T(x, y, z) = \frac{T_h + T_c}{2} \quad (3.14)$$

By putting all these together and writing (3.7) for all the (nx)x(ny)x(nz) points in the volume, a linear system for the unknown temperatures at those points will be formulated.

This system of equations will be solved iteratively using the TriDiagonal Matrix Algorithm (*TDMA*) method for the solution of tridiagonal systems. This will be discussed in Section 3.4. The iterative solution will be useful to help solve large number of equations which is beyond the means of direct method such as Gaussian elimination. It will solve the equation semi-implicitly, where the values at each iteration, which are not yet known, will be used in order to proceed. Convergence of the solution is obtained when the average difference in temperature between iterations over the average temperature in the previous iteration is too small, typically 10^{-5} , or when a maximum number of iterations is reached, typically a few thousand.

Therefore, the mean temperature difference between the TEG surface on both the cold and hot side is shown in (3.15) below,

$$\Delta T_1 = \text{mean}(T(x, y, z = 0) - T(x, y, z = H)) \quad (3.15)$$

The mean temperature difference between the opposite side of the TEG surface on both the cold and hot side is as shown in (3.16) below,

$$\Delta T_2 = \text{mean}(T(x, y, z = w) - T(x, y, z = w + w_{PN})) \quad (3.16)$$

3.3 Modeling of Heat Sink

Heat sinks are the most common thermal management hardware, used to enhance heat transfer through its extended surface, commonly known as fins. This happens because of the entrainment of air with increasing height and a high velocity of impingement [79]. This theory has been proven to be cost effective too by Maveety and Jung [80] whom in their research concluded that beyond a particular height of fin, gain in heat transfer is offset by material and manufacturing costs.

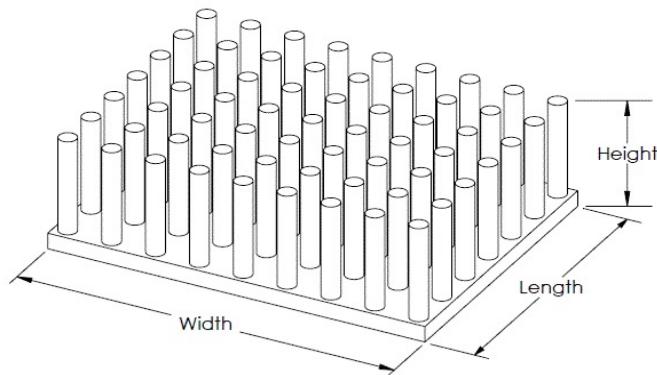


Figure 3.8 Geometric arrangement of a heat sink

In this research, the function of the heat sink will be used to assist in the removal of heat from the TEG surface on the cold side to create a larger temperature gradient across the thermoelement. This is equivalent to a larger output voltage generated by the TEG module.

The heat sink used in this research consists of two regions, the base and the fins. The base is assumed to adopt the same dimensions as the ceramic plates of the TEG and height H_b . The fins are assumed cylindrical in shape with diameter D and height H_f , and made from the same material as the base. The total height of the heat sink is $H_{hs}=H_b + H_f$. Their geometric arrangement is that of an array as is shown Figure 3.8, with N_x fins per dimension and $N = N_x^2$ fins in total. Khan et

al [81] carried out a series of analytical work to identify the impact of surrounding fluid friction on the heat profile of the semiconductor and relating this to the performance of the TEG.

Each fin will remove heat from its lateral surface which has an area of

$$A_f = \pi D H_f \quad (3.17)$$

while its top surface is assumed insulated. Similarly, the base area removes heat from the surface not occupied by the fins, that has an area

$$A_b = A - N \frac{\pi D^2}{4} \quad (3.18)$$

The heat sink cools the TEG by allowing cold air to flow through it at a constant velocity U_w . As air passes through the fins. It gets compressed due to the smaller cross section that it encounters and thus its approaching velocity is higher than U_w . This is given by

$$U_{app} = \frac{U_w L H_{hs}}{(L - N_x D) H_f} \quad (3.19)$$

It can be derived from mass continuity equation. This is further modulated by the geometrical arrangement of the fins, and becomes

$$U_{max} = \max\left(\frac{S_l}{S_l - 1}, \frac{S_d}{S_d - 1}\right) U_{app} \quad (3.20)$$

Here S_l is the distance between the center of two consecutive fins also known as pin spacing as shown in Figure 3.7, is normalized to their diameter,

$$S_l = \frac{L/(N_x - 1)}{D} \quad (3.21)$$

This parameter is assumed to be the same in both horizontal directions, and then the respective

dimensionless diagonal is

$$S_d = \sqrt{S_l^2 + (S_l/2)^2} \quad (3.22)$$

The maximum velocity of (3.20) is used in the computation of the Reynolds number of the air flow as

$$Rn = \frac{U_{max}D}{\nu_{air}} \quad (3.23)$$

with ν_{air} defined as its kinematic viscosity. That is interpolated from the properties of air [82]. Together with Prandtl number of the flow, they determine the mean heat transfer coefficients for the fins h_f and for the base h_b as

$$h_{f/b} = C_{f/b} Rn^{1/2} Pr^{1/3} \frac{K_{air}}{D} \quad (3.24)$$

The constants, C , are given by the empirical relations

$$C_f = (0.2 + e^{-0.55S_l})S_l^{1/2} \quad (3.25)$$

for the fins, and

$$C_b = 0.75 \left(\frac{S_l - 1}{N_x S_l^2} \right)^{1/2} \quad (3.26)$$

for the base. The thermal resistance of each fin is

$$R_f = \frac{1}{\eta h_f A_f} \quad (3.27)$$

where the efficiency of the fins is given by

$$\eta = \frac{\tanh(\mu H_f)}{\mu H_f} \quad (3.28)$$

where

$$\mu = \sqrt{\frac{4h_f}{k_b D}}. \quad (3.29)$$

Next, the thermal resistance of the heat sink base is similarly

$$R_b = \frac{1}{h_b A_b}, \quad (3.30)$$

and thus the total resistance of the entire heat sink, taking into considerations the fins plus base system is

$$R = \left(\frac{N}{R_f} + \frac{1}{R_b} \right)^{-1} \quad (3.31)$$

Using the total resistance, the average heat sink thermal conductivity is as shown below

$$K_f = \frac{H_f}{RA}. \quad (3.32)$$

3.3.1 Numerical Implementation with Heat Sink

The TEG with heat sink is divided in regions of different volume and different thermal conductivity. There will be a few more regions to add on to what was indicated in Section 3.2.2 above in the scenario with the heat sink.

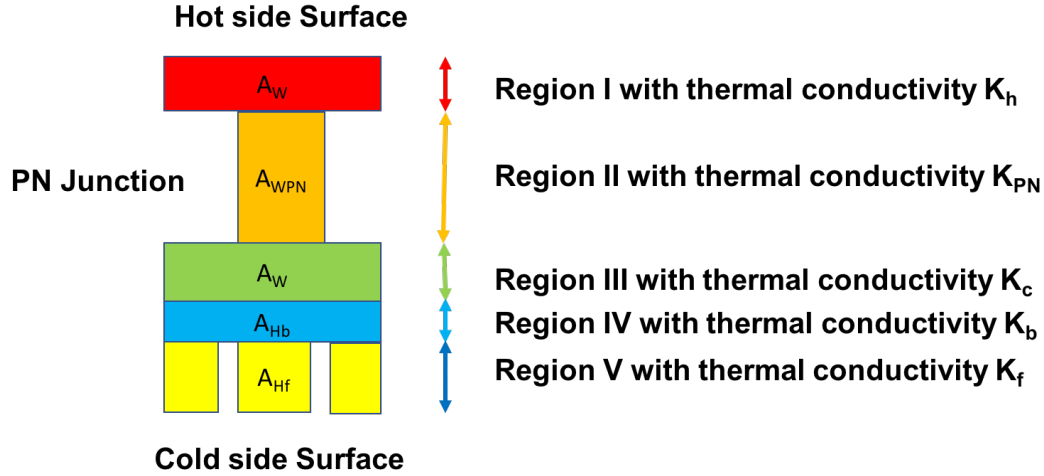


Figure 3.9 Segmentation of TEG with Heat Sink

They are:

- iv. Region IV: This is the base of the heat sink, with volume AH_b and thermal conductivity K_b , that is discretized by $(nx) \times (ny) \times (nz_3)$ points, where nz_3 is proportional to H_b/H_{hs} .
- v. Region V: This is the fins, with volume AH_f and thermal conductivity K_f , that is discretized by $(nx) \times (ny) \times (nz_{hs} - nz_3)$ points.

Since the length of the heat sink can be comparable to, or even larger than the length of the whole TEG, there is the option for the grid spacing along z -axis to be finer in regions iv and v. The thermal conductivity is in total,

$$K = \left\{ \begin{array}{l} K_h, 0 \leq z < w \\ K_{PN}, w < z < w + w_{PN} \\ K_C, w + w_{PN} < z < H \\ K_b, H < z < H + H_b \\ K_f, H + H_b < z \leq H + H_{hs} \end{array} \right\}. \quad (3.33)$$

and in transition regions (such as $z=w$) the harmonic mean is taken. Boundary conditions used were the same as in the scenario without the heat sink, except that from the bottom boundary which now corresponds to the insulated tips of the fins, thus it is seen as

$$(x, y, z = H + H_{hs}) = 0 \quad (3.34)$$

$$q(x, y, z = H + H_{hs}) = 0 \quad (3.35)$$

the same relation that replaces (3.11).

The resulting $(nx)(ny)(nz+nz_{hs})$ equations are solved as in the no-sink case. The outputs in this case is the mean temperature difference between the bottom of the top ceramic plate and the top of the bottom ceramic plate,

$$\Delta T_3 = \text{mean}(T(x, y, z = w) - T(x, y, z = w + w_{PN})), \quad (3.36)$$

This is different than ΔT_2 , although given by the same relation, since the heat sink removes more heat from the system.

3.4 Tri Diagonal Matrix Method

In solving the heat equation to derive the surface temperature on the ceramic substrate of the TEG, a large linear system of equation is formed. The complexity and size of the set of equations depend on the dimensionality of the problem, the number of grid nodes and the discretization practice. A robust method for the solution of such a system is by using the TDMA, also known as Thomas algorithm. The TDMA is a direct method for one dimensional situations but can be applied iteratively in a line by line fashion to solve multi-dimensional problem.

This algorithm is designed to solve the linear system of N equations

$$A_i X_{i-1} + B_i X_i + C_i X_{i+1} = D_i, i = 1, \dots, N, \quad (3.37)$$

for the vector X given the vectors A, B, C, D , and the consistency constraint

$$A_1 = 0, C_N = 0 \quad (3.38)$$

The algorithm solves the system by first performing Gaussian elimination and then backward substitution [83]. The Thomas algorithm is exact for systems obtained from 1D heat equations

since the one-dimensional analog of (3.7) (with $a_S=a_N=a_B=a_T=0$) is a tridiagonal system of the exact form of (3.37). It can however be applied in a line-by-line fashion to systems obtained from 2D and 3D heat equations as show below.

Consider the 2D case shown in Figure 3.8. The corresponding two-dimensional discretized heat Equation is obtained from (3.6) by setting $a_B=a_T=0$, and can be rewritten as

$$-a_S T_S + a_P T_P - a_N T_N = a_W T_W + a_E T_E + S_U \quad (3.39)$$

The right-hand side of (3.39) is assumed to be temporally known, and in the form required by the Thomas algorithm. Thus, it can be utilized to obtain a temporary solution along north-south lines (in the direction of y axis), as shown in Figure 3.8. This is then repeated for all other lines of the plane until an overall temporary solution is obtained. The same procedure is iterated many times, in the order of a few thousands, until the temporary solution does not change anymore and this is then taken as the solution of the system.

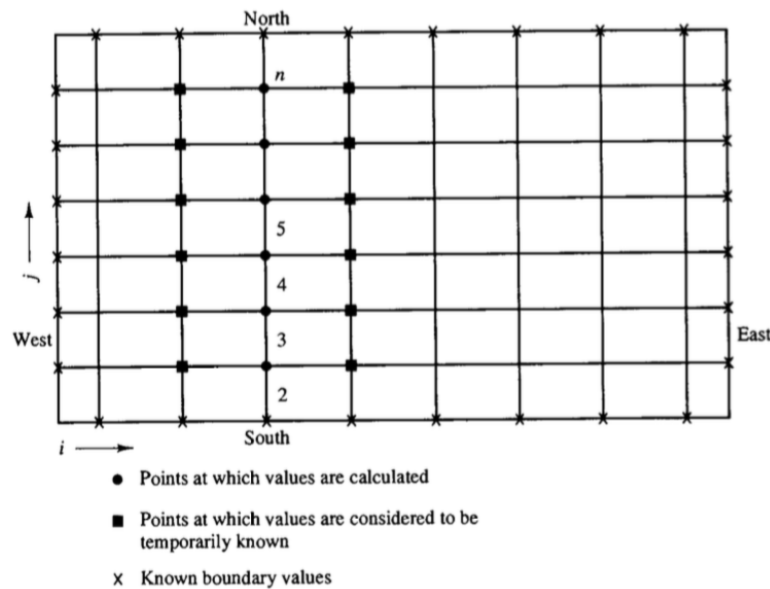


Figure 3.10 Line by line application of the TDMA method [83]

In the 3D scenario, the line-by-line solution is done for each plane separately until the whole volume is scanned plane-by-plane. This way, a temporary solution is obtained and will be iterated until a converged solution is produced.

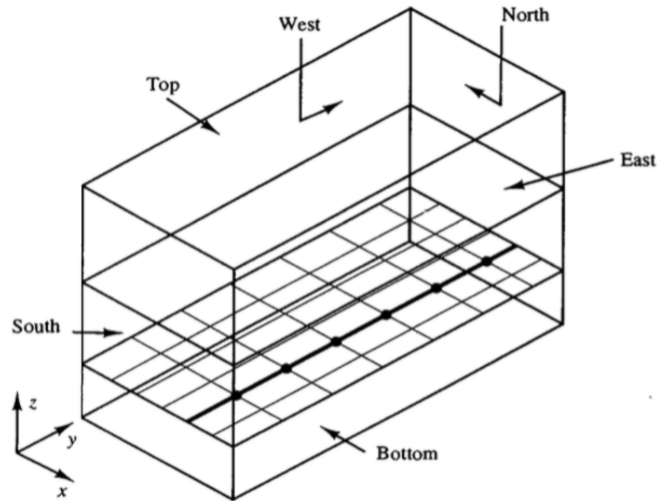


Figure 3.11 TDMA method in a 3D volume of TEG [83]

The line by line application of the TDMA method used will therefore provide users with an accurate surface temperature on the ceramic substrates of the TEG, factoring in the environmental parameters. This will eventually generate a temperature gradient across the TEG. These data collected will be collated into an Excel spreadsheet that will be used as inputs to train the ANN model.

3.5 Summary

Conventionally, deriving of the output voltage from a TEG for the manufacturer specification sheet has always been done in a simplified way, whereby the outputs derived are often obtained from a laboratory environment where all the environmental factors are being omitted. This often results in a variation from the actual output voltages generated by a TEG in its operating environment.

In this chapter, the method of obtaining the output voltage of the TEG obtained together with the interaction of its operating environmental parameter is explained in detail. The physics involved in the calculating of heat transfer across the TEG together with environmental parameters has increased the complexity of calculating the output voltage generated by the TEG and using finite volume method for 3D diffusion, to have the subdivided domain of the TEG structure thereafter using the TDMA. This is to solve the equation iteratively, in a line by line fashion.

Chapter 4 Research Methodology for Artificial Neural Network Model

4.1 Artificial Neural Network Model

This ANN model is aimed at developing an accurate model for predicting the output voltage generated by the TEG in its operating environment. This will allow the understanding of how these environmental parameters will affect the energy generation of the TEG as ANN models are very useful to problems that depend on many physical phenomena [84].

The accuracy on the predicted values of the output voltage from the ANN can be verified from both the calculated and measured values from mathematical model as well as actual experimental setup respectively as shown in Figure 4.1. As there are a range of input parameters and the fact that the inputs are a range of unpredictable values adopted from the surrounding environmental parameters of the TEG and the dimensions of the TEG, the ANN, with its ability to generalized, will be a better option for this research. This means that after training, the ANN could classify data from the same class as the learning data that it has never seen before.

This model can be applied to a wide range of applications in various sectors. Applications such as energy generator using thermoelectric windows, wall mount heater, automobile exhaust and even for space exploration mission as discussed in section 2.5. Therefore, from the range of application that is operating across a wide range of temperature under different circumstances, it is eminent that the dataset generated should also be able to cover the wide range of parameters for the training of the ANN.

Given the space and environmental constraints that this research is facing, the setup of the apparatus shown in Figure 5.1, the measurement of actual output voltages generated from the TEG can only be done in just one environment, which is the office environment. Hence the need of a robust mathematical model to anticipate the output voltages generated by the TEG in various operating environment is required for the training of the ANN in this research.

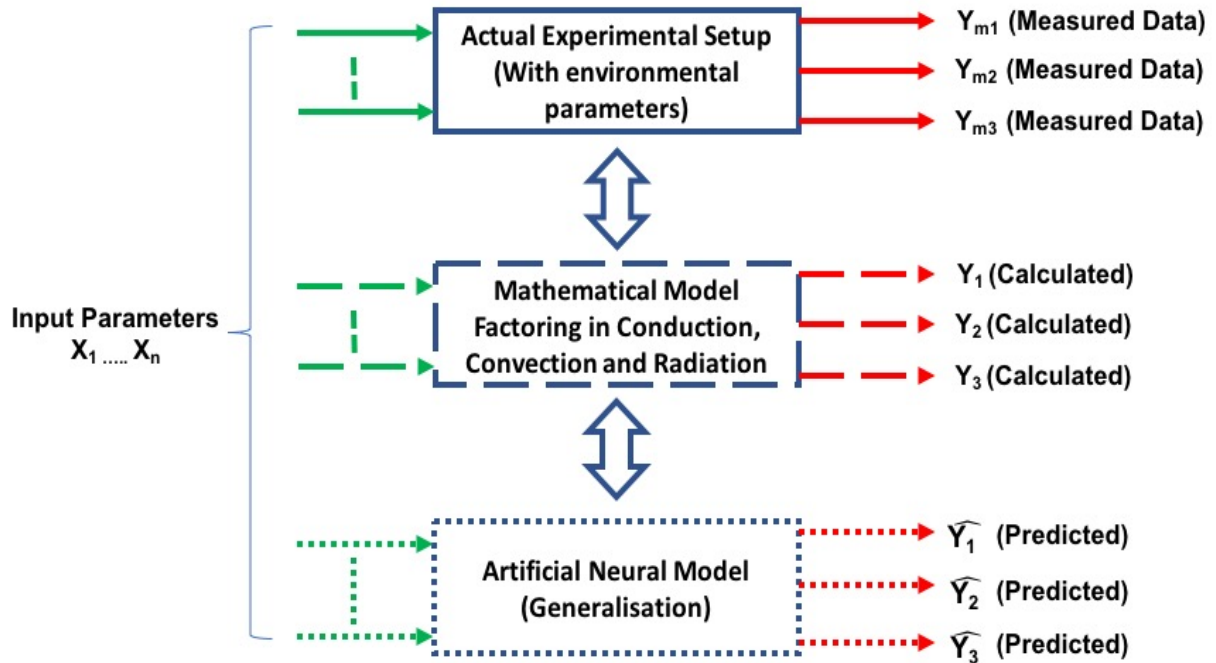


Figure 4.1 Generalization of artificial neural network

One of the key elements of a neural network is its ability to learn. It is not just a complex system but it is a complex adaptive system, meaning to say that it can change its internal structure based on the information flowing through it, by reading the input, process it and generate an output value. Network made up of many neurons can exhibit incredibly rich and intelligent behaviors. This is much more superior to the conventional mathematical model that was derived through physics on heat transfer although it too can derive accurate results but may lack the adaptively of an ANN.

In this model, we will be using a range of datasets generated from the mathematical model and leveraging on this set of data to train the ANN. The range of datasets will also have to be realistic in order to reduce the training time required by the ANN. As this model is meant to be used in an environment with natural ventilation, the wind velocity of the surrounding environment will not exceed 5m/s, assuming that the environment is exposed to gentle breeze according to the beaufort scale [85] and ambient temperature to be kept within the range of 293.15K – 299.15K, which is commonly used in an office environment. They are also empirical models which can predict the output results with high variability and fluctuations from the various input parameters used, as compared to traditional statistical techniques.

This model learns in a supervised way, performing training on the data set gathered from the finite volume analysis method performed on the TEG with the environmental parameters that surround the operating environment of the TEG. The input to the ANN model is a set of 12 input parameters, to predict the values of output voltages under three different scenarios.

In general, it is almost impossible to have access to all the variable input parameters that determine the output voltage of the TEG as there might still be some hidden parameters which will influence the dynamics of the model. The result will be model ambiguity in the sense that for the same input values, different outputs might have been obtained. The degree of ambiguity may vary widely across the whole range of input environmental parameters that the TEG is operating in. Therefore, the ANN model used in this research will comprise of a two coupled neural networks configuration, the first one to compute on the average predicted value and the other to evaluate the reliability of the output, which is learned from the error values of the first.

The ANN model will also be equipped with two extra add-on features. They are the prediction of an input parameter value by the ANN model when given an output voltage value of a particular scenario and the identification of key input parameters that have a strong influence in the output value through sensitivity analysis.

The function for prediction of an input values when given an output value will be useful when an application requires a specific output voltage to operate. The users will have the knowledge of the best value to use for certain selected input parameter to achieve the required output voltage. These will allow the user to better design the TEG according to their needs without having to tweak other input parameters, which will directly affect the efficiency and cost of the TEG setup.

All the 12 input parameters used for this ANN model has a role to play in getting the output voltages of the TEG. The sensitivity analysis function that is incorporated into this program will provide users with an overview on the influence of each input parameter on the output voltage, ranking from the most influential parameter to the least, graphically. This will allow the users to better select the particular input parameter to change or modify when designing the TEG with limited resources, rather than to make changes to a few parameters to obtain the required outcome which at times can be inefficient or costly.

4.1.1 Proposed Method of Artificial Neural Network Model

The ANN model uses a multilayer, feedforward, back propagation error neural network for heat segmentation. It is to distinguish the output voltage generated by the TEG, with and without the aid of a heat sink, as the region of interest which was illustrated in Figure 4.2. It has three layers, namely the input, hidden and output.

In each layer, every neuron is connected to a neuron of adjacent layer having different weights. Each neuron as indicated in Figure 4.2 receives signals from the neurons of the previous layer weighted by the interconnect values between neurons, except for the input layer. The neurons then produce an output signal, by passing the summed signal through an activation function.

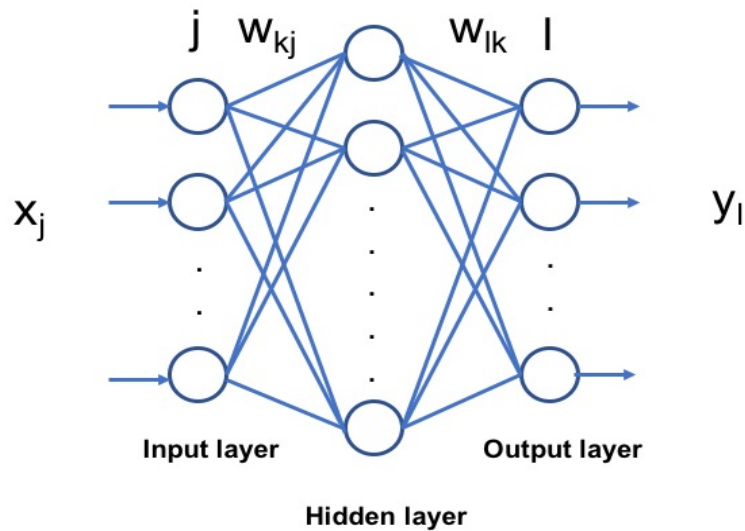


Figure 4.2 Three-layered artificial neural network

The activation function acts as an entity to transform the output range between 0 to 1 or -1 to 1 as shown in Figure 2.11. As the model uses feedforward networks, there are usually one or more hidden layers having the activation function of sigmoid neurons, and the output layer contains neurons of linear transfer function. The use of nonlinear functions in hidden layers enable the neural networks to learn nonlinear scenarios, while linear transfer function in the output layer is used in the cases where the output is of the nonlinear regression type. When the output value is between 0 and 1, a sigmoid function is used instead of a linear function. In this research, when a

new neural network is defined, the transfer function for each layer is automatically selected by the model during training from all the available activation functions.

The training procedure of this ANN model requires the weights of the connection between the neurons to be readjusted to achieve the desired input or output relation of the network. This entire procedure will go through many training cycles known as the epoch, until the mean squared error (MSE) is reduced to an acceptably low value. By then it would be suitable to classify the test set correctly, after which the ANN model should be ready to test data that are not seen previously.

The network has 12 unit of input as shown in Table 4.1 below,

Table 4.1. Inputs parameters for ANN model

Input	Abbreviation
Hot Side Ambient Temperature	T_{ambh}
Cold Side Ambient Temperature	T_{ambc}
Hot Side Wind Velocity	V_{wh}
Cold Side Wind Velocity	V_{wc}
Width of Ceramic Substrate	W_c
Thermal Conductivity of Hot Side Ceramic Substrate	K_{csh}
Thermal Conductivity of Cold Side Ceramic Substrate	K_{csc}
Length of PN junction	L_{pn}
Thermal Conductivity of PN Junction	K_{pn}
Length of Heat Sink Fins	L_{fin}
Area of Thermoelectric Generator	A_{teg}
Surface Temperature	T_{sur}

The number of processing elements per layer, as well as the number of layers, will greatly affect the abilities of the ANN model. Too few of them will slow down the learning process, and too many of them can alter the generalizing abilities of the ANN model, due to overfitting or memorization of the input training set data.

The changes in heat intensity on the TEG influenced by the 12 environmental and TEG

construction parameters will lead to a range of output voltages generated by the TEG under three scenarios. All the output data generated from the finite volume analysis by the various input parameters defined are combined to produce a set of data that reflects the behavior of the TEG used for the neural network. The data set used for the training of the model in this research comprises 2048 sets of parameters.

Hidden layer nodes will be required for the ANN to be trained. In most situation, there is no way to determine the best number of hidden layer nodes without having to go through the tedious process of training several networks and estimating the generalization of each. In situations where there are too few hidden layer nodes, the model will end up with high training error and high generalization error, due to under fitting and high statistical bias. On the contrary, if there are too many hidden layer nodes, the model may get low training error but still with a high generalization error, due to overfitting and high variance.

There are a range of books and articles that state the “rule of thumb” for the number of hidden layer nodes. Some suggest that the size of the hidden layer node to be somewhere between the input layer size and the output layer size [86] or that the hidden layer nodes should not be twice as large as the input value [87]. These rules are not realistic as they ignore the number of training cases. Hence it is recommended that the number of training cases in the formulation of the hidden layer nodes should be included. In this research, the number of hidden layer nodes in each network for the three layers network will be determined by applying the formula as shown in (4.1) [88]

$$n_h = \left(\frac{n_i + n_o}{2} \right) + \sqrt{(n_p)} \quad (4.1)$$

Where n_h , n_i and n_o are the number of hidden input and output layer nodes respectively, and n_p is the number of training samples in the dataset used. Therefore, the number of hidden layer nodes used for each neural network in this research is 53 nodes ($n_i=12$, $n_o=3$ and $n_p=2048$).

The output layer of the model will provide user with three units of output layers for different scenarios as shown in Table 4.2 below,

Table 4.2. Output parameter from ANN model

Output	Abbreviation
Output voltage obtained from manufacturer specification sheet using temperature differential obtained from hot and cold side TEG ceramic substrate surface	V_{ss}
Output voltage obtained from manufacturer specification sheet using temperature differential obtained from PN junction with environmental parameters	V_{ep}
Output voltage obtained from manufacturer specification sheet using temperature differential obtained from PN junction with environmental parameters and a heat sink	V_{ephs}

The three outputs generated from the ANN model will present the output voltage for each scenario, hence allowing users to better estimate the amount of energy generated by the TEG under different circumstances with different configuration, with and without the use of heat sink. The users will also be able to compare the output voltage obtained with reference to the manufacturer specification sheet when using the temperature differential obtained from both hot and cold side of the TEG ceramic substrate against those that were generated using temperature differential obtained at the PN junction. This also factors in the environmental parameters. Lastly the effect when using a heat sink of the same footprint as the TEG ceramic substrate will dissipate more heat away from the surface.

In this model, the sigmoidal logistic function as shown in Figure. 2.11, will be used for both the hidden and output layers as an activation function. The function is as shown below,

$$y = \left(\frac{1}{1 + e^{-x}} \right) \quad (4.2)$$

This is the most commonly used transfer function which restricts the nodes between 0 and 1. A typical operation of an artificial neuron is schematically shown in Figure 4.3.

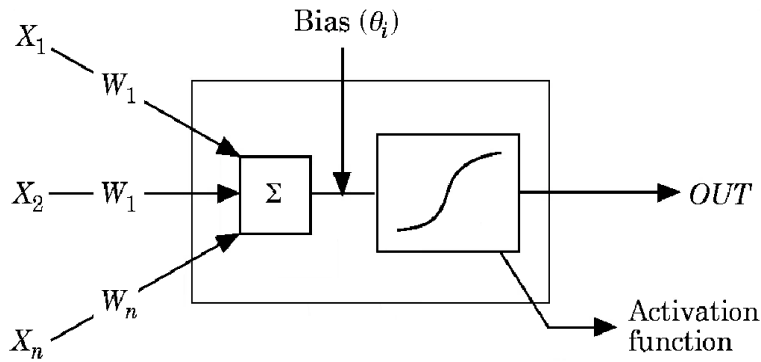


Figure 4.3 Operation of an artificial neuron in a layer

4.1.2 Coupled Neural Networks

With a total of 12 input variables identified from the surrounding environmental parameters as well as the construction of the TEG, there may still be hidden variables that will influence the dynamics of the system. Thus, there will be a degree of ambiguity that may vary widely across the whole range of input values. To evaluate the accuracy of a model, it is important to devise a method to ensure that results obtained from the model has a degree of reliability of each output voltage presented by the ANN model.

In this research, uncertainty in the construction of models from the data set will be of concern. These uncertainties may arise either from inaccuracies in the measurement of the observed variables, or from the fact that the measurable variables do not provide a complete specification of the behavior of the model. In general, the uncertainties are not uniform throughout. There might be areas where the input parameters provide users with an unambiguous answer, or others which are unable to provide precise answers due to lack of information. Hence a coupled neural network model as shown in Figure 4.4 is adopted in this ANN model to provide the user with the most probable outcome. At the same time, it also indicates the reliability of the output voltage calculated.

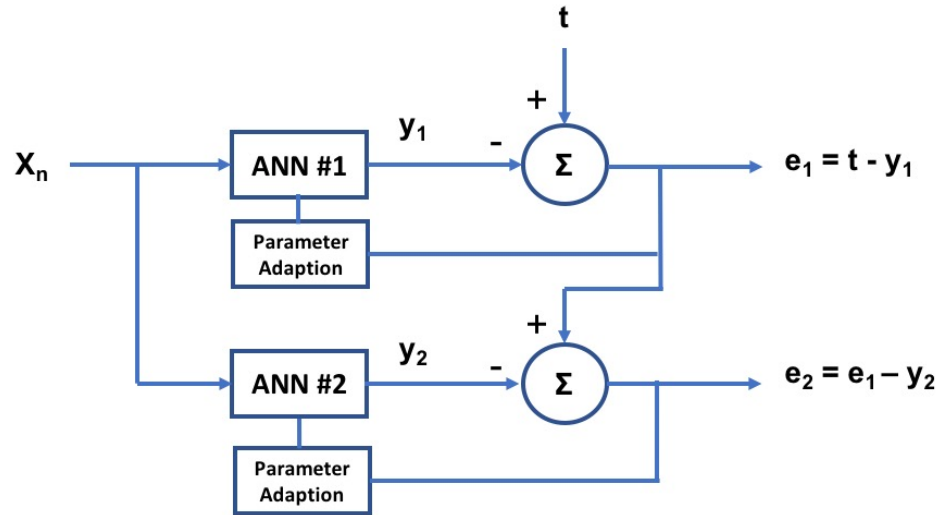


Figure 4.4 Schematic of a coupled neural network

For the coupled network model, one is to learn the most probable output value for each set of inputs and the other to provide the expected error of the output voltage. The first network will converge to an average of the corresponding outputs for each region of the input space while the second network will compute the expected errors for each region of the parameter space. The main aim of coupled neural network for this research is not to remove the fluctuations in the data to obtain an approximate output, but instead is used to characterize the ambiguity of the output voltages generated [89].

However, the actual function that the system provides is the joint information on the average output and the expected uncertainty in each region of the input parameter space. The second network because of the interpolating features of the network, does it in a more accurate way. Having done all the above is not to smooth out fluctuations in the data to obtain an approximate. Instead it characterizes the ambiguity of the answer and there is a need to quantify this ambiguity for each input.

In this ANN model as shown in Figure 4.3, the first network on the left-hand side calculates the output values having highest probability for each input value and the second network on the right calculates the expected error for that specific input value. Both networks used in this ANN model are same in architecture and properties with the same input data set for processing. The only difference is that the first network calculates values of output, while the second network calculates

the error values of output for each input data.

In the first network, the difference between the way the actual output and predicted output is calculated is referred to as network error, and the second network calculates the difference between the predicted output of second network and the network error values calculated for the first network. The absolute value is taken after calculating the difference between the predicted output of second network and the network error values calculated for the first network.

As shown in Fig 4.3, \vec{x} values are the inputs to a multilayer network. $\{W\}$ denoting the full set of connection strengths, the output being $fw(\vec{x})$. The aim is to choose a set of connection strengths $\{W\}$ that annihilates the expectation value [89],

$$E \left\{ W \sum_{\{\vec{x}\}} (fw(\vec{x}) - y(\vec{x}))^2 \right\} = 0 \quad (4.3)$$

When put through the backpropagation algorithm, (4.3) will be minimize as shown below,

$$E(fw(\vec{x}) - y(\vec{x}))^2 \quad (4.4)$$

Therefore, fixing \vec{x} and considering $fw(\vec{x})$ evolving in learning time, the time-evolution of the network output is framed as,

$$fw(\vec{x}, t + 1) = fw(\vec{x}, t) - 2\eta \frac{\partial fw}{\partial w} \times (fw(\vec{x}) - y(\vec{x})) \frac{\partial fw}{\partial w} \quad (4.5)$$

Where $\Delta W = -\eta \frac{\partial e}{\partial w}$, η being the learning rate and $e = (fw(\vec{x}) - y(\vec{x}))^2$ the error function.

When the η is sufficiently small for the learning time scale to be much smaller than the sampling rate of the $y(\vec{x})$ random variable, the last equality may be approximated by

$$fw(\vec{x}, t + 1) = fw(\vec{x}, t) - 2\eta \frac{\partial f}{\partial w} \times (fw(\vec{x}) - y(\vec{x})) \frac{\partial fw}{\partial w} \quad (4.6)$$

Where $y(\vec{x})$ is the average value of the random variable y at the argument \vec{x} . A fixed point is obtained for

$$(fw(\vec{x}) = \bar{y}(\vec{x})) \quad (4.7)$$

Where the average value of the random variable y at \vec{x} is tend by $fw(\vec{x})$.

Similarly, for the second network where the output is defined as $gw'(\vec{x})$ and with the same input, \vec{x} , as shown in Fig 4.3, is constructed according to the learning law

$$gw(\vec{x}, t + 1) = gw'(\vec{x}, t) + \frac{\partial gw'}{\partial W'} \times \Delta W' \quad (4.8)$$

With the error function, as

$$e' = (gw'(\vec{x}) - (fw(\vec{x}) - \bar{y}(\vec{x}))^2)^2 \quad (4.9)$$

Where

$$\Delta W = -\eta \frac{\partial e'}{\partial W'} \quad (4.10)$$

Hence,

$$gw'(\vec{x}, t + 1) = gw'(\vec{x}, t) - 2\eta' \frac{\partial gw'}{\partial W'} \times \frac{\partial gw'}{\partial W'} (gw'(\vec{x}) - (fw(\vec{x}) - \bar{y}(\vec{x}))^2)^2 \quad (4.11)$$

Under the same assumptions as the first network, concerning the smallest of the learning rate, it is shown as:

$$gw'(\vec{x}) = \overline{(y(\vec{x}) - \bar{y}(\vec{x}))^2} \quad (4.12)$$

The rationale for taking the absolute value is that only the difference in values is required. It does

not matter whether the error value is a positive or negative number. Also, to present the values in the histogram plot, the absolute values are needed to plot the graph in one direction. This will allow for easy identification of errors within the error plot.

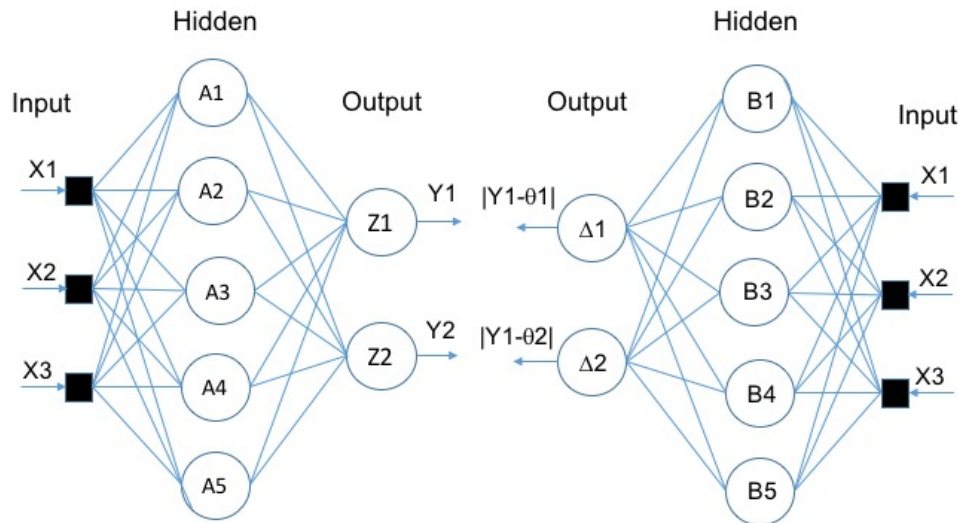


Figure 4.5 Coupled neural network

4.1.3 Training Algorithms

There are many different types of functions available for the training of the neural network, and the selection of suitable functions depends upon many factors such as the number of inputs, weights, biases, the problem complexity and the goals for error. It also depends upon the type of problem for example whether it is a pattern recognition problem or regression type problem.

Four types of functions which are very efficient and are commonly used for regression type of problems will be programmed into the ANN Model. These functions are mostly used for regression type of problem where there are not many number of weights. These functions include the Levenberg-Marquardt back propagation [90], Bayesian regularization back propagation [70], Scaled conjugate gradient back propagation [70] and Resilient back propagation [91].

The Levenberg-Marquardt algorithm was designed to approach second order training speed without having to compute the Hessian matrix. When the performance function has the form of a sum of squares, the Hessian matrix can then be approximated and the gradient can be computed

as,

$$H = J^T J \quad (4.13)$$

$$g = J^T e \quad (4.14)$$

Where J is a Jacobian matrix. This contains first order derivatives of the network errors with respect to the weights and biases, where e is a vector of network errors. The Jacobian matrix can be computed through a standard backpropagation technique that is much less complex than computing the Hessian matrix. The Levenberg-Marquardt algorithm uses this approximation to the Hessian matrix in the following Newton-like update, where x represents the connection weights.

$$x_{k+1} = x_k - [J^T J + \mu I]^{-1} J^T e \quad (4.15)$$

This algorithm was used for this model as it appears to be the fastest method for training moderate size feedforward neural networks. It also has an efficient implementation in MATLAB as the solution of the matrix equation is a built-in function. As such its attributes become even more pronounced in a MATLAB environment. There are also limitations in this function as it is using the Jacobian for calculations, which assumes that performance is a mean or sum of squared errors.

The Bayesian regularization backpropagation is a network training function that updates the weight and bias values according to Levenberg-Marquardt optimization. It minimizes a combination of squared errors and weights, and then determines the correct combination so as to produce a network that generalizes well. Bayesian regularization introduces network weights into the training objective function which is denoted as $F(\omega)$,

$$F(\omega) = \alpha E_\omega + \beta E_D \quad (4.16)$$

Where E_ω is the sum of the squared network weights and E_D is the sum of network errors. Both α and β are the objective function parameters. The α and β factors are defined using Bayes' theorem.

The Bayes' theorem relates two variables, A and B, based on their prior probabilities and posterior probabilities as shown in

$$P(A|B) = \frac{P(B|A)P(A)}{P(B)} \quad (4.17)$$

Where $P(A|B)$ is the posterior probability of A conditional on B, $P(B|A)$ the prior of B conditional on A and $P(B)$ the non-zero prior probability of event B, which functions as a normalizing constant. To find the optimal weight space, objective function needs to be minimized, which is the equivalent of maximizing the posterior probability function given as,

$$P(\alpha, \beta|D, M) = \frac{P(D|\alpha, \beta, M)P(\alpha, \beta|M)}{P(D|M)} \quad (4.18)$$

Where α and β are the factors needed to be optimized, D is the weight distribution, M is the particular neural network architecture, $P(D|M)$ is the normalization factor. Next $P(\alpha, \beta|M)$ is the uniform prior density for the regularization parameters and $P(D|\alpha, \beta, M)$ is the likelihood function of D for given α, β, M . Maximizing the posterior function $(\alpha, \beta|D, M)$ is equivalent of maximizing the likelihood function $(D|\alpha, \beta, M)$. Because of this process, optimum values for α and β for a given weight space are found. Afterwards, algorithm moves into LM phase where Hessian matrix calculations take place and updates the weight space in order to minimize the objective function. Then, if the convergence is not met, algorithm estimates new values for α and β and the whole procedure repeats itself until convergence is reached

This network training function can be used to train any network if its weight, net input, and transfer functions have derivative functions. This network training function has the same limitation as the Levenberg-Marquardt algorithm.

The scaled conjugate gradient backpropagation can be used to train any network as long as its weight, net input, and transfer functions have derivative functions. In this method, as described in (4.19), where s is the Hessian matrix approximation, E is the total error function and E' is the gradient of E, scaling factors λ_k and σ_k are introduced to approximate the Hessian matrix. They are initialized by user at the beginning of the algorithm such that $0 < \lambda_k < 10^{-6}$ and $0 < \sigma_k < 10^{-4}$. For

Scaled conjugate gradient, β_k factor calculation and direction of the new search can be shown as in (4.20) (4.21):

$$s_k = \frac{E'(w_k + \sigma_k p_k) - E'(w_k)}{\sigma_k} + \lambda_k p_k \quad (4.19)$$

$$\beta_k = \frac{(|g_{k+1}|^2 - g_{k+1}^T g_k)}{g_k^T g_k} \quad (4.20)$$

$$p_{k+1} = -g_{k+1} + \beta_k p_k \quad (4.21)$$

The resilient backpropagation is a network training function that updates weight and bias values according to the resilient backpropagation algorithm. The purpose of the Resilient backpropagation training algorithm is to eliminate the harmful effects of the magnitudes of the partial derivatives. Only the sign of the derivative can determine the direction of the weight update. Also the magnitude of the derivative has no effect on the weight update. The size of the weight change is determined by a separate update value. The update value for each weight and bias is increased by a factor whenever the derivative of the performance function, with respect to that weight, has the same sign for two successive iterations. The update value is decreased by a factor whenever the derivative, with respect to that weight, changes sign from the previous iteration. If the derivative is zero, the update value remains the same. Whenever the weights are oscillating, the weight change is reduced. If the weight continues to change in the same direction for several iterations, the magnitude of the weight change increases.

Large amount of data will be required to train, validate and test the network. The training of this model will be done in two scenarios. The first scenario will be training 50% of the dataset and the remaining 50% will be used for verification. The second scenario will be solely training 100% of the dataset. The Quasi-Newton algorithm, specifically the Levenberg-Marquardt backpropagation (*trainlm*) method will be used for this research.

The Quasi-Newton algorithm method is chosen as it will give better and faster optimization when compared to the conjugate gradient methods. The basic step of the Quasi-Newton method is the Hessian Matrix of the performing index at the current values of the weights and biases. This

method will usually converge faster than the conjugate gradient methods. However, these methods are much more complex and will require a longer time to compute the Hessian matrix for the feed-forward neural networks.

The *trainlm* algorithm locates the minimum of a multivariate function that can be expressed as the sum of squares of non-linear real-valued functions. It is an iterative technique that works in such a way that performance function will always be reduced in each iteration of the algorithm. This feature makes *trainlm* the fastest training algorithm for networks of moderate size. However, this algorithm has its drawback of memory and computation overhead caused by the calculation of the gradient and approximated Hessian matrix [69].

4.1.4 Sensitivity Analysis

The ANN model has the capacity to predict the output variables but the mechanism that occurs within the network is often neglected and is usually known as the “black box”. Researchers have been exploring the roles of each individual variable in the ANN model as well as the algorithm.

Analyzing the input variables used for the ANN model will help to eliminate irrelevant inputs or to identify key inputs that will influence and affect the outputs of the ANN model. The “Weights” method, a computation using the connecting weights, will be used for the analysis. The “Weights” method is adopted for this research due to its functionality as compared to other methods in terms of time, memory and complexity.

While the other methods use partial derivatives of input and output and perturbation of input variables, the “Weights” method uses only the weight values of the trained neural network. With the methodology of changing one variable and fixing others for other methods, it will require a much longer time and processing for each run. There is a need to save all input and output data for sensitivity analysis (SA). In contrast, the “Weights” method, only the weights values for SA need to be saved. Hence this requires less memory and is therefore considered as a better method when compared to the rest.

The “Weights” method uses the partitioning of the connection weights to determine the relative importance of the various inputs as proposed by Garson [92]. This method essentially involves partitioning of the hidden output connection weights of each hidden neuron into components associated with each input neuron. M.Gevrey et al. [93] suggested a methodology to

simplify the algorithm that gives identical results as proposed by Garson. The alternative is to divide the absolute values of the input hidden layer connection weight by the sum of the absolute value of the input hidden layer connection weights. This include all input neurons for each hidden neuron, as shown in (4.22),

$$Q_{ih} = \left(\frac{|W_{ih}|}{\sum_{i=1}^{ni} |W_{ih}|} \right) \quad (4.22)$$

For each input neuron i , divide the sum of (4.22) for each hidden neuron by the sum of each hidden neuron of the sum for each input neuron of (4.22), and multiply by 100. The relative importance (RI) of all output weights attributable to the given input variable is then obtained, as shown in (4.23).

$$RI(\%)_i = \left(\frac{\sum_{h=1}^{nh} Q_{ih}}{\sum_{i=1}^{ni} \sum_{h=1}^{nh} Q_{ih}} \right) \times 100 \quad (4.23)$$

The SA will be presented in a line graph format where all 12 inputs for the three different outputs will be shown and compared against each other. Those with higher sensitivity values will therefore have more influence over all the output voltages generated.

4.2 Graphical User Interface

To enhance the user experience for this ANN model, a set of graphical user interfaces (GUI) have been designed.

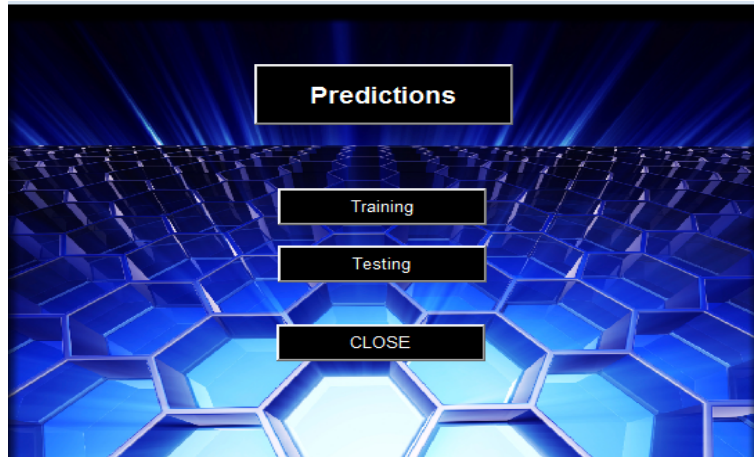


Figure 4.6 Main GUI

The interface shown in Figure 4.6 provides the user with two options: to perform training on a new set of data, and to predict the output voltage generated by the TEG that has been trained, refer to Appendix A.

Upon choosing the option of training, refer to Appendix C, the ANN model will allow the user to select the type of network that is preferred to train the data set. As mentioned in Chapter 4.1.3, there are four kinds of training algorithm. Each training algorithm will have its own training functions. There are four options, namely,

- i. Levenberg-Marquardt back propagation
- ii. Bayesian regularization back propagation
- iii. Scaled conjugate gradient back propagation
- iv. Resilient back propagation

The training button for the GUI is programmed in a way whereby an option must be chosen for the network. If no options are chosen for the network, the program will not proceed.

When a network has been chosen for the training of the data set, three feedforward neural network will be trained. They are output 1 and output 2, where only 11 inputs will be used for the

training as the 12th input is specifically used to determine the length of the heat sink used. This is not applicable to both output 1 and output 2. For output 3, all 12 inputs will be required for the training as a heat sink is used together with the TEG, refer to Appendix B. Figure 4.6 shows the training process of the ANN model.



Figure 4.7 Training GUI

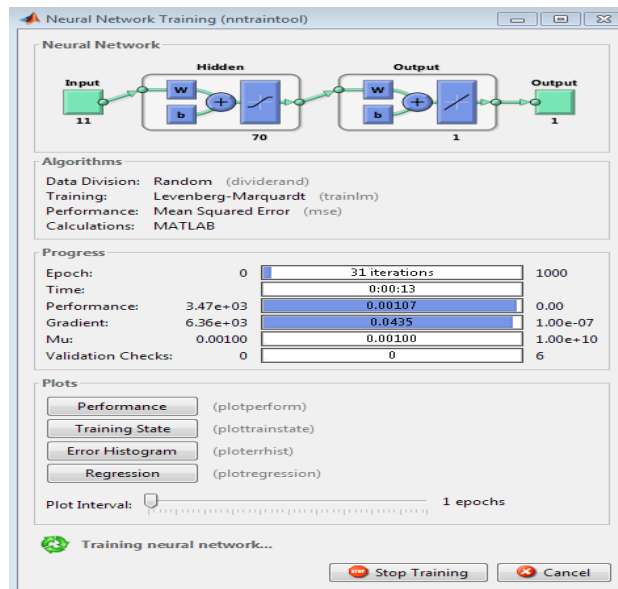


Figure 4.8 Training of ANN model

After training of the network has been completed, sensitivity analysis, discussed in Chapter 4.1.4, can be carried out for the data set, referring to Appendix D. This function will allow the user to rank the 12 inputs according to their influence to the output voltage, from the most critical to the least. The information generated will assist the users to obtain their required output voltage generated by the TEG by changing the most critical parameter given a limited budget or constrained environment as discussed in Chapter 4.1.

The ANN model will also allow the users to predict one of the input parameters for the TEG when the requirement by the application has to meet a stipulated output voltage. This function is particularly useful when the user wants to know the predicted values for the chosen input when given a prescribed output voltage. Constraints will also be set for each of input values to keep the ANN model input and output values realistic, as shown in Figure 4.10.

Upon insertion of some unknown input values into their respective box, the system can be tested to predict the values of Output 1, Output 2 or Output 3. There are three buttons on Testing GUI window for this purpose. Predict Output 1 will predict the value of Output 1 on the basis of saved Neural Network after the training. Similarly, Output 2 and Output 3 will be predicted by utilizing saved neural networks after the training.

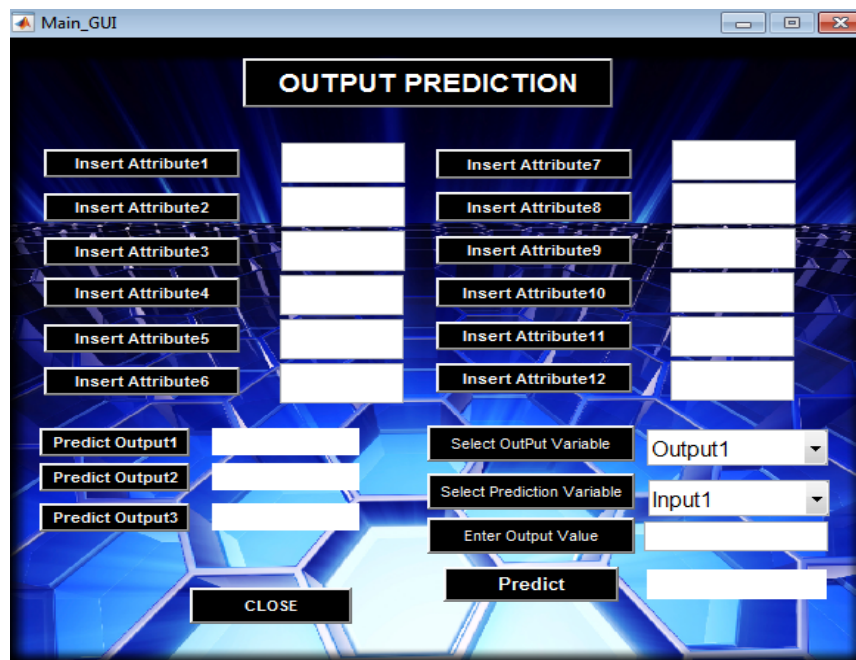


Figure 4.9 Testing GUI

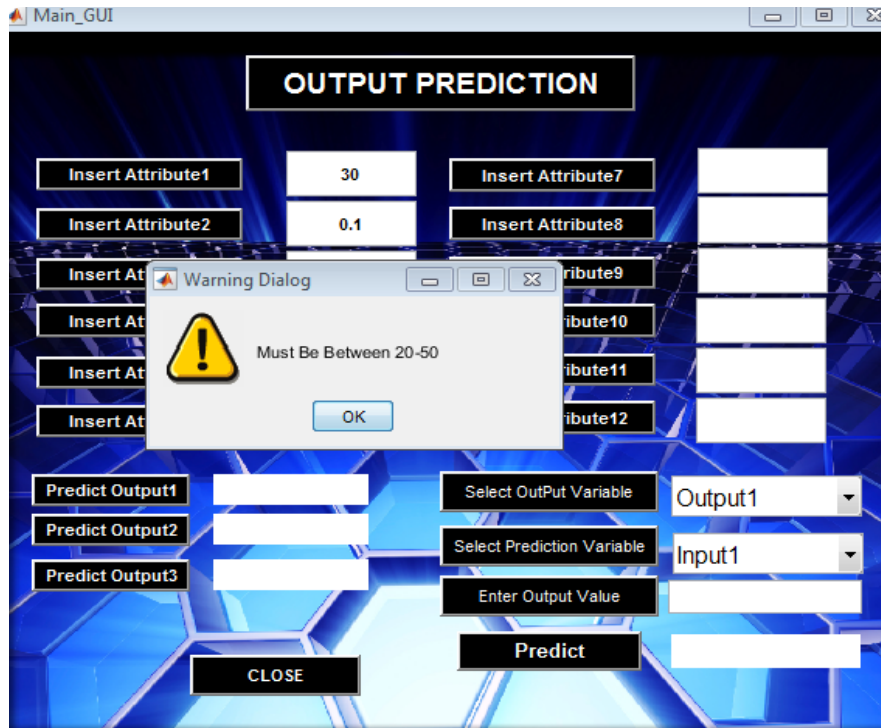


Figure 4.10 Input value range constraint

4.3 Summary

This chapter has provided an insight on the conceptualization of the novel ANN model with the inclusion of a coupled neural network that can evaluate the accuracy and degree of reliability of predictive models. The function to predict both input parameters and its output parameters. Lastly, it also addressed the sensitivity analysis of all the input parameters. In this ANN model, a simple GUI that has been added to allow users to navigate more easily.

The use of ANN in this application has proved its efficiency as an estimated tool for predicting outputs values through a set of 12 input parameters which do not have any specific relationship. An example is the use of ANN to carry out the convective heat transfer prediction of evaporative processes which is a very sophisticated process due to the fact that the physical phenomena involved are very complex and varies with the change in the environment [65].

In this research, the same set of physical phenomena will be the input parameters too, but with extra parameters such as the thermal conductivity of the TEG material, the wind viscosity, wind velocity, the design of the TEG itself and many more.

Chapter 5 Results Analysis and Discussions

This chapter will discuss the process of obtaining the data set used for training the ANN model and the training results from the ANN model. The data set will be segregated into 50% training as well as 50% validation. Subsequently, verification of the robustness of the ANN model will be done through experiments with comparisons to real life scenarios and the laboratory based data obtained.

5.1 Data Set Generation and Validation

To generate a wide range of data set to train the ANN model, an experimental set up shown in Figure 5.1 has been designed for this purpose but it will not be productive and feasible to generate thousands of data sets from this set up, as the dynamic operating environmental parameters are also taken into consideration. This is a mathematical model with a huge range of variable parameters. Therefore, a mathematical model that factors in the construction setup and operating environmental parameters of the TEG has been designed to help with the generation of thousands of data sets for the training of the ANN model.

To ensure that the data generated by the mathematical model has a degree of accuracy for the user to obtain the temperature difference across the TEG, the validation of the mathematical model prior to generating the data set will be required. This validation experiment will be carried out using a conventional TEG bought commercially off the shelves, TEG1-1263-4.3 from Thermal Electronics Corp, an 11-volt light emitting diode as the heat source on the hot side of the TEG and a metal heat sink. The heat sink will have the same footprint as the TEG used.

The experimental setup is done in an air-conditioned laboratory environment with a constant surrounding ambient temperature of approximately 294.15K. This temperature is taken from a type T temperature sensor and wind draft from the air conditioner is approximately 0.1m/s. The heat sink of the 11-volt light emitting diode is used as the heat source, generating approximately 303.15K to 313.15K of thermal heat onto the hot side substrate surface of the TEG. The temperature gradient across the thermocouple is measured and logged by a type T thermocouple sensor on both the hot and cold side ceramic substrate. The ambient air temperature

around the experiment will also be monitored and logged to ensure that it remains consistent or with minimal disruptions throughout the experiment. The TEG is clamped together with the heat sink of the heat source, which is a LED lighting, to provide it with the heat required on the hot side of the TEG. Type T thermocouples were set in place at various point of the TEG, the hot side, cold side and as well as one that is expose to the environmental parameters of the laboratory. Data such as the TEG hot side surface temperature, cold side surface temperature, ambient temperature as well as wind draft speed flowing towards the TEG are all logged and trend by data loggers.

The main constrain that this experimental setup faced is the range of data that it can trend as the experiment is being carried out in a functional student laboratory where only a single scenario can be experimented and not the rest of the environmental conditions such as a plant room or freezer room used in commercial buildings hence only a small data range can be derived from the experiment to be compared with the mathematical model. The experiment setup is as shown in Figure 5.1 and the schematic overview as shown in Figure 5.2.

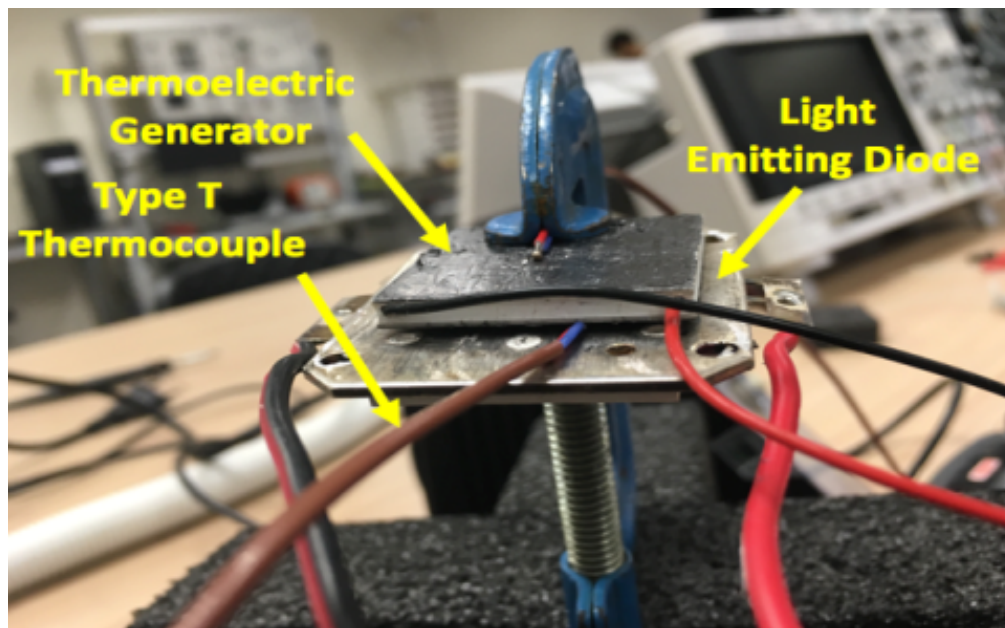


Figure 5.1 Experimental setup of TEG with LED heat source

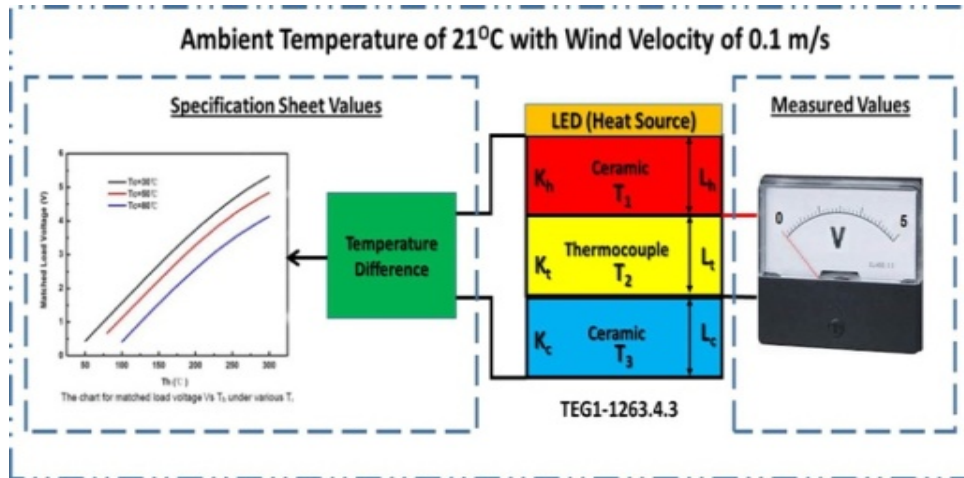


Figure 5.2 Experiment setup schematic overview.

Using a range of temperature gradients measured across the TEG from the actual experiment setup in the functional student laboratory as shown in Figure 5.1 and subsequently correlating it to the output voltage graphs provided by manufacturer's specifications sheet graph, a range of output voltage generated was obtained. This range of output voltages anticipated by the manufacturer will be compared against the output voltage measured by a digital voltmeter connected to the experimental setup and the output voltage calculated by the mathematical model.

This comparison serves to validate the output voltage obtained from the actual setup shown in Figure 5.1 with both output voltages obtained from the manufacturer's specification sheet graph and the mathematical model respectively.

The output voltage bar graph shown in Figure 5.3 indicates that there are indeed some differences in the output voltages obtained from all the three scenarios carried out, with those output voltages obtained from the manufacturer's specification sheet being the most unsynchronized when compared to the rest. This is due to the fact that the manufacturers produced the graph using the results that were generated without taking into the surrounding operating environmental parameters. This has been confirmed by manufacturers when asked how they conducted their experiment to derive the voltage output graphs based on temperature difference. In contrast, both the output voltages measured from the actual setup and the mathematical model prediction tool show that they have almost similar output voltage.

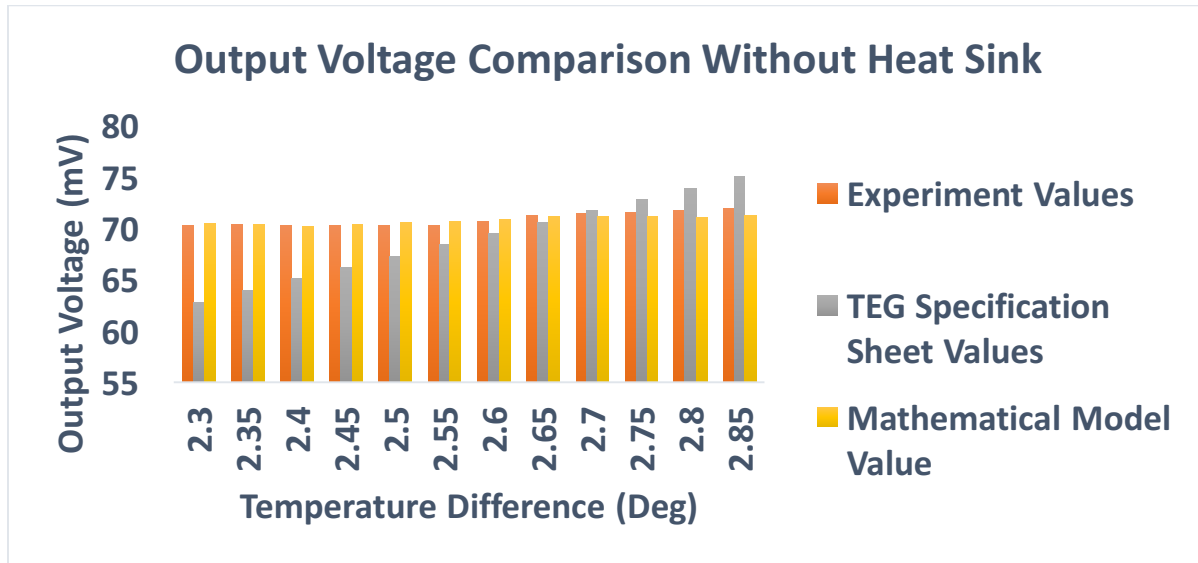


Figure 5.3 Graph comparisons between measured, technical sheet data and mathematical model for TEG without heat sink.

The difference between the output voltage obtained from the actual experiment setup when compared to the output voltage obtained from the mathematical model and manufacturer's specification sheet is approximately +/- 0.15% and +/- 0.9% respectively. Therefore, with the small difference in the output voltage generated, the mathematical model which takes into consideration the operating environmental and construction parameters of the TEG, has been proven to be a much more reliable and precise tool that is to be used for the future prediction of the energy generated by the TEG hence it can be used to generate a range of data set under various circumstances for the training of the ANN.

However, as seen in Figure 5.1, the manufacturer's specifications sheet data which is obtained in an operating environment that does not factor in the environmental parameters, cannot be used if accuracy of the data generated is the primary concern for the experiment. Based on conventional theory of the TEG, as the temperature difference across the TEG increases, so will the output voltage but when exposed to the operating environmental parameters, the temperature difference across the TEG will be affected as there are the elements of conduction, convection as well as radiation hence it is recommended that this method of obtaining data through the manufacturer's specification sheet graph can only be used as a guide that can at times have a huge deviation in terms of the output values.

In order to generate a range of data set that is to be used for the training of the ANN model, a range of parameters as shown in Table 3 has been chosen for the generation of data set for the TEG using our validated mathematical model.

This set of parameters will generate a total of 2048 sets of data for the training of the ANN model. These ranges are chosen as TEG that are commonly used in building applications and are usually exposed to ambient temperature range between 293.15K to 299.15K as well as wind velocity of 0.1 m/s to 5.1 m/s under a natural ventilation scenario.

The common parameter ranges used for the construction of the TEG are usually defined from the commercial TEG sizes that users can get off the shelves and the material properties of the TEG is based on the commonly used materials such as Bismuth telluride and these are discussed in Chapter 2 when reviewing the literature of TEG. The heating elements used to heat up the hot side surface of the TEG is a 11V LED light and the maximum temperature on the heat sink will be approximately at 313.15K when the LED light is turned on fully. When dimmed, it will produce approximately 303.15K of heat on its heat sink hence the range stated in Table 5.3.

Table 5.3 Parameter range for data set generation

Parameter	Range
Hot Side Ambient Temperature	293.15K – 299.15K
Cold Side Ambient Temperature	293.15K – 299.15K
Hot Side Wind Velocity	0.1 m/s – 5.1 m/s
Cold Side Wind Velocity	0.1 m/s – 5.1 m/s
Thickness of TEG Substrate	0.001m – 0.003m
Thermal Conductivity of Hot Side Substrate	1 W/m ² – 4 W/m ²
Thermal Conductivity of Cold Side Substrate	1 W/m ² – 4 W/m ²
Height of PN Junction	0.001 m – 0.003 m
Thermal Conductivity of PN Junction	1 W/m ² – 2 W/m ²
Length of Heat Sink Fin	0.002m – 0.008m
Total Surface Area of TEG	0.0009m ²
Hot Side Substrate Surface Temperature	303.15K – 313.15K

5.2 Training of the Artificial Neural Network

The training of the data set generated was done using the Levenberg-Marquardt algorithm and they are divided equally into 50% for training and the remaining 50% for validation. In this ANN model, there are three output values, namely output voltage obtained from the manufacturer's specification sheet, the output voltage obtained from mathematical model with environmental parameters. Lastly, the output voltage from the mathematical model is tied to the environmental parameters with the inclusion of a heat sink. Therefore, the three sets of neural network will be trained. The error distribution in the first network for the three output voltages are as shown in Figure 5.4 below.

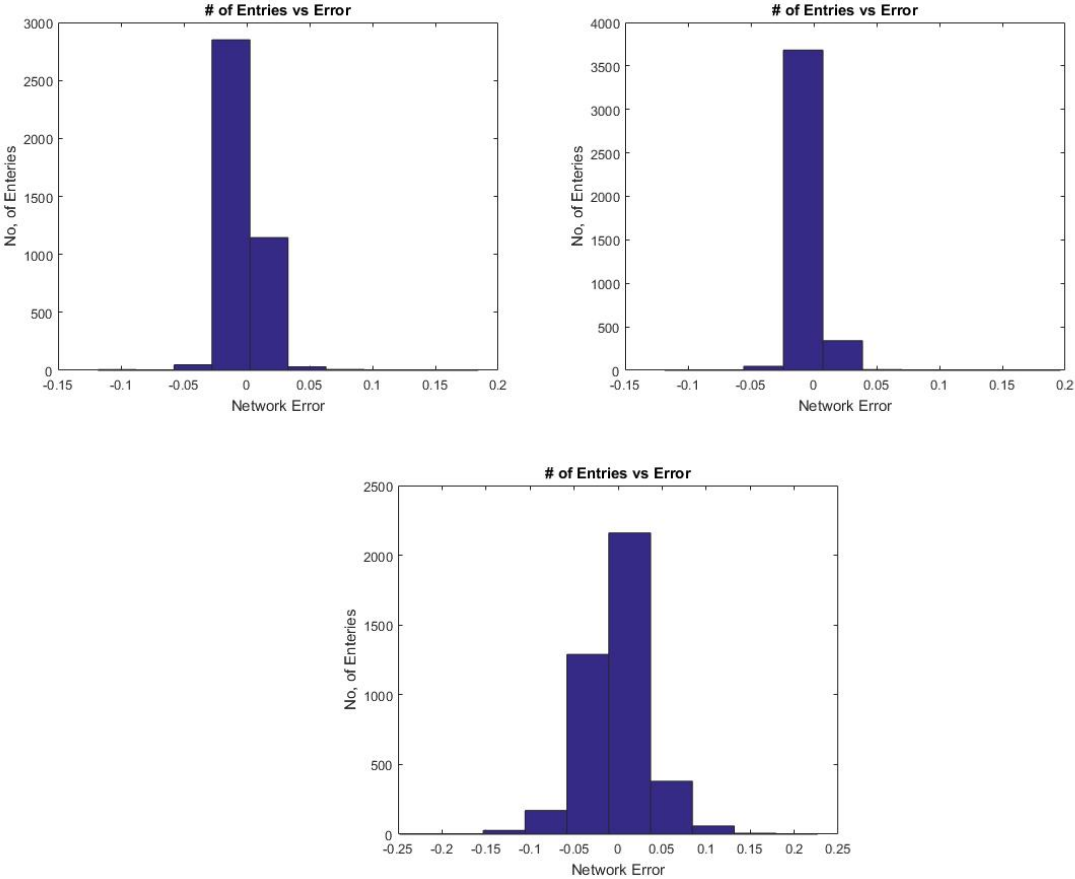


Figure 5.4 Error distributions in the first network

The results presented in Figure 5.4 shows that the networks are performing well and are giving good prediction values as the error values indicated in each of the bar chart are not too far extended towards the higher network error range.

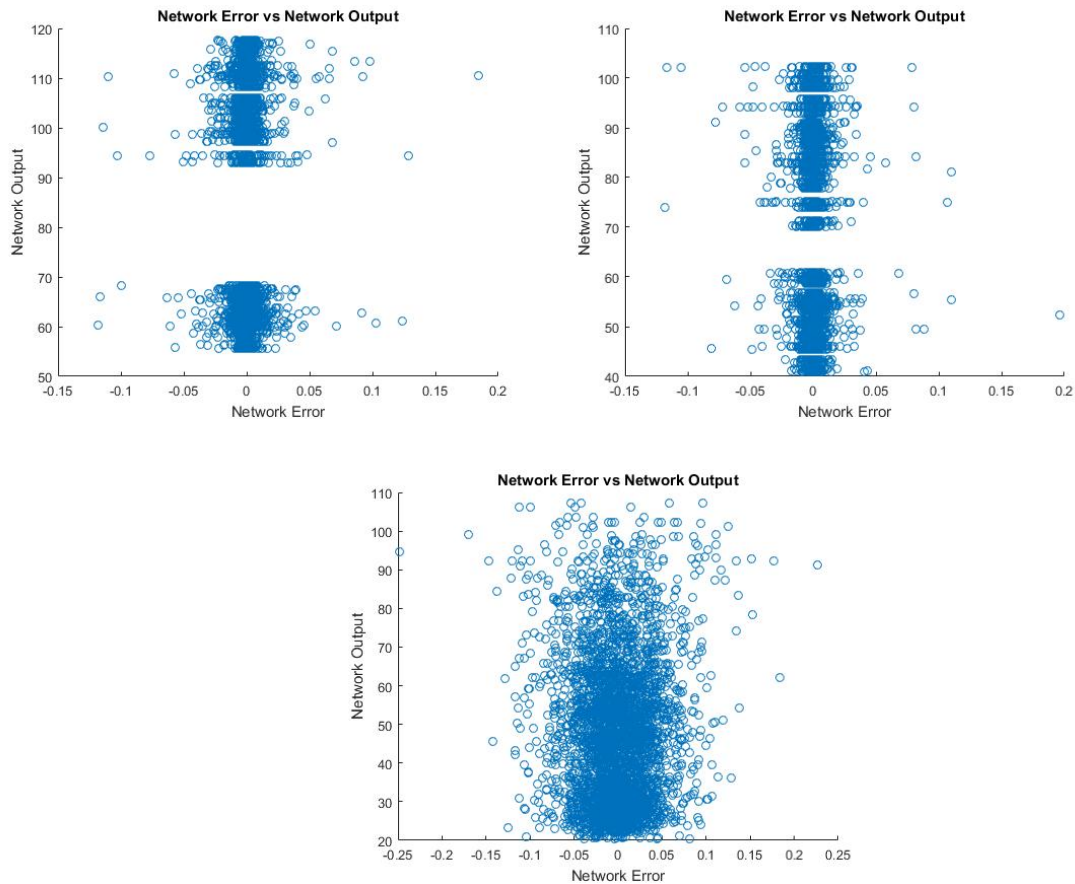


Figure 5.5 Comparison of the actual error of the first network and the estimated uncertainty predicted by the second network

Figure 5.5 shows the comparison of the actual error of the first network and the estimated uncertainty predicted by the second network. In these plots, higher values of network error and prediction values of second network highlighted that network will be robust enough to deal with a variety of data set input into the model. When there are outlier entries in the data set, the network will be able to deal with those. Similarly, some small value of network error and higher value of prediction shows that network is unreliable for the prediction of such data values.

This is the case for both output 1 and output 2 where there are some slight ambiguities in

the predictions. Hence there is some ambiguity in the dataset for the two outputs.

Upon completion of the training, the trained system will be tested for unknown data, and the performance of system is estimated through performance, error histogram, regression and training state plots.

In the learning network, the degree of convergence can be expressed in a mean square error (MSE) as follows,

$$MSE = \frac{1}{N} \sum_{i=1}^N (Y_i - X_i)^2 \quad (5.1)$$

where N is the number of objects, Y_i is the neural network predicted values and X_i is the actual output values. The value of the MSE lies within the range of 0 to 1.

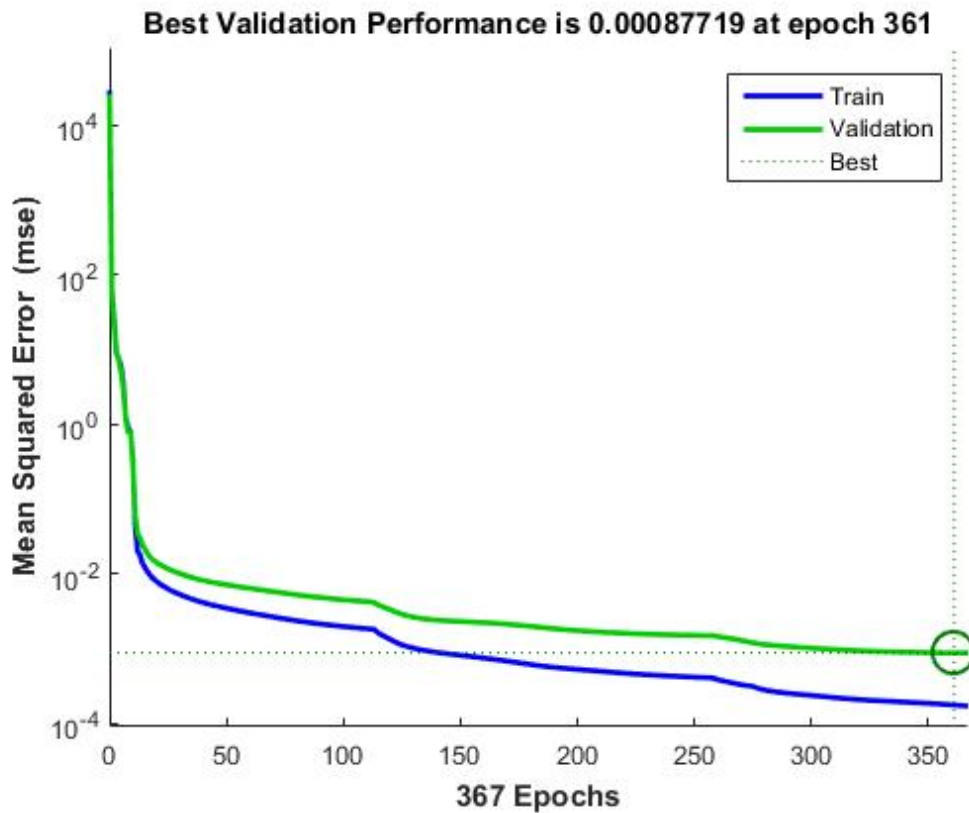


Figure 5.6 Performance plot

Figure 5.6 shows the variation of the learning cycle with MSE and the performance plot where the MSE become smaller as number of epoch increases. Here the maximum epoch is determined as 361 and the training least mean square error is obtained as 0.00087719, which is considered good as it is within the range stipulated above and almost at 0.

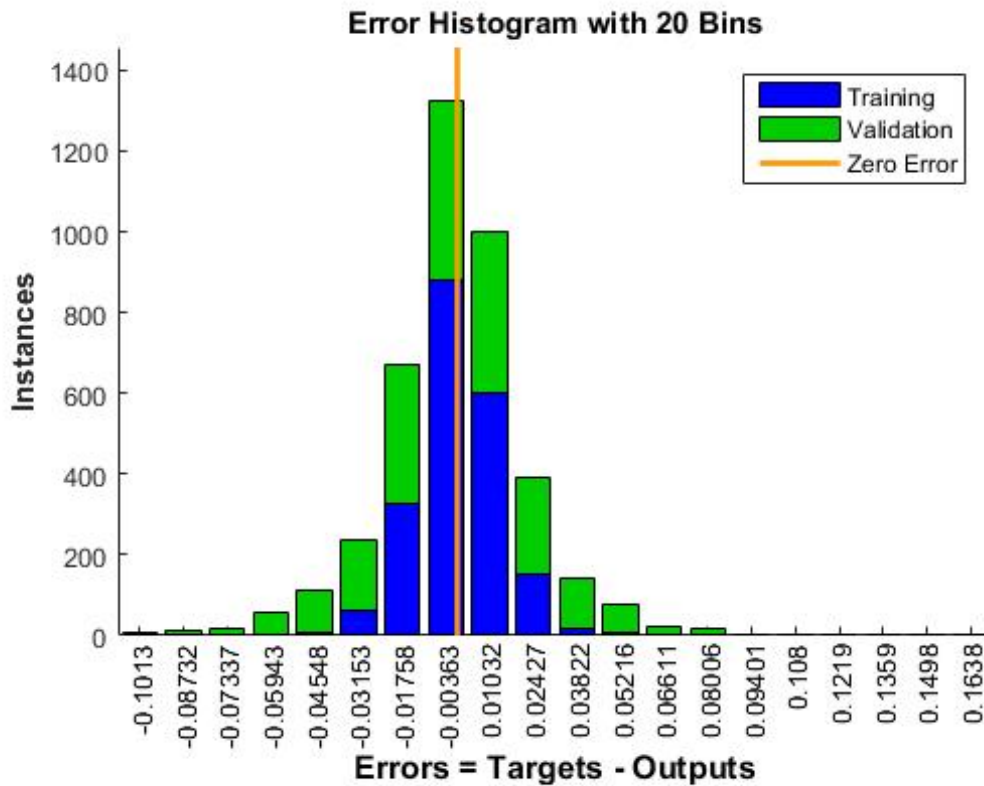


Figure 5.7 Error histogram plot

The error histogram plot for training data is as shown in Figure 5.7. This graph is to provide additional verification of network performance and it indicates outliers. The blue and green bars represent training data and validation data respectively. Most of the data falls on the zero-error line. This provides an opportunity to check the outliers to determine if the data is precise or if those data points are different from the rest of the data. The outliers in Figure 5.7 are considered valid data point but are unlike the rest of the data. Hence the network has to extrapolate for these points.

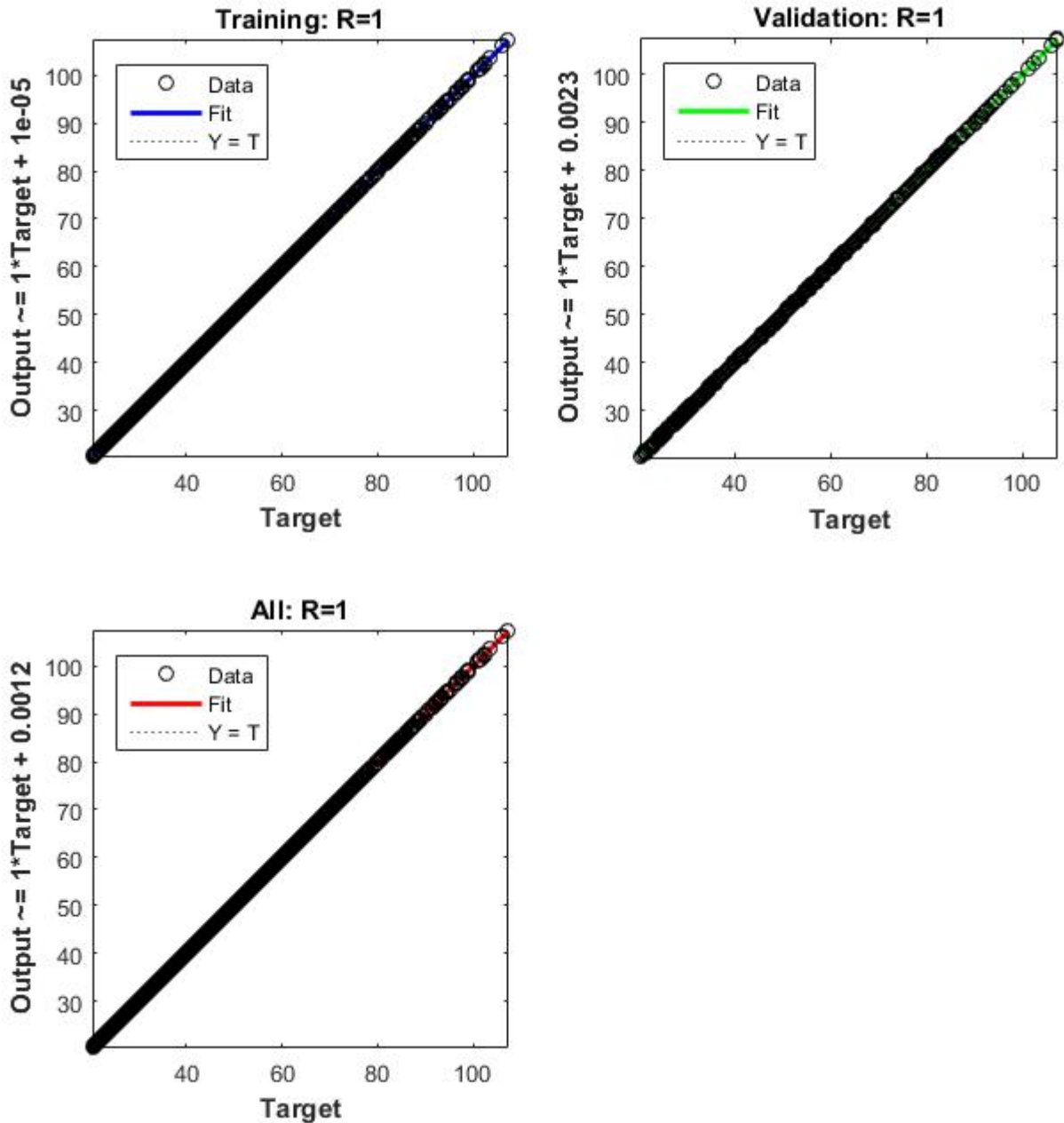


Figure 5.8 Regression plot

The correlation coefficient (*R-Value*) measures the correlation between the outputs and targets. The R-Value between the predicted and the actual values of the output voltages are shown in Figure 5.8 for training, validation. Next the entire data set. R value of 1 has been obtained for training, validation and the entire data set. This means that the predicted output voltages match the actual values in the data set.

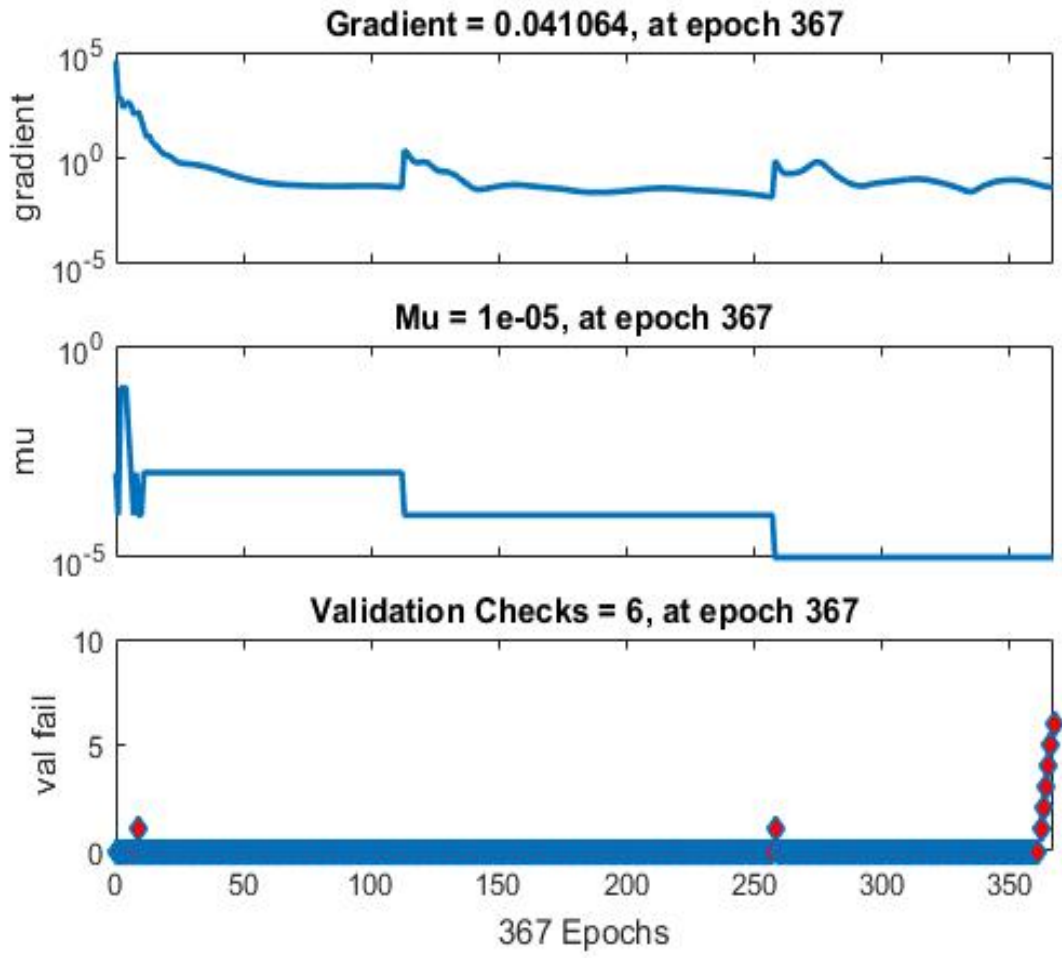


Figure 5.9 Training state plots

Figure 5.9 shows the training state plot for the network. The first graph describes the results of the gradient value in every iteration. With a gradient of 0.041064, we can expect a good performance can be expected for the network. With Mu valued at 0.00001, the convergence of the network will be slower as a smaller Mu will cause the network to converge slowly. The training stops when the validation parameter reached a maximum of six validation checks at epoch 367.

5.3 Sensitivity Analysis Output

Much information can be generated from the sensitivity analysis of the data set. The sensitivity results are as shown in Figure 5.10 and is done using the “Weights’ method. It works on the values of connection weights between layers after the training of network is complete. For the sake of comparing methods, the composite sensitivity rankings are based on the RI value. The parameter with the highest RI value will be considered as the variable with the greatest sensitivity therefore it will have a higher influence on the output generated by the TEG.

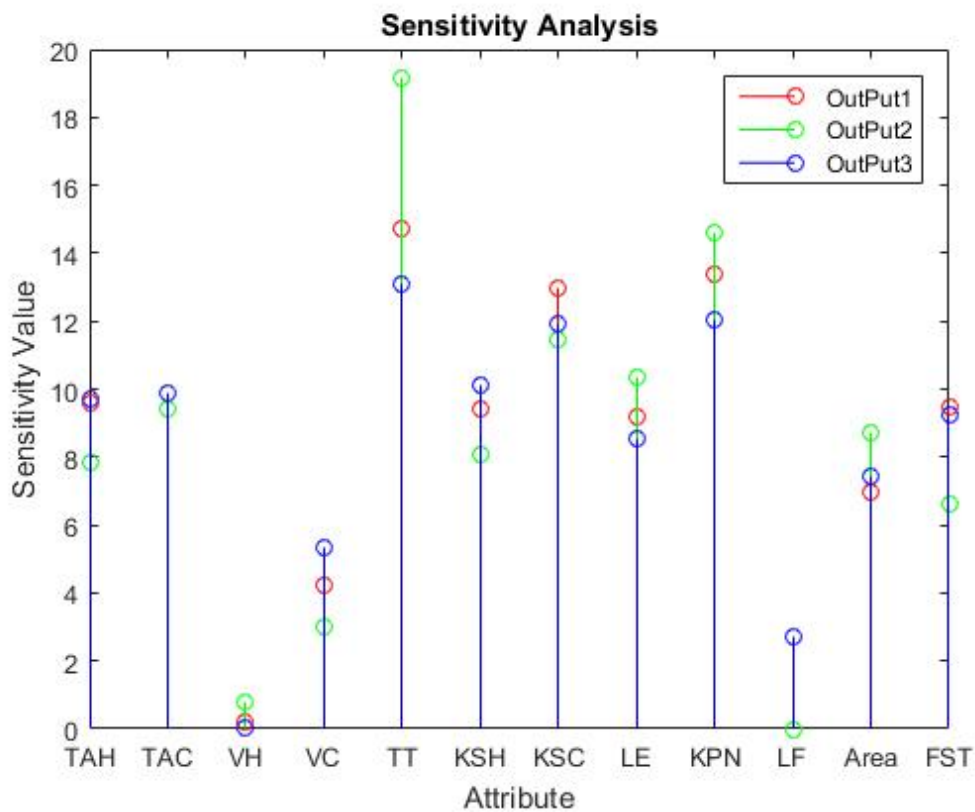


Figure 5.10 Sensitivity analysis

The red lines, output 1, represent the RI values of the variable used for generating the output voltage when compared with the manufacturer’s specification sheet. The green lines, output 2, represent the RI values of the variables used to generate the output voltage when the operating environmental factors are factored into the equation. Lastly, the blue lines, output 3, represent the

RI values of the variables used to generate the output voltage with the aid of a heat sink.

From the sensitivity analysis results shown in Figure 5.10, the 12 input variables can be ranked according to their sensitivities in the mathematical model for all the three output voltages as shown in Table 5.4.

Table 5.4. Ranking on the sensitivities of the input variables on the output voltages across the three scenarios.

Input Parameter	Output 1	Output 2	Output 3
Hot Side Ambient Temperature (TAH)	5	8	6
Cold Side Ambient Temperature (TAC)	4	5	5
Hot Side Wind Velocity (VH)	11	11	12
Cold Side Wind Velocity (VC)	10	10	10
Thickness of TEG Substrate (TT)	1	1	1
Thermal Conductivity of Hot Side Substrate (KSH)	6	7	4
Thermal Conductivity of Cold Side Substrate (KSC)	3	3	3
Height of PN Junction (LE)	8	4	8
Thermal Conductivity of PN Junction (KPN)	2	2	2
Length of Heat Sink Fin (LF)	Not Applicable	Not Applicable	11
Total Surface Area of TEG (Area)	9	6	9
Hot Side Substrate Surface Temperature (FST)	7	9	7

The sensitivity analysis results shown in Figure 5.1 has been summarized in Table 5.4. It can be concluded from the results obtained that the operating environmental parameters such as the hot and cold side ambient temperature together with the hot and cold side wind velocity do play a role in the mathematical model but they are not as critical as the construction parameters of the TEG. The thickness of the ceramic substrate that sandwiched the TE is the most important parameter in the mathematical model and this is consistent throughout the three scenarios. The

consistency also applies for both the thermal conductivity of the TE material and thermal conductivity of the cold side substrate respectively after the thickness of the ceramic substrate.

Most of the environmental parameters are not as critical as the construction of the TEG. Amongst them, the cold side ambient temperature stands out from the rest and this is due to the fact that the cold side ambient temperature helps in the dissipation of heat transferred from the hot side and by doing so, increasing the temperature difference across the TEG. The hot side ambient temperature, wind velocity on the cold side and wind velocity on the hot side followed on after the cold side ambient temperature.

The thermal conductivity of the material used on the hot side of the TEG is not as critical as the cold side as the heat is constantly supplied by the heat source whereas for the cold side, the material properties of the ceramic substrate will dictate how fast the heat can be dissipated away to create a larger temperature difference. Height of the TE sandwiched in between the ceramic substrate is much more critical when comparing it to the scenario with a heat sink on the cold side as the speed at which heat can be transferred to the other end of the TE will depend on the length of the TE as the longer it is, the more time is required for the heat to conduct towards the cold side whereas for the scenario with heat sink, is not that critical as the heat will be dissipated with the help of a heat sink which is of the same footprint as the TEG.

This sensitivity analysis test will be useful for users to better understand the performance of the TEG as well as their capabilities hence allowing users to make changes to either the operating environmental or construction parameters with limited resources, in order to achieve higher efficiency from the TEG.

5.4 Results and Discussion

The 12 input parameters used for the ANN model can be categorized into two areas, the operating environmental parameters and construction parameters of the TEG. The operating environmental parameters are the parameters that include the surrounding temperature as well as the wind velocity that will aid in the dissipating of heat from the TEG. Next the construction parameters of the TEG will include the material that is used to manufacture the TEG, as well as its dimensions, which will affect the rate of heat transfer across the TEG.

To perform the experiment, a set of values, which is within the range of the data used to train the ANN model, have been input into the model to derive the output voltages that the TEG can generate. Most of the values related to the construction parameters of the TEG are provided by the manufacturer specification sheet and the operating environmental parameters are obtained from the environmental parameters that the TEG is operating in. The parameters are shown in Table 5.5.

Table 5.5. Default parameters used for validation

Parameter	Range
Hot Side Ambient Temperature	293.15K
Cold Side Ambient Temperature	293.15K
Hot Side Wind Velocity	0.1m/s
Cold Side Wind Velocity	0.1m/s
Thickness of TEG Substrate	0.001m
Thermal Conductivity of Hot Side Substrate	2W/m ²
Thermal Conductivity of Cold Side Substrate	2W/m ²
Height of PN Junction	0.0025m
Thermal Conductivity of PN Junction	1.3W/m ²
Length of Heat Sink Fin	0.006m
Total Surface Area of TEG	0.0009m ²
Hot Side Substrate Surface Temperature	303.15K

5.4.1 Operating Environmental Parameters

There are four operating environmental parameters that have been taken into consideration for the mathematical model. They are the hot and cold side ambient temperature as well as the hot and cold side wind velocity.

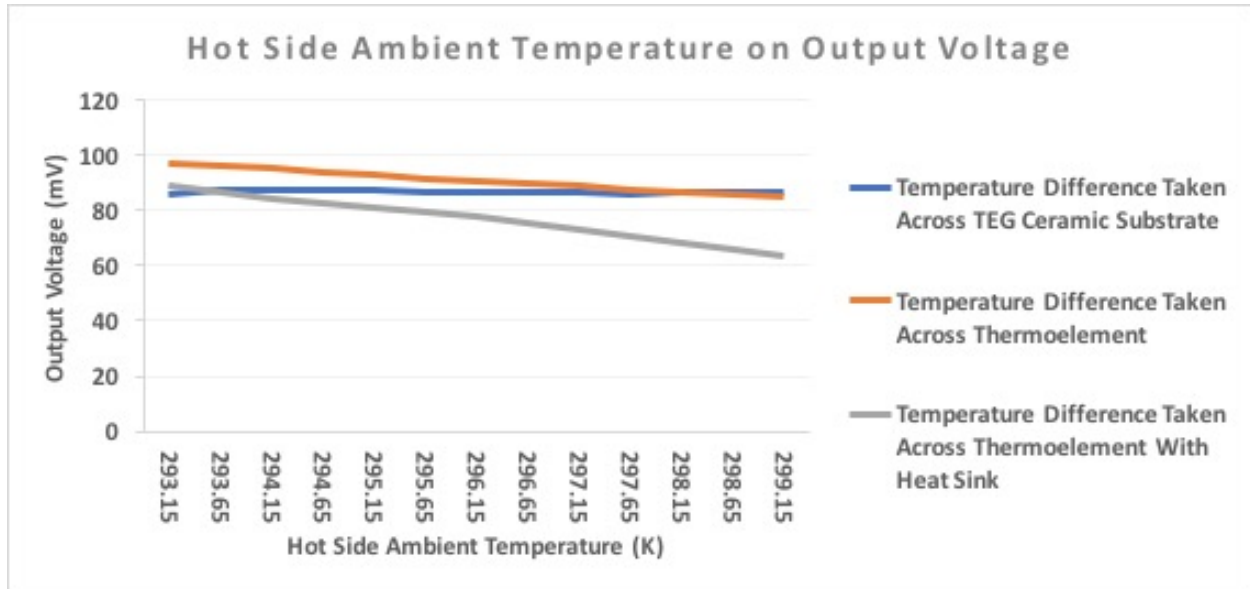


Figure 5.11 Hot side ambient temperature effects on output voltage

Figure 5.11 shows the output voltage pattern when the hot side ambient temperature increases from 293.15K to 299.15K. For the first scenario where the temperature gradient is taken from the ceramic substrate surface of the TEG, there is a slight increase of approximately 2% in the output voltage. This is because the temperature of the ceramic substrate increase under the influence of the ambient temperature and as the temperature gradient of the TEG is taken from the surface of the ceramic substrate, the voltage increases. The ambient temperature loss its effect on the hot side ceramic substrate surface after a 2K increment. The scenario where temperature gradient is taken from the TE, has a slight drop in the output voltage as the hot side ambient temperature increases. This shows that the increment in the ambient temperature has no effect on the TE temperature gradient as the TE is being separated away from the ambient temperature by the ceramic substrate hence the temperature gradient continues to reduce and therefore the output

voltage. For the scenario where temperature gradient is taken from the TE with the aid of a heat sink, there is a drop of approximately 3% in the output voltage as the temperature gradient increases. This could be because the heat on the cold side could not be dissipated effectively as the ambient temperature and wind velocity on the cold side remains the same hence the drop in the output voltage.

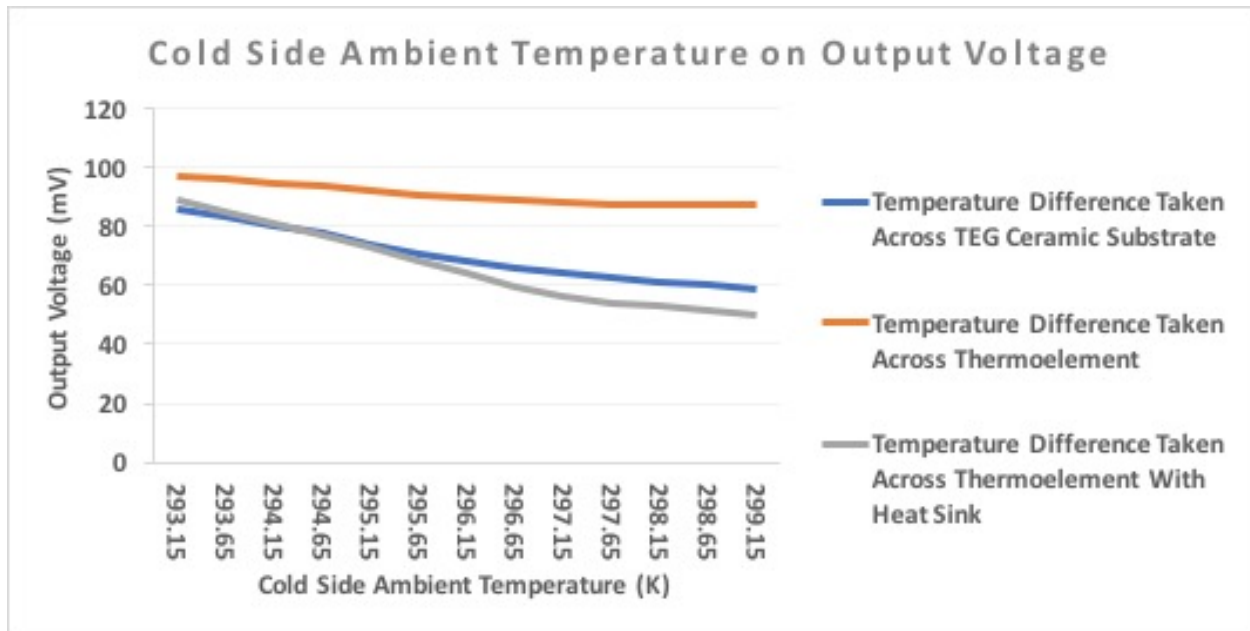


Figure 5.12 Cold side ambient temperature effects on output voltage

Figure 5.12, shows that as the cold side ambient temperature starts to increase, there is a drop in the output voltage generated across all the scenario with the output voltage generated from the temperature gradient taken from the TE with the aid of a heat sink. This is because as the ambient temperature increases, it hinders the dissipation of heat from the heat sink fins hence causing a drop in the temperature measured across the TE. For the scenario that generates the output voltage from the temperature taken from the ceramic substrate of the TEG, as the ambient temperature on the cold side increases, it affects the ceramic substrate surface temperature on the cold side too hence reducing the temperature gradient measured across both the ceramic substrate surface. For the temperature gradient taken at the TE, there isn't any significant change in the output voltage as it is shielded from the ceramic substrate, the same for the previous example

where the increment on the hot side ambient temperature do not have much influence on the output voltage.

As shown in Figure 5.11 and Figure 5.12, it can be concluded that with the ambient temperature fluctuation on the hot and cold side of the TEG, it will not greatly affect the generation of output voltage from the TEG under the three different scenarios. Both only showed a slight decrease in the output voltage of the TEG as the hot side and cold side ambient temperature increases respectively. When incorporating the change with the other environmental parameters such as an increase in the wind velocity on the cold side of the ceramic substrate surface or having a higher thermal conductivity for the ceramic substrate material, there could be some slight increment to the output voltage generated.

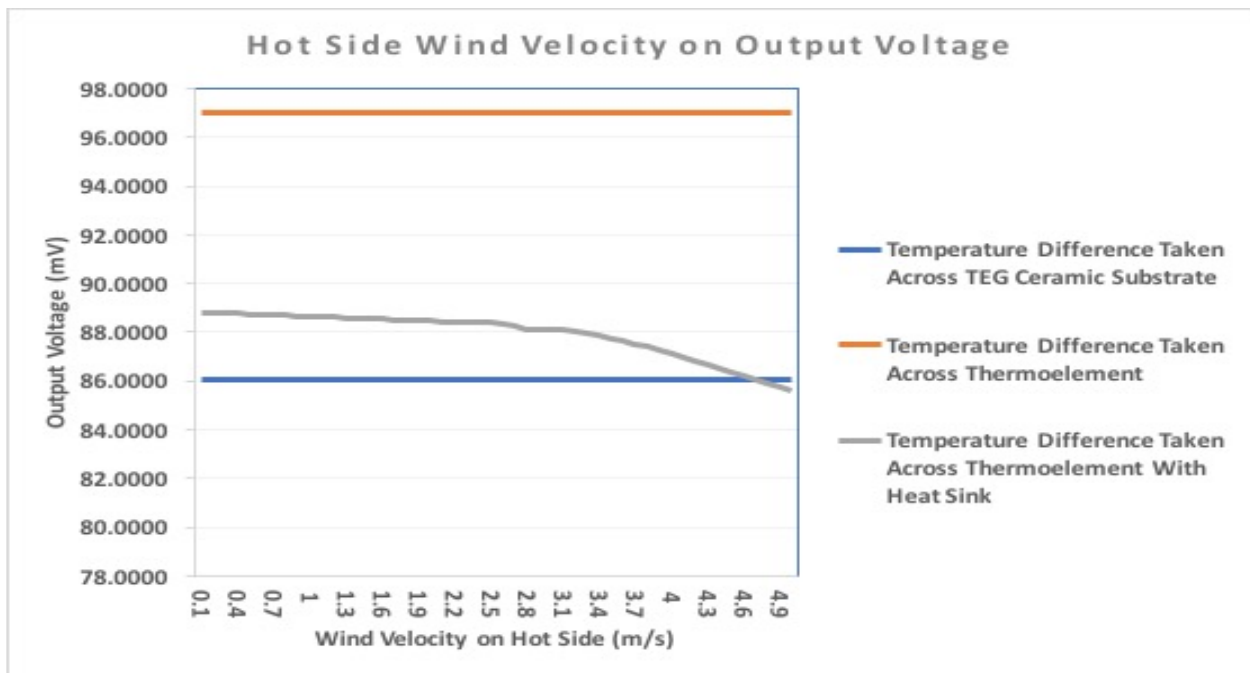


Figure 5.13 Hot side wind velocity effect on output voltage

Figure 5.13 shows the output voltage trending with the gradual increment of the hot side wind velocity. As shown, there isn't any significant changes to two scenarios when temperature difference is taken across the TEG ceramic substrate and across the TE as the heat source is assumed to be affixed onto the hot side ceramic substrate and that the wind velocity will not be able

to dissipate away the heat on hot side ceramic substrate also for the temperature gradient taken at the TE, it will be shielded away from the wind velocity. The scenario with temperature taken across the TE together with the heat sink shows an insignificant drop in the output voltage when the wind velocity reaches 3.2 m/s. This can be related back to what was encountered in Figure 5.12 where the heat sink instead of helping to dissipate away the heat, hinders the process hence leading to a decrease in the temperature difference across the TEG which affects the output voltage.

For the increment in the wind velocity on the cold side as shown in Figure 5.14, the only scenario that reacted to the change in terms of the output voltage is the scenario when temperature gradient is measured across the TE together with a heat sink. In this case, the heat sink will be able to perform its function unlike the other scenario where it hinders the dissipation of heat as the wind velocity and ambient temperature remains the same. As the wind velocity increases, the heat sink will help to remove some heat from the cold side ceramic substrate but it has also been noted that there is a dip in the output voltage when the wind velocity reached approximately 2.8m/s.

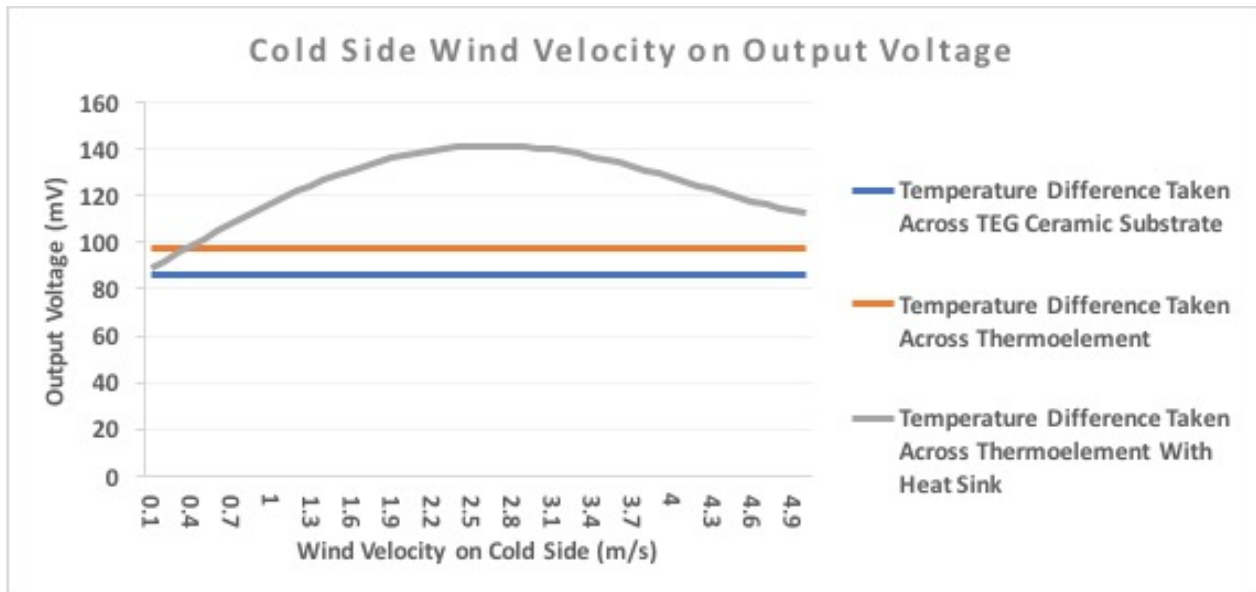


Figure 5.14 Cold side wind velocity effect on output voltage

The dip in the output voltage is due to the length of the fins of the heat sink. When the fin reaches its maximum efficiency to dissipate heat away to its surrounding environment, it stops functioning hence leading to a buildup of heat on the cold side [94], leading to a drop in the temperature gradient and hence the drop in output voltage.

This example indicates that having a high wind velocity might not be always useful to help dissipate the heat into the surrounding environment and it will only be useful when used with the correct parameters.

5.4.2 TEG Construction Parameters

The TEG construction parameters comprise of both material and physical aspects of the TEG. They are the properties of the material used, as well as the dimensions and height of the TEG and TE respectively. For the scenario with the heat sink, the length of the heat sink fins will also be discussed.

The TEs are all sandwiched in between two layers of ceramic substrate. Therefore, it is crucial to find out how various parameters of the ceramic substrate can affect the generation of energy from the TEG.

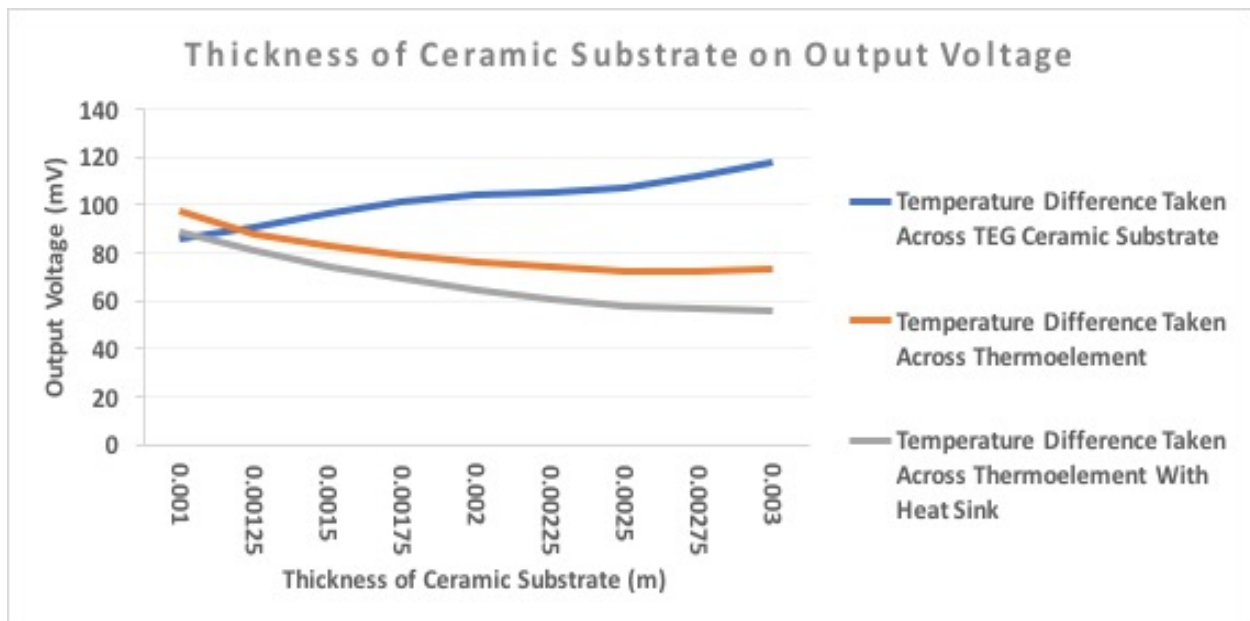


Figure 5.15 Thickness of the ceramic substrate effect on output voltage

The thickness of the ceramic substrate will affect how heat is being transferred into and out of the TE. Figure 5.15, shows the relationship of the thickness of the TEG and the amount of energy that is being generated from the TEG. This thickness is assumed to be the same for both ceramic

substrates that sandwich the TE.

The gradual increment in the thickness of the ceramic substrate for the TEG will affect how heat is being transferred across the TEG as the ceramic substrate is used to sandwich and transfer the heat to the TE. For the first scenario where the temperature gradient is taken from ceramic substrate surface of the TEG, the increment in the thickness of the ceramic substrate actually helps to increase the output voltage gradually. This is because as the thickness of the ceramic substrate increase, the heat transfer from the hot side of the TEG will be slowed down as heat will need to penetrate a thicker material to reach to the cold side of the TEG. This will therefore create a larger temperature difference across the TEG which in turn increase the output voltage.

For the other two scenarios, as temperature gradient is taken from the TE itself, being sandwich by thick ceramic substrate on both the hot and cold side of the TEG will reduce the temperature gradient as heat will take time to penetrate through the hot side to reach the TE as well as heat will take a while to dissipate from the TE to the cold side of the TEG. This will eventually lead to a small temperature difference across the TE which resulted in the low output voltage as shown in Fig 5.15. Heat sink for this case doesn't seems to help with the generating of energy instead a hindrance.

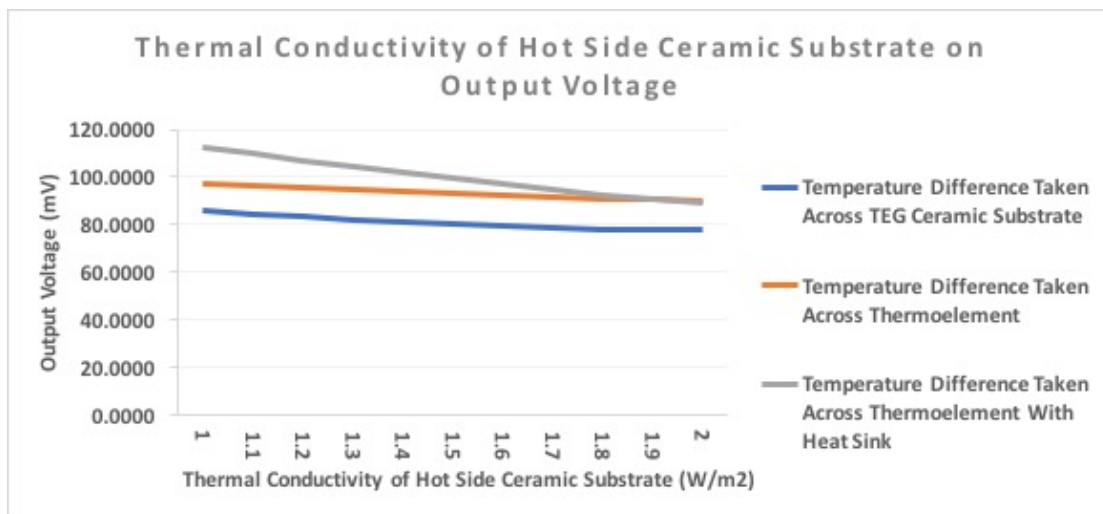


Figure 5.16 Thermal conductivity of the ceramic substrate on hot side effect on output voltage

Ceramic substrate material properties will influence the output voltage of the TEG. As the thermal conductivity of the ceramic substrate increases, it will affect the temperature gradient

hence the output voltage from the TEG. When temperature difference across the TEG is taken from both the ceramic substrate surface on the hot and cold side, there is a gradual decrease in all the three output voltages as the thermal conductivity of the ceramic substrate material on the hot side increases. With the high thermal conductivity value, heat gets transferred across the ceramic substrate on the hot side at a faster rate but as the cold side substrate thermal conductivity still remains at the minimum, most of the heat gets trapped and are not able to dissipate through the cold side ceramic substrate hence decreasing the temperature gradient across the TEG. As the ambient temperature and the wind velocity on the cold side remains unchanged, the heat sink will not be able to dissipate the heat fast enough hence the highest decline in the output voltage is from the temperature gradient measured at the TE and with the aid of a heat sink.

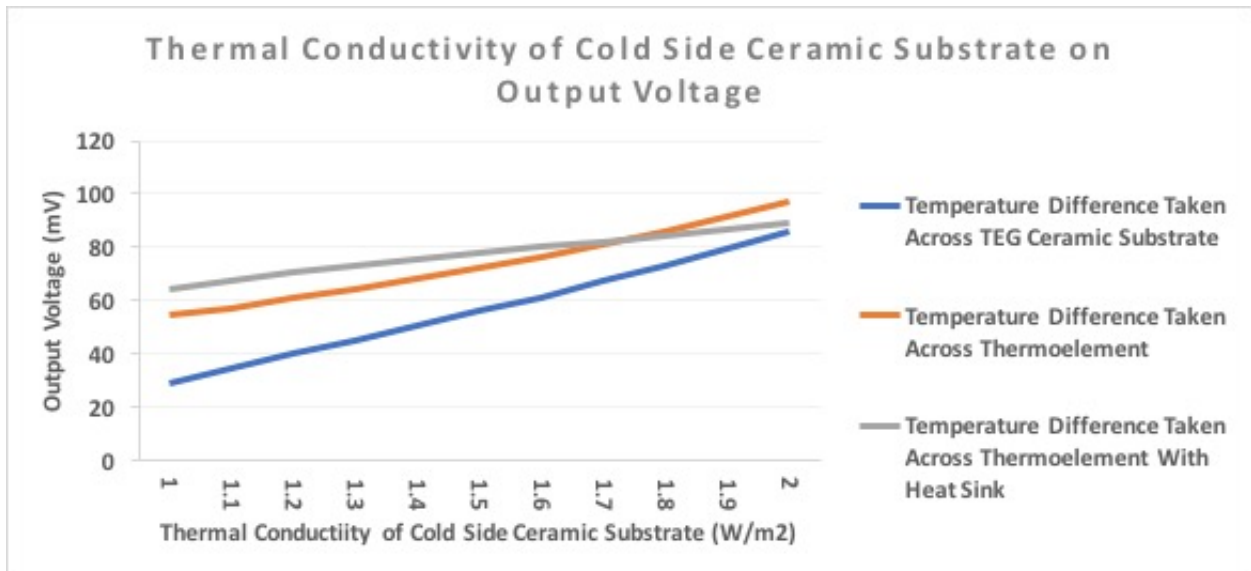


Figure 5.17 Thermal conductivity of the ceramic substrate on cold side effect on output voltage

Figure 5.17 shows an increase in the output voltage trending when thermal conductivity on the cold side ceramic substrate increases. With a good thermal conductivity on the cold side ceramic substrate, heat transferred from the hot side ceramic substrate will be able to dissipate into the surrounding environment at a faster rate hence creating a large temperature gradient across the TEG.

The steepest increment is from the scenario where the temperature gradient is taken from

the surface of the two ceramic substrates. The least output voltage increment is from the scenario where the temperature is taken from the TE with the aid of a heat sink as the heat sink tends to hinder the heat transfer from the cold side ceramic substrate with default ambient temperature as well as wind velocity.

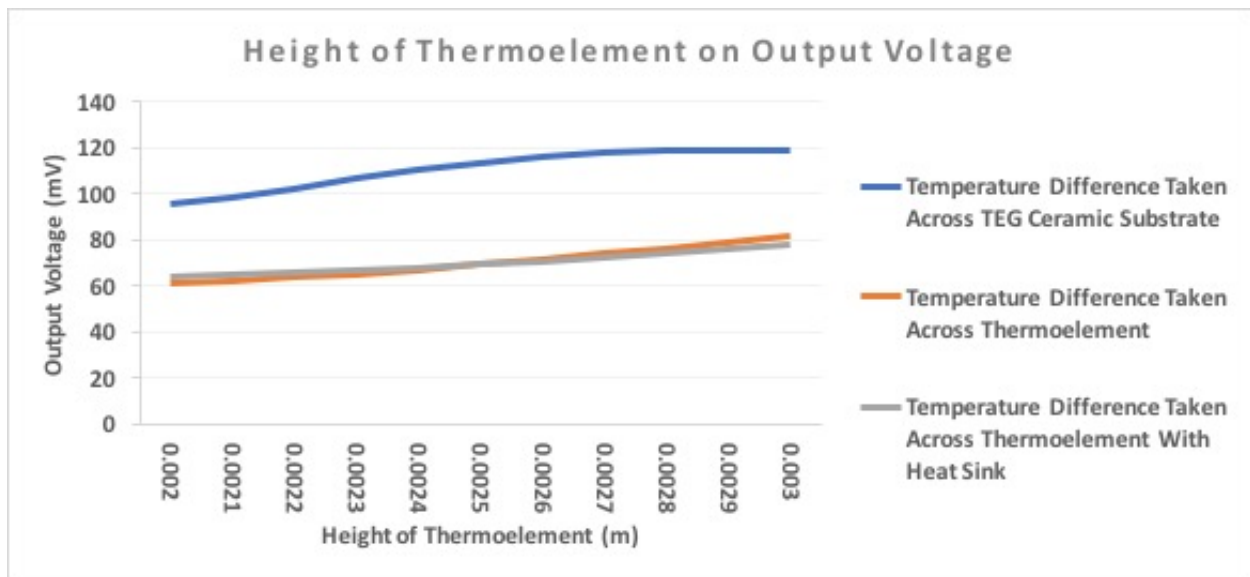


Figure 5.18 Height of TE effect on output voltage

As the height of the TE increases, the heat generated from the hot side of the TEG will take a longer time to transfer over to the cold side. As the heat transfer towards the cold side duration increases, the cold side heat on the ceramic substrate surface will have ample time to dissipate the existing heat on its surface into the surrounding environment, in the process, creating a large temperature gradient across the TE junction which correlates to the increment in the output voltage as shown in Figure 5.18.

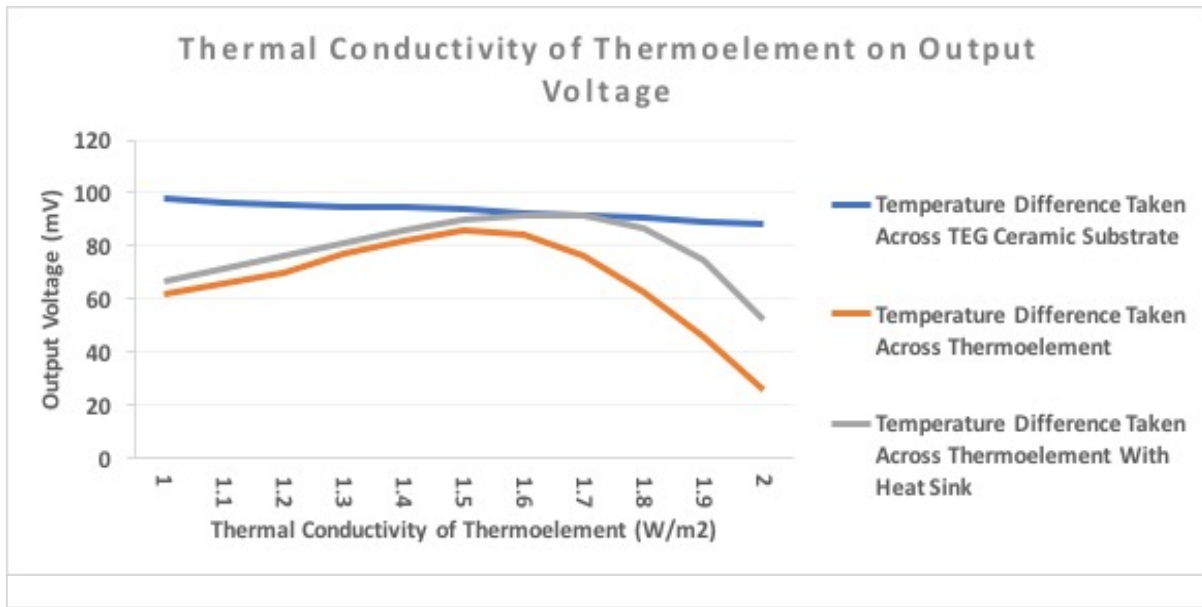


Figure 5.19 Thermal conductivity of TE effect on output voltage

The TE being the main energy generating platform for the TEG will dictate the output voltage generated hence the material that the TE is made of plays an important role in the prediction of the output voltage. Figure 5.19 shows the output voltage trending for the various scenario as the thermal conductivity of the TE increases.

When temperature gradient is taken from the surface of the ceramic substrate, the drop in the output voltage is negligible as temperature is not taken from the TE but rather the surface of the ceramic substrate. For both temperature taken at the TE with and without the use of a heat sink, there is a significant increase and drop in the output voltage. For the scenario when temperature gradient is taken from the TE without the use of the heat sink, there is a gradual increase in the output voltage as the thermal conductivity increases. This increment in the output voltage will reach a peak when the thermal conductivity is at approximately 1.5W/m^2 and started to decline. As the height of the TE is at its default value, the transfer of heat from the hot side will be expedited hence causing the entire TE to heat up which leads to a low temperature gradient.

For the scenario where temperature gradient is taken at the TE with the aid of a heat sink, it has the same trending pattern as the earlier scenario discussed above but with the help of a heat sink, the decline of the output voltage will start at around 1.6W/m^2 .

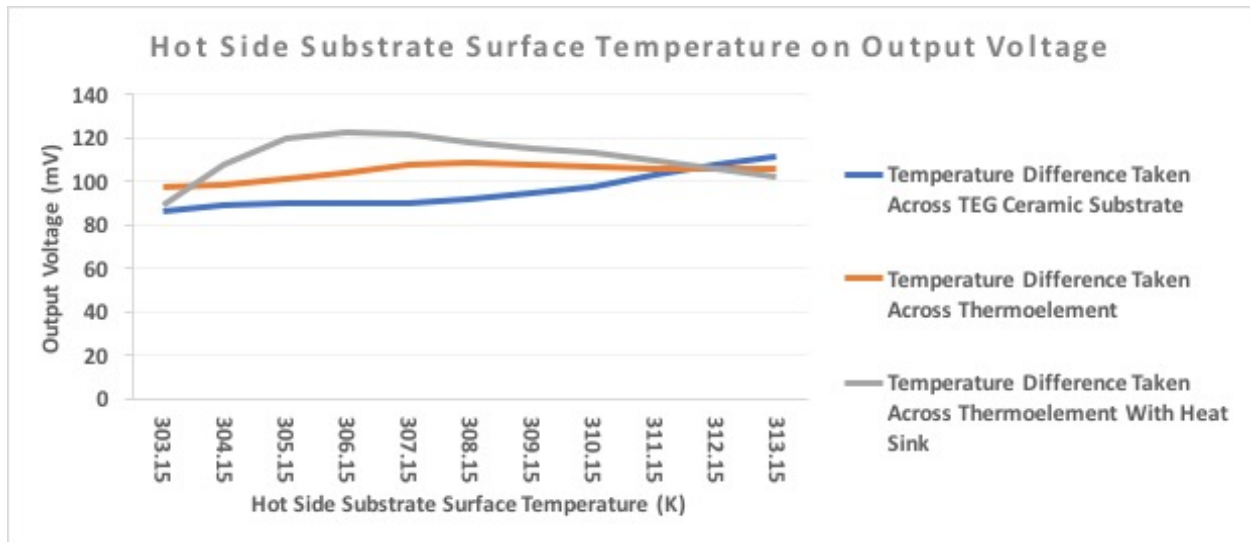


Figure 5.20 Input heat on hot side surface effect on output voltage

Figure 5.20 shows the output voltage pattern with increment of the hot side surface temperature on the TEG. For the scenario where temperature gradient is taken from both the hot and cold side of the ceramic substrate surfaces, there is a gradual increase in the output voltage as temperature for this scenario is taken from the surface of the ceramic substrate. This can also be because the environmental parameters as well as construction parameters are all at its default value hence the transfer of heat is not as efficient therefore when the heat source temperature increases, it creates a larger temperature difference across the TEG.

For the scenario where the temperature gradient is taken from the TE without the aid of a heat sink, there is a slight increase in the output voltage. The increment is slow as the heat on the surface of the ceramic substrate will take time to reach the TE and will decrease when the heats up. When used with a heat sink, the output voltage will increase as the heat sink will help to remove the excess heat from the TE but there is a limitation to the performance of the heat sink. Once the heat saturates at the heat sink fins, the temperature gradient will be small and hence a low output voltage.

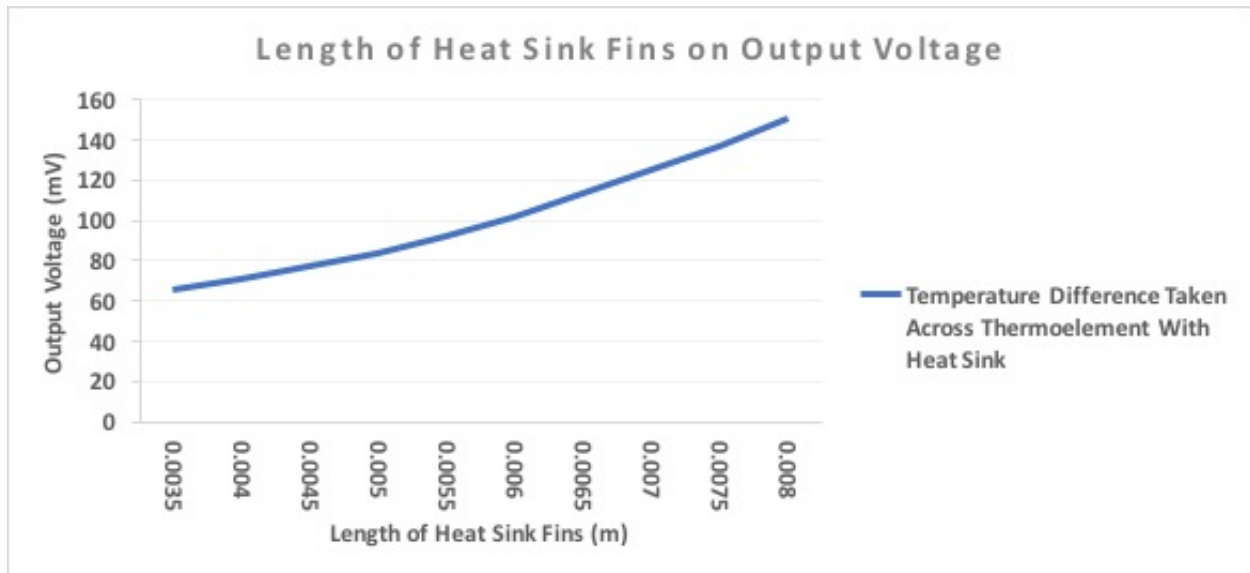


Figure 5.21 Length of heat sink fin effect on output voltage

Most of the scenarios that were discussed in the previous session indicated that most of the time, the heat sink is a hindrance to the dissipation of heat from the cold side to the surrounding environments. The dissipation of heat will depend on the number of fins incorporated into the design of the heat sink as well as its height.

There is only one scenario shown as the other two scenarios do not have a heat sink attached and therefore no need for the output voltage trend. The results also indicated that as the height of the fins increase, it has a bigger surface area and can be used to help dissipate more heat from the cold side surface which will create a higher temperature gradient and therefore higher output voltage.

5.5 Summary

This chapter discussed the process of achieving various results from the mathematical model generated and the prediction of output voltages generated by the TEG using various input parameters. They are broadly categorized as operating environmental parameters and TEG construction parameters. The training process of the ANN model was also presented to ensure that the ANN model can predict the output voltages with a certain level of accuracy.

The analysis of the results shown in this chapter are set to change. This is because changes

in any of the input parameters and those input parameters with higher sensitivities in the mathematical model has been identified through the sensitivity analysis carried out. The sensitivity function will be extremely useful to users with limited resources as the identification of input parameters with higher sensitivities will also allow the users to focus and allocate their resources on these inputs parameters that will increase or reduce the output voltage significantly.

The various graphs shown above co-relate the relationship between the input parameter to the output voltage generated for this experiment. This ANN model will be useful for the prediction of the energy output as the behavior and efficiency of the TEG will change constantly according to the operating environmental parameters, or the construction of the TEG. Thus, it is important to understand this relationship as it allows users to choose the right TEG to be used for the application required which will in return, boost the efficiency of the TEG.

Chapter 6 Conclusion and Future Work

The materials that are used for the construction of the TEG do not seem to be a competitive solution for renewable energy power generation. Even for a material with a high ZT, the efficiency of the TEG is still not as competitive as compared to other renewable energy sources currently available on the market. This direction of constant material research to improve the TEG has not achieved any significant breakthrough in the recent years. As such, an alternative form or method to improve the optimization and designing of TEG has been suggested.

In this work, a novel mathematical model used to predict the energy generated by a TEG has been developed. This mathematical model optimizes and determines the output voltage generated by the TEG system designed for a given set of operating environmental and construction parameters. Three sets of scenarios, output voltage generated based on the temperature difference measured across both ceramic substrate surface according to the manufacturer's specification sheet, output voltage generated with environmental parameters based on temperature difference measured across the thermoelement and output voltage measured across the thermoelement with environmental parameters and the aid of heat sink were studied and validated in this research.

Many of the TEG bought commercially off the shelves are often dismissed as inaccurate because the output voltages obtained from the manufacturer's specification sheet are often out of the specified range because the values are usually generated from a laboratory or vacuum environment. Therefore, the results obtained are often inaccurate and of unknown precision when used by a TEG application in the real world. Attention has been focused on the accuracy of the mathematical model used to predict the output voltage generated by using finite volume method. This is to calculate the heat transfer across the TEG. Data obtained using the mathematical model will be used to train the ANN model for the prediction of output voltage by the end user of the TEG. Two coupled neural networks were also used in the ANN model to ensure the degree of reliability of each output result generated by the model.

This research has identified the relationship of the environmental parameters that the TEG application is operating in, as well as the construction of the TEG with the output voltage generated. It has been concluded from the three scenarios that was carried out on the TEG that, the operating environment although can influence the output voltage generated by the TEG, it is still not as critical as the construction material of the TEG. It has been shown by the experiments carried

out that there is a larger difference in output voltage generated when there is a change in the thermal conductivity of the ceramic substrate on both the hot and cold side of the TEG. This refers specifically the thermal conductivity on the cold side substrate.

The physics involved in this research, specifically from the surrounding environmental parameters such as conduction, convection and radiation of heat and wind velocity across the TEG, has increased the complexity to derive the output voltage generated. For these reasons, it is now even harder to have a good correlation for prediction of the temperature gradient across the TEG when compared to those TEG that considered the operating environmental parameters as a separate phenomenon.

It has been observed in this research that for a given TEG bought commercially off the shelves and with the inclusion of environmental conditions such as the TEG material used and wind velocity on the cold side of the TEG, the output voltage produced by the TEG has a variation when compared to the values obtained from the manufacturer's specification sheet. Furthermore, when used with a heat sink on the cold side ceramic substrate of the TEG, the output voltage generated by the TEG will be significantly higher as compared to those without heat sink. However, this increment will decrease overtime due to the heat dissipation limitation of the heat sink given its size.

An ANN model has been trained and validated using the data set generated by the mathematical model. This ANN model has been packaged into a programme with an interactive GUI that allows end users to predict the output voltage of a TEG when given the operating environmental parameters, as well as its construction and material usage. This programme will allow the users to predict an input parameter when provided with the output voltage required. This function will be useful for the end users to identify the best fit input parameter required to generate the output voltage required.

Sensitivity analysis of the input parameters has been incorporated into the program too. This will allow end users to identify the input parameter that has the most influence on the output voltage. All 12 inputs will be ranked according to their sensitivity. Should there be a limitation in the budget of the TEG application, this function will be useful to allow user to increase or reduce the output voltage by changing only one input parameter rather than a few, especially when there are challenges such as financial and space constrains.

This thesis contributes to the existing body of knowledge about TEG with original works

and experiments carried out using various novel ideas incorporated into the model. The results obtained come from testing and characterizing the performance of the TEG. This programme will allow a flexible adaptation to both the input parameters as well as output parameters.

6.1 Future Work

In this work, a novel TEG model was developed and a preliminary set of studies were performed with the use of actual experimental set up. As discussed, several of the TEG system design aspects (i.e. Sensitivity analysis) have been included into the model as well as the design optimization itself. However further refinements to the novel TEG model and additional design optimization studies are necessary to further maximize the efficiency of the TEG. This is critical especially when it is used in an environment where the environmental parameters which the TEG is operating in is taken into consideration.

In general, all TE properties varies with temperature. Thus, precision in TEG output measurement requires precise temperature measurement even with the use of the novel TEG model. To obtain an accurate value, precise input values must be used.

From the sensitivity analysis results obtained from Table 5.4, it has been shown that thermal conductivity of the TEG material plays a critical role in the output voltage generated. Through heat transfer studies performed, thermal conductivity has turned out to be one of the most difficult to analyze among TE measurement.

Principal errors of direct methods are caused by thermal losses, thermal resistivity of interfaces and available sample size. Therefore, to maximize the efficiency of the TEG, a library of commercially available TEG with an accurate measurement of the thermal conductivity properties of materials, used for the construction of the TEG, needs to be incorporated into the novel TEG model. The need to calculate output voltage for anisotropic thermoelement must be used when interacting with operating environmental parameters.

6.1.1 Standardization of Thermoelectric Generator Material Specification Library

The standardization of the material properties for the TEG that is to be used in the measurements of the TEG materials cannot be overvalued, since without it the commercialization of research

ideas and device will be threatened. This can undermine the green energy generation capabilities of TEG. In the context of standardization, it means to implement a common set of techniques and customized procedures while leveraging on the novel TEG model to set guidelines. This is done to have a consistent accuracy levels of output results.

In the case of TEG and the heat sink materials, heat removal on the cold side, together with the environmental parameters that the TEG is operating in, plays a key role in TEG research. Evolutionary improvement of TEG materials requires a continuous feedback cycle between preparation and characterization so as to assess the influence of variation in material composition. Together with its interaction with the operating environmental parameters on the output energy obtained from the TEG, standardization and customization in TE appears as a prerequisite to enter stable interaction with large markets. This would eventually be established a stable demand in TEG.

Prior to the development of this novel TEG model, the conventional TE measurement technology, which is done in a vacuum environment, has been used on a laboratory scale for decades. However, it has yet to achieve a level of commercial availability and distribution due to the inaccuracy in their output values when compared to real life scenarios.

With the implementation of a standardize material thermal conductivity library used in the novel TEG model, the prediction of the output voltage generated by the TEG will be more accurate and precise overtime.

6.1.2 Calculation for Anisotropic Thermolement

Temperature difference creates a potential electric field in a homogeneous isotropic medium. However, to produce an emf, a non-conservative electric field is required. Therefore, only an inhomogeneity can create the TE power in an isotropic material.

In general, junctions between two different materials provide the required inhomogeneity. Due to the presence of the transverse component of the TE field, the occurrence of a thermos-emf even in a thermoelectrically homogeneous medium, is possible. The TE energy converter which utilizes the transverse thermos-emf is an anisotropic medium commonly referred to as the anisotropic thermoelement (AT).

In recent years, there has been an increase in the use of AT for energy generation. The

energy conversion efficiency using TE technology is mainly dominated by the materials ZT. Currently, advanced materials such as Bi_2Te_3 , PbTe, skutterudites, clathrates, Mg_2Si , Half-heusler have been developed to increase the current ZT value.

It has been shown that a high ZT of 2.6 has been achieved at 923K in SnSe single crystal, far above the values of other state of the art materials. SnSe is a typical narrow band gap semiconductor and belong to Pnma space group with orthorhombic structure at room temperature. It derives from the NaCl-type structure. The tin atoms are surrounded by highly distorted octahedron of selenium atoms to form a zig-zag structure.

The differences and advantages of using AT in comparison with the usual TEG is that the geometrical factor is contained in the expression for the EMF of an AT. The thermo-emf of the AT depends on the geometry of the sample, whereas the thermo-emf of the thermocouple does not.

This dependence gives an important advantage to the AT whereby the thermo-emf can be increase by increasing the length or decreasing the sample thickness. This method of increasing the thermo-emf appears to be much simpler than the traditional method of combining the P and N type semiconductors by linking the branches in series. Moreover, the AT has no junction. This is the other important advantage that results in an increased reliability. Thus it is good to recommend ways to better incorporate the calculation of output voltage for AT when taking into consideration of the operating environmental parameters.

6.1.3 Unsupervised Learning

Through literature researches, it has been shown that using unsupervised learning is beneficial to learn for better data representations in Deep Learning architectures, including multi-layer neural network and deep belief networks. They do so particularly by capitalizing on the availability of large amounts of unlabeled data hence for future work, the use of unsupervised learning will be explored.

These future works planned will provide the TEG users with a more precise and reliable means to understand the generation of energy from a TEG under various environmental circumstances. It has and will continue to open up more opportunities for the advancement of the TEG research.

Appendix A

This set of codes will present user with the options to choose on the option to train a new set of data or to execute the program to predict the output voltage of the TEG.

```
function varargout = Start(varargin)
% START MATLAB code for Start.fig
% Begin initialization code
gui_Singleton = 1;
gui_State = struct('gui_Name',       mfilename, ...
                  'gui_Singleton',   gui_Singleton, ...
                  'gui_OpeningFcn',  @Start_OpeningFcn, ...
                  'gui_OutputFcn',  @Start_OutputFcn, ...
                  'gui_LayoutFcn',   [], ...
                  'gui_Callback',    []);

if nargin && ischar(varargin{1})
    gui_State.gui_Callback = str2func(varargin{1});
end

if nargout
    [varargout{1:nargout}] = gui_mainfcn(gui_State, varargin{:});
else
    gui_mainfcn(gui_State, varargin{:});
end
% End initialization code
% --- Executes just before Start is made visible.
function Start_OpeningFcn(hObject, eventdata, handles, varargin)
% Choose default command line output for Start
handles.output = hObject;
ah = axes('unit', 'normalized', 'position', [0 0 1 1]);
% import the background image and show it on the axes
bg = imread('Background.jpg'); imagesc(bg);
% prevent plotting over the background and turn the axis off
axis off
% Update handles structure
guidata(hObject, handles);
% --- Outputs from this function are returned to the command line.
function varargout = Start_OutputFcn(hObject, eventdata, handles)
```

```

% Get default command line output from handles structure
varargout{1} = handles.output;
% --- Executes on button press in pushbutton1.
function pushbutton1_Callback(hObject, eventdata, handles)
% --- Executes on button press in pushbutton2.
function pushbutton2_Callback(hObject, eventdata, handles)
close(Start);
Train_GUI();
% --- Executes on button press in pushbutton3.
function pushbutton3_Callback(hObject, eventdata, handles)
close(Start);
Main_GUI();
% --- Executes on button press in pushbutton4.
function pushbutton4_Callback(hObject, eventdata, handles)
close(Start);
clear all;
close all;
clc;

```

Appendix B

This code present user with the interface to input the 12 parameters required for the analysiing of the output voltage generated by the TEG. Range of values will be controlled by this set of codings.

```
function varargout = Main_GUI(varargin)
% MAIN_GUI MATLAB code for Main_GUI.fig
% Begin initialization code
gui_Singleton = 1;
gui_State = struct('gui_Name',       mfilename, ...
                  'gui_Singleton',   gui_Singleton, ...
                  'gui_OpeningFcn',  @Main_GUI_OpeningFcn, ...
                  'gui_OutputFcn',   @Main_GUI_OutputFcn, ...
                  'gui_LayoutFcn',   [], ...
                  'gui_Callback',    []);
if nargin && ischar(varargin{1})
    gui_State.gui_Callback = str2func(varargin{1});
end
if nargout
    [varargout{1:nargout}] = gui_mainfcn(gui_State, varargin{:});
else
    gui_mainfcn(gui_State, varargin{:});
end
% End initialization code
% --- Executes just before Main_GUI is made visible.
function Main_GUI_OpeningFcn(hObject, eventdata, handles, varargin)
% Choose default command line output for Main_GUI
handles.output = hObject;
ah = axes('unit', 'normalized', 'position', [0 0 1 1]);
% import the background image and show it on the axes
bg = imread('Background.jpg'); imagesc(bg);
% prevent plotting over the background and turn the axis off
axis off
outputt=[];
handles.outputt=outputt;
% Update handles structure
guidata(hObject, handles);
```



```

% --- Outputs from this function are returned to the command line.
function varargout = Main_GUI_OutputFcn(hObject, eventdata, handles)
% Get default command line output from handles structure
varargout{1} = handles.output;
% --- Executes on button press in pushbutton1.
function pushbutton1_Callback(hObject, eventdata, handles)
% --- Executes on button press in pushbutton2.
function pushbutton2_Callback(hObject, eventdata, handles)
% --- Executes on button press in pushbutton3.
function pushbutton3_Callback(hObject, eventdata, handles)
% --- Executes on button press in pushbutton4.
function pushbutton4_Callback(hObject, eventdata, handles)
% --- Executes on button press in pushbutton5.
function pushbutton5_Callback(hObject, eventdata, handles)
% --- Executes on button press in pushbutton6.
function pushbutton6_Callback(hObject, eventdata, handles)
% --- Executes on button press in pushbutton7.
function pushbutton7_Callback(hObject, eventdata, handles)

% --- Executes on button press in pushbutton8.
function pushbutton8_Callback(hObject, eventdata, handles)
% --- Executes on button press in pushbutton9.
function pushbutton9_Callback(hObject, eventdata, handles)
% --- Executes on button press in pushbutton10.
function pushbutton10_Callback(hObject, eventdata, handles)
% --- Executes on button press in pushbutton11.
function pushbutton11_Callback(hObject, eventdata, handles)
% --- Executes on button press in pushbutton12.
function pushbutton12_Callback(hObject, eventdata, handles)
% --- Executes on button press in pushbutton13.
function pushbutton13_Callback(hObject, eventdata, handles)
function edit1_Callback(hObject, eventdata, handles)
handles.phi = (get(hObject, 'String'));
outputt=handles.outputt;
outputt(1)=str2num(handles.phi);
if((outputt(1)>50) | (outputt(1)<20))
warningMessage = sprintf('Must Be Between 20-50');
uiwait(warndlg(warningMessage)); % Pop up message.

```

```

end;
handles.outputt=outputt;
guidata(hObject, handles);
% --- Executes during object creation, after setting all properties.
function edit1_CreateFcn(hObject, eventdata, handles)
if ispc && isequal(get(hObject,'BackgroundColor'),
get(0,'defaultUicontrolBackgroundColor'))
    set(hObject,'BackgroundColor','white');
end
function edit3_Callback(hObject, eventdata, handles)
handles.phi = (get(hObject,'String'));
outputt=handles.outputt;
outputt(2)=str2num(handles.phi);
if((outputt(2)>50) | (outputt(2)<20))
warningMessage = sprintf('Must Be Between 20-50');
uiwait(warndlg(warningMessage)); % Pop up message.
end;
handles.outputt=outputt;
guidata(hObject, handles);
% --- Executes during object creation, after setting all properties.
function edit3_CreateFcn(hObject, eventdata, handles)
if ispc && isequal(get(hObject,'BackgroundColor'),
get(0,'defaultUicontrolBackgroundColor'))
    set(hObject,'BackgroundColor','white');
end
function edit4_Callback(hObject, eventdata, handles)
handles.phi = (get(hObject,'String'));
outputt=handles.outputt;
outputt(3)=str2num(handles.phi);
if((outputt(3)>5) | (outputt(3)<0.1))
warningMessage = sprintf('Must Be Between 0.1-5');
uiwait(warndlg(warningMessage)); % Pop up message.
end;
handles.outputt=outputt;
guidata(hObject, handles);
% --- Executes during object creation, after setting all properties.
function edit4_CreateFcn(hObject, eventdata, handles)

```

```

if ispc && isequal(get(hObject,'BackgroundColor'),
get(0,'defaultUicontrolBackgroundColor'))
    set(hObject,'BackgroundColor','white');
end
function edit5_Callback(hObject, eventdata, handles)
handles.phi = (get(hObject,'String'));
outputt=handles.outputt;
outputt(4)=str2num(handles.phi);
if((outputt(4)>5) | (outputt(4)<0.1))
warningMessage = sprintf('Must Be Between 0.1-5');
uiwait(warndlg(warningMessage)); % Pop up message.
end;
handles.outputt=outputt;
guidata(hObject, handles);
% --- Executes during object creation, after setting all properties.
function edit5_CreateFcn(hObject, eventdata, handles)
if ispc && isequal(get(hObject,'BackgroundColor'),
get(0,'defaultUicontrolBackgroundColor'))
    set(hObject,'BackgroundColor','white');
end
function edit6_Callback(hObject, eventdata, handles)
handles.phi = (get(hObject,'String'));
outputt=handles.outputt;
outputt(5)=str2num(handles.phi);
if((outputt(5)>0.005) | (outputt(5)<0.001))
warningMessage = sprintf('Must Be Between 0.001-0.005');
uiwait(warndlg(warningMessage)); % Pop up message.
end;
handles.outputt=outputt;
guidata(hObject, handles);
% --- Executes during object creation, after setting all properties.
function edit6_CreateFcn(hObject, eventdata, handles)
if ispc && isequal(get(hObject,'BackgroundColor'),
get(0,'defaultUicontrolBackgroundColor'))
    set(hObject,'BackgroundColor','white');
end
function edit7_Callback(hObject, eventdata, handles)
handles.phi = (get(hObject,'String'));

```

```

outputt=handles.outputt;
outputt(6)=str2num(handles.phi);
if((outputt(6)>2) | (outputt(6)<0.1))
warningMessage = sprintf('Must Be Between 0.1-2');
uiwait(warndlg(warningMessage)); % Pop up message.
end;
handles.outputt=outputt;
guidata(hObject, handles);
% --- Executes during object creation, after setting all properties.
function edit7_CreateFcn(hObject, eventdata, handles)
if ispc && isequal(get(hObject,'BackgroundColor'),
get(0,'defaultUiControlBackgroundColor'))
    set(hObject,'BackgroundColor','white');
end
function edit8_Callback(hObject, eventdata, handles)
handles.phi = (get(hObject,'String'));
outputt=handles.outputt;
outputt(7)=str2num(handles.phi);
if((outputt(7)>2) | (outputt(7)<0.1))
warningMessage = sprintf('Must Be Between 0.1-2');
uiwait(warndlg(warningMessage)); % Pop up message.
end;
handles.outputt=outputt;
guidata(hObject, handles);
% --- Executes during object creation, after setting all properties.
function edit8_CreateFcn(hObject, eventdata, handles)
if ispc && isequal(get(hObject,'BackgroundColor'),
get(0,'defaultUiControlBackgroundColor'))
    set(hObject,'BackgroundColor','white');
end
function edit9_Callback(hObject, eventdata, handles)
handles.phi = (get(hObject,'String'));
outputt=handles.outputt;
outputt(8)=str2num(handles.phi);
if((outputt(8)>0.008) | (outputt(8)<0.001))
warningMessage = sprintf('Must Be Between 0.001-0.008');
uiwait(warndlg(warningMessage)); % Pop up message.
end;

```

```

handles.outputt=outputt;
guidata(hObject, handles);
% --- Executes during object creation, after setting all properties.
function edit9_CreateFcn(hObject, eventdata, handles)
if ispc && isequal(get(hObject,'BackgroundColor'),
get(0,'defaultUicontrolBackgroundColor'))
    set(hObject,'BackgroundColor','white');
end
function edit10_Callback(hObject, eventdata, handles)
handles.phi = (get(hObject,'String'));
outputt=handles.outputt;
outputt(9)=str2num(handles.phi);
if((outputt(9)>2) | (outputt(9)<0.5))
warningMessage = sprintf('Must Be Between 0.5-2');
uiwait(warndlg(warningMessage)); % Pop up message.
end;
handles.outputt=outputt;
guidata(hObject, handles);
% --- Executes during object creation, after setting all properties.
function edit10_CreateFcn(hObject, eventdata, handles)
if ispc && isequal(get(hObject,'BackgroundColor'),
get(0,'defaultUicontrolBackgroundColor'))
    set(hObject,'BackgroundColor','white');
end
function edit11_Callback(hObject, eventdata, handles)
handles.phi = (get(hObject,'String'));
outputt=handles.outputt;
outputt(10)=str2num(handles.phi);
if((outputt(10)>0.05) | (outputt(10)<0.01))
warningMessage = sprintf('Must Be Between 0.01-0.05');
uiwait(warndlg(warningMessage)); % Pop up message.
end;
handles.outputt=outputt;
guidata(hObject, handles);
% --- Executes during object creation, after setting all properties.
function edit11_CreateFcn(hObject, eventdata, handles)
if ispc && isequal(get(hObject,'BackgroundColor'),
get(0,'defaultUicontrolBackgroundColor'))

```

```

        set(hObject, 'BackgroundColor', 'white');
end
function edit12_Callback(hObject, eventdata, handles)
handles.phi = (get(hObject, 'String'));
outputt=handles.outputt;
outputt(11)=str2num(handles.phi);
if((outputt(11)>0.0005) | (outputt(11)<0.0001))
warningMessage = sprintf('Must Be Between 0.0001-0.0005');
uiwait(warndlg(warningMessage)); % Pop up message.
end;
handles.outputt=outputt;
guidata(hObject, handles);
% --- Executes during object creation, after setting all properties.
function edit12_CreateFcn(hObject, eventdata, handles)
if ispc && isequal(get(hObject, 'BackgroundColor'),
get(0, 'defaultUiControlBackgroundColor'))
    set(hObject, 'BackgroundColor', 'white');
end
function edit13_Callback(hObject, eventdata, handles)
handles.phi = (get(hObject, 'String'));
outputt=handles.outputt;
outputt(12)=str2num(handles.phi);
if((outputt(12)>70) | (outputt(12)<40))
warningMessage = sprintf('Must Be Between 40-70');
uiwait(warndlg(warningMessage)); % Pop up message.
end;
handles.outputt=outputt;
guidata(hObject, handles);
% --- Executes during object creation, after setting all properties.
function edit13_CreateFcn(hObject, eventdata, handles)
if ispc && isequal(get(hObject, 'BackgroundColor'),
get(0, 'defaultUiControlBackgroundColor'))
    set(hObject, 'BackgroundColor', 'white');
end
function edit14_Callback(hObject, eventdata, handles)
% --- Executes during object creation, after setting all properties.
function edit14_CreateFcn(hObject, eventdata, handles)
if ispc && isequal(get(hObject, 'BackgroundColor'),

```

```

get(0,'defaultUicontrolBackgroundColor'))
    set(hObject,'BackgroundColor','white');
end
function edit15_Callback(hObject, eventdata, handles)
% --- Executes during object creation, after setting all properties.
function edit15_CreateFcn(hObject, eventdata, handles)
if ispc && isequal(get(hObject,'BackgroundColor'),
get(0,'defaultUicontrolBackgroundColor'))
    set(hObject,'BackgroundColor','white');
end
function edit16_Callback(hObject, eventdata, handles)
% --- Executes during object creation, after setting all properties.
function edit16_CreateFcn(hObject, eventdata, handles)
if ispc && isequal(get(hObject,'BackgroundColor'),
get(0,'defaultUicontrolBackgroundColor'))
    set(hObject,'BackgroundColor','white');
end
% --- Executes on button press in pushbutton14.
function pushbutton14_Callback(hObject, eventdata, handles)
outputt=handles.outputt;
load net1;
outputt1=outputt(1:9);
outputt1(10:11)=outputt(11:12);
Result1=net1(outputt1');
set(handles.text2, 'String', num2str(Result1));
% --- Executes on button press in pushbutton15.
function pushbutton15_Callback(hObject, eventdata, handles)
outputt=handles.outputt;
load net2;
outputt1=outputt(1:9);
outputt1(10:11)=outputt(11:12);
Result2=net2(outputt1');
set(handles.text3, 'String', num2str(Result2));
% --- Executes on button press in pushbutton16.
function pushbutton16_Callback(hObject, eventdata, handles)
outputt=handles.outputt;
load net3;
Result3=net3(outputt');

```

```

set(handles.text4, 'String', num2str(Result3));
% --- Executes on button press in pushbutton17.
function pushbutton17_Callback(hObject, eventdata, handles)
close(Main_GUI);
Start();
% --- Executes on selection change in popupmenu3.
function popupmenu3_Callback(hObject, eventdata, handles)
selection_out=handles.selection_out;
selection_in = get(handles.popupmenu3, 'Value');
if(selection_out==1 & selection_in==10)
    warningMessage = sprintf('Must Not Be Input10');
    uiwait(warndlg(warningMessage)); % Pop up message.
end;
if(selection_out==2 & selection_in==10)
    warningMessage = sprintf('Must Not Be Input10');
    uiwait(warndlg(warningMessage)); % Pop up message.
end;
handles.selection_in=selection_in;
guidata(hObject, handles);
% --- Executes during object creation, after setting all properties.
function popupmenu3_CreateFcn(hObject, eventdata, handles)
if ispc && isequal(get(hObject, 'BackgroundColor'),
get(0, 'defaultUiControlBackgroundColor'))
    set(hObject, 'BackgroundColor', 'white');
end
% --- Executes on button press in pushbutton20.
function pushbutton20_Callback(hObject, eventdata, handles)
% --- Executes on selection change in popupmenu4.
function popupmenu4_Callback(hObject, eventdata, handles)
selection_out = get(handles.popupmenu4, 'Value');
handles.selection_out=selection_out;
guidata(hObject, handles);
% --- Executes during object creation, after setting all properties.
function popupmenu4_CreateFcn(hObject, eventdata, handles)
if ispc && isequal(get(hObject, 'BackgroundColor'),
get(0, 'defaultUiControlBackgroundColor'))
    set(hObject, 'BackgroundColor', 'white');
end

```



```

% --- Executes on button press in pushbutton21.
function pushbutton21_Callback(hObject, eventdata, handles)
% --- Executes on button press in pushbutton22.
function pushbutton22_Callback(hObject, eventdata, handles)
outputt=handles.outputt;
output_val=handles.output_val;
selection_in=handles.selection_in;
selection_out=handles.selection_out;
Data=dlmread('test1.xls');%% Read Data %%
ind_mat=[1:9 11 12];
ind_mat1=1:12;
if(selection_out==1)
    x=Data(:,[ind_mat(find(ind_mat~=selection_in) 13)]);%% Features %%
    t=Data(:,selection_in);%% Values %%
    net = feedforwardnet(20);%% Network Design %%
    [nett,tr1] = train(nett,x,t);%% Network Training %%
    ntraintool('close');
    pred_input=nett([outputt(ind_mat(find(ind_mat~=selection_in))
output_val]));
    if(selection_in==3)
        pred_input = str2num(num2str(pred_input, '%10.0e'));
    elseif(selection_in==4)
        pred_input = str2num(num2str(pred_input, '%10.0e'));
    elseif(selection_in==5)
        pred_input = str2num(num2str(pred_input, '%10.2e'));
    elseif(selection_in==6)
        pred_input = str2num(num2str(pred_input, '%10.0e'));
    elseif(selection_in==7)
        pred_input = str2num(num2str(pred_input, '%10.0e'));
    elseif(selection_in==8)
        pred_input = str2num(num2str(pred_input, '%10.2e'));
    elseif(selection_in==9)
        pred_input = str2num(num2str(pred_input, '%10.0e'));
    elseif(selection_in==10)
        pred_input = str2num(num2str(pred_input, '%10.1e'));
    elseif(selection_in==11)
        pred_input = str2num(num2str(pred_input, '%10.3e'));
    end;

```

```

        set(handles.text5, 'String', num2str(pred_input));
elseif(selection_out==2)
    x=Data(:,[ind_mat(find(ind_mat~=selection_in) 14)]');%% Features %%
    t=Data(:,selection_in)';%% Values %%
    net = feedforwardnet(20);%% Network Design %%
    [net, tr1] = train(net,x,t);%% Network Training %%
    ntraintool('close');
    pred_input=net([outputt(ind_mat(find(ind_mat~=selection_in))
output_val)]');
        if(selection_in==3)
            pred_input = str2num(num2str(pred_input, '%10.0e'));
elseif(selection_in==4)
            pred_input = str2num(num2str(pred_input, '%10.0e'));
elseif(selection_in==5)
            pred_input = str2num(num2str(pred_input, '%10.2e'));
elseif(selection_in==6)
            pred_input = str2num(num2str(pred_input, '%10.0e'));
elseif(selection_in==7)
            pred_input = str2num(num2str(pred_input, '%10.0e'));
elseif(selection_in==8)
            pred_input = str2num(num2str(pred_input, '%10.2e'));
elseif(selection_in==9)
            pred_input = str2num(num2str(pred_input, '%10.0e'));
elseif(selection_in==10)
            pred_input = str2num(num2str(pred_input, '%10.1e'));
elseif(selection_in==11)
            pred_input = str2num(num2str(pred_input, '%10.3e'));
end;
set(handles.text5, 'String', num2str(pred_input));
else
    x=Data(:,[ind_mat1(find(ind_mat1~=selection_in) 15)]');%% Features %%
    t=Data(:,selection_in)';%% Values %%
    net = feedforwardnet(20);%% Network Design %%
    [net, tr1] = train(net,x,t);%% Network Training %%
    ntraintool('close');
    pred_input=net([outputt(ind_mat1(find(ind_mat1~=selection_in))
output_val)]');
        if(selection_in==3)

```

```

        pred_input = str2num(num2str(pred_input, '%10.0e'));
elseif(selection_in==4)
        pred_input = str2num(num2str(pred_input, '%10.0e'));
elseif(selection_in==5)
        pred_input = str2num(num2str(pred_input, '%10.2e'));
elseif(selection_in==6)
        pred_input = str2num(num2str(pred_input, '%10.0e'));
elseif(selection_in==7)
        pred_input = str2num(num2str(pred_input, '%10.0e'));
elseif(selection_in==8)
        pred_input = str2num(num2str(pred_input, '%10.2e'));
elseif(selection_in==9)
        pred_input = str2num(num2str(pred_input, '%10.0e'));
elseif(selection_in==10)
        pred_input = str2num(num2str(pred_input, '%10.1e'));
elseif(selection_in==11)
        pred_input = str2num(num2str(pred_input, '%10.3e'));
end;
set(handles.text5, 'String', num2str(pred_input));
end
% --- Executes on button press in pushbutton23.
function pushbutton23_Callback(hObject, eventdata, handles)
function edit17_Callback(hObject, eventdata, handles)
handles.phi = (get(hObject, 'String'));
output_val=str2num(handles.phi);
if((output_val>1000) | (output_val<0))
warningMessage = sprintf('Must Be Between 0-1000');
uiwait(warndlg(warningMessage)); % Pop up message.
end;
handles.output_val=output_val;
guidata(hObject, handles);
% --- Executes during object creation, after setting all properties.
function edit17_CreateFcn(hObject, eventdata, handles)
if ispc && isequal(get(hObject, 'BackgroundColor'),
get(0, 'defaultUiControlBackgroundColor'))
set(hObject, 'BackgroundColor', 'white');
end
% --- Executes on selection change in popupmenu5.

```

```

function popupmenu5_Callback(hObject, eventdata, handles)
selection_out = get(handles.popupmenu5, 'Value');
handles.selection_out=selection_out;
guidata(hObject, handles);
% --- Executes during object creation, after setting all properties.
function popupmenu5_CreateFcn(hObject, eventdata, handles)
if ispc && isequal(get(hObject, 'BackgroundColor'),
get(0, 'defaultUicontrolBackgroundColor'))
    set(hObject, 'BackgroundColor', 'white');
end
% --- Executes on selection change in popupmenu6.
function popupmenu6_Callback(hObject, eventdata, handles)
selection_out=handles.selection_out;
selection_in = get(handles.popupmenu6, 'Value');
if(selection_out==1 & selection_in==10)
    warningMessage = sprintf('Must Not Be Input10');
    uiwait(warndlg(warningMessage)); % Pop up message.
end;
if(selection_out==2 & selection_in==10)
    warningMessage = sprintf('Must Not Be Input10');
    uiwait(warndlg(warningMessage)); % Pop up message.
end;
handles.selection_in=selection_in;
guidata(hObject, handles);
% --- Executes during object creation, after setting all properties.
function popupmenu6_CreateFcn(hObject, eventdata, handles)
if ispc && isequal(get(hObject, 'BackgroundColor'),
get(0, 'defaultUicontrolBackgroundColor'))
    set(hObject, 'BackgroundColor', 'white');
end
% --- Executes during object creation, after setting all properties.
function text5_CreateFcn(hObject, eventdata, handles)

```

Appendix C

This set of code will be used present user with few training networks and will execute the program after user selected the training option.

```
function varargout = Train_GUI(varargin)
% TRAIN_GUI MATLAB code for Train_GUI.fig
% Begin initialization code
gui_Singleton = 1;
gui_State = struct('gui_Name',       mfilename, ...
                  'gui_Singleton',   gui_Singleton, ...
                  'gui_OpeningFcn',  @Train_GUI_OpeningFcn, ...
                  'gui_OutputFcn',  @Train_GUI_OutputFcn, ...
                  'gui_LayoutFcn',   [] , ...
                  'gui_Callback',    []);
if nargin && ischar(varargin{1})
    gui_State.gui_Callback = str2func(varargin{1});
end
if nargout
    [varargout{1:nargout}] = gui_mainfcn(gui_State, varargin{:});
else
    gui_mainfcn(gui_State, varargin{:});
end
% End initialization code
% --- Executes just before Train_GUI is made visible.
function Train_GUI_OpeningFcn(hObject, eventdata, handles, varargin)
% Choose default command line output for Train_GUI
handles.output = hObject;
ah = axes('unit', 'normalized', 'position', [0 0 1 1]);
% import the background image and show it on the axes
bg = imread('Background.jpg'); imagesc(bg);
% prevent plotting over the background and turn the axis off
axis off
% Update handles structure
guidata(hObject, handles);
% --- Outputs from this function are returned to the command line.
```

```

function varargout = Train_GUI_OutputFcn(hObject, eventdata, handles)
varargout{1} = handles.output;
% --- Executes on button press in pushbutton3.
function pushbutton3_Callback(hObject, eventdata, handles)
function popupmenu1_Callback(hObject, eventdata, handles)
% --- Executes during object creation, after setting all properties.
function popupmenu1_CreateFcn(hObject, eventdata, handles)
if ispc && isequal(get(hObject,'BackgroundColor'),
get(0,'defaultUiControlBackgroundColor'))
    set(hObject,'BackgroundColor','white');
end
% --- Executes on button press in pushbutton4.
function pushbutton4_Callback(hObject, eventdata, handles)
% --- Executes on button press in pushbutton5.
function pushbutton5_Callback(hObject, eventdata, handles)
selection=handles.selection;
Data=xlsread('results.xls');%% Read Data %%
ind_mat=1:length(Data);
for i=1:length(Data);
    i
x=Data(ind_mat(find(ind_mat~=i)),1:9)';%% Features %%
x(10:11,:)=Data(ind_mat(find(ind_mat~=i)),11:12)';
t=Data(ind_mat(find(ind_mat~=i)),13)';%% Values %%
net1 = feedforwardnet(70);%% Network Design %%
if(selection==1)
    net1.trainFcn = 'trainlm';
elseif(selection==2)
    net1.trainFcn = 'trainbr';
elseif(selection==3)
    net1.trainFcn = 'trainscg';
else
    net1.trainFcn = 'trainrp';
end;
net1.inputs{1}.processFcns={'fixunknowns','mapminmax'};
net1.divideParam.trainRatio = 100/100;
net1.divideParam.valRatio = 0/100;
net1.divideParam.testRatio = 0/100;
[net1,tr1] = train(net1,x,t);%% Network Training %%

```

```

save net1 net1; %% Saving Trained Network %%
in1=Data(i,1:9)';%% Features %%
in1(10:11,:)=Data(i,11:12)';
output(i)=net1(in1);
e1(i)=(Data(i,13)-output(i));
e2(i)=(e1(i)-output(i));
e2(i)=abs(e2(i));
end;
figure;
hist(e1);xlabel('Network Error');ylabel('No, of Enteries');title('# of
Entries vs Error');figure;
scatter(e1,output);xlabel('Network Error');ylabel('Network
Output');title('Network Error vs Network Output');figure;
for i=1:length(Data);
    i
x=Data(ind_mat(find(ind_mat~=i)),1:9)';%% Features %%
x(10:11,:)=Data(ind_mat(find(ind_mat~=i)),11:12)';
t=Data(ind_mat(find(ind_mat~=i)),14)';%% Values %%
net2 = feedforwardnet(70);%% Network Design %%
if(selection==1)
    net2.trainFcn = 'trainlm';
elseif(selection==2)
    net2.trainFcn = 'trainbr';
elseif(selection==3)
    net2.trainFcn = 'trainscg';
else
    net2.trainFcn = 'trainrp';
end;
net2.inputs{1}.processFcns={'fixunknowns','mapminmax'};
net2.divideParam.trainRatio = 100/100;
net2.divideParam.valRatio = 0/100;
net2.divideParam.testRatio = 0/100;
[net2,tr1] = train(net2,x,t);%% Network Training %%
% nntraintool('close');%% Closing Training window %%
save net2 net2; %% Saving Trained Network %%
in1=Data(i,1:9)';%% Features %%
in1(10:11,:)=Data(i,11:12)';
output(i)=net2(in1);

```

```

e1(i)=(Data(i,14)-output(i));
e2(i)=(e1(i)-output(i));
e2(i)=abs(e2(i));
end;
figure;
hist(e1);xlabel('Network Error');ylabel('No, of Enteries');title('# of
Entries vs Error');figure;
scatter(e1,output);xlabel('Network Error');ylabel('Network
Output');title('Network Error vs Network Output');figure;
for i=1:length(Data);
    i
x=Data(ind_mat(find(ind_mat~=i)),1:12)';%% Features %%
t=Data(ind_mat(find(ind_mat~=i)),15)';%% Values %%
net3 = feedforwardnet(70);%% Network Design %%
if(selection==1)
    net3.trainFcn = 'trainlm';
elseif(selection==2)
    net3.trainFcn = 'trainbr';
elseif(selection==3)
    net3.trainFcn = 'trainscg';
else
    net3.trainFcn = 'trainrp';
end;
net3.inputs{1}.processFcns={'fixunknowns','mapminmax'};
net3.divideParam.trainRatio = 100/100;
net3.divideParam.valRatio = 0/100;
net3.divideParam.testRatio = 0/100;
[net3,tr1] = train(net3,x,t);%% Network Training %%
% nntraintool('close');%% Closing Training window %%
save net3 net3; %% Saving Trained Network %%
in1=Data(i,1:12)';%% Features %%
output(i)=net3(in1);
e1(i)=(Data(i,15)-output(i));
e2(i)=(e1(i)-output(i));
e2(i)=abs(e2(i));
end;
figure;
hist(e1);xlabel('Network Error');ylabel('No, of Enteries');title('# of

```



```

Entries vs Error');figure;
scatter(e1,output);xlabel('Network Error');ylabel('Network
Output');title('Network Error vs Network Output');figure;
% --- Executes on button press in pushbutton6.
function pushbutton6_Callback(hObject, eventdata, handles)
% --- Executes on button press in pushbutton7.
function pushbutton7_Callback(hObject, eventdata, handles)
close(Train_GUI);
Start();
% --- Executes on button press in pushbutton8.
function pushbutton8_Callback(hObject, eventdata, handles)
figure;
load net1;
IW1=net1.IW{1};
for h=1:size(IW1,1)
for i=1:size(IW1,2)
Q1(i,h)=(abs(IW1(h,i)))/(sum(abs(IW1(h,:))));
end;
for i=1:size(IW1,2)
RI1(i)=(sum(Q1(i,:)))/(sum(sum(Q1(:,:))))*100;
end
RI1(11:12)=RI1(10:11);
RI1(10)=0;
stem(RI1,'r');title('Sensitivity Analysis');hold on;
load net2;
IW2=net2.IW{1};
for h=1:size(IW2,1)
for i=1:size(IW2,2)
Q2(i,h)=(abs(IW2(h,i)))/(sum(abs(IW2(h,:))));
end;
end;
for i=1:size(IW2,2)
RI2(i)=(sum(Q2(i,:)))/(sum(sum(Q2(:,:))))*100;
end
RI2(11:12)=RI2(10:11);
RI2(10)=0;
stem(RI2,'g');title('Sensitivity Analysis');hold on;
load net3;

```

```

IW3=net3.IW{1};
for h=1:size(IW3,1)
for i=1:size(IW3,2)
Q3(i,h)=(abs(IW3(h,i)))/(sum(abs(IW3(h,:))));
end;
end;
for i=1:size(IW3,2)
RI3(i)=((sum(Q3(i,:)))/(sum(sum(Q3(:,:)))))*100;
end
stem(RI3,'b');title('Sensitivity Analysis');
legend('OutPut1','OutPut2','OutPut3');
xlim([1 12]);xlabel('Attribute');ylabel('Sensitivity Value');
ax = gca;
set(ax,'XTickLabel',{'TAH','TAC','VH','VC','TT','KSH','KSC','LE','KPN','LF','Area','FST'});
% --- Executes on button press in pushbutton10.
function pushbutton10_Callback(hObject, eventdata, handles)
% --- Executes on button press in pushbutton11.
function pushbutton11_Callback(hObject, eventdata, handles)
% --- Executes on selection change in popupmenu2.
function popupmenu2_Callback(hObject, eventdata, handles)
% --- Executes during object creation, after setting all properties.
function popupmenu2_CreateFcn(hObject, eventdata, handles)
if ispc && isequal(get(hObject,'BackgroundColor'),
get(0,'defaultUicontrolBackgroundColor'))
    set(hObject,'BackgroundColor','white');
end
% --- Executes on selection change in popupmenu3.
function popupmenu3_Callback(hObject, eventdata, handles)
selection = get(handles.popupmenu3,'Value');
handles.selection=selection;
guidata(hObject, handles);
% --- Executes during object creation, after setting all properties.
function popupmenu3_CreateFcn(hObject, eventdata, handles)
if ispc && isequal(get(hObject,'BackgroundColor'),
get(0,'defaultUicontrolBackgroundColor'))
    set(hObject,'BackgroundColor','white');
end

```

Appendix D

This set of code will be used to present user with the sensitivity analysis. It will adopt the results after the training of data base.

```
clc;
clear all;
close all;
load net1;
IW1=net1.IW{1};
for h=1:size(IW1,1)
    for i=1:size(IW1,2)
        Q1(i,h)=(abs(IW1(h,i)))/(sum(abs(IW1(h,:))));
    end;
end;
for i=1:size(IW1,2)
    RI1(i)=(sum(Q1(i,:)))/(sum(sum(Q1(:,:))))*100;
end
stem(RI1,'r');figure;
load net2;
IW2=net2.IW{1};
for h=1:size(IW2,1)
    for i=1:size(IW2,2)
        Q2(i,h)=(abs(IW2(h,i)))/(sum(abs(IW2(h,:))));
    end;
end;
for i=1:size(IW2,2)
    RI2(i)=(sum(Q2(i,:)))/(sum(sum(Q2(:,:))))*100;
end
stem(RI2,'g');figure;
load net3;
IW3=net3.IW{1};
for h=1:size(IW3,1)
    for i=1:size(IW3,2)
        Q3(i,h)=(abs(IW3(h,i)))/(sum(abs(IW3(h,:))));
    end;
end;
```

```
for i=1:size(IW3,2)
    RI3(i)=(sum(Q3(i,:)))/(sum(sum(Q3(:,:))))*100;
end
stem(RI3,'b');figure;
```

References

- [1] S. Maharaj and P. Govender, "Waste Energy Harvesting With A Thermoelectric Generator," *2013 Proceedings of the 21st Domestic Use of Energy Conference (DUE)*, pp. 1 - 6, 3-4 April 2013.
- [2] S.-C. Tzeng, T.-M. Jeng, and Y.-L. Lin, "Parametric study of heat-transfer design on the thermoelectric generator system," *International Communications in Heat and Mass Transfer*, vol. 52, pp. 97-105, 2014.
- [3] O. L. Ayodele and M. T. E. Kahn, "Underutilise waste heat as potential to generate environmental friendly energy," presented at the International Conference on the Industrial and Commercial Use of Energy (ICUE), 2014 Cape Town, 2014.
- [4] D. T. Hendricks, "Engineering Scoping Study of Thermoelectric Generator Systems for Industrial Waste Heat Recovery," Pacific Northwest National Laboratory 2006.
- [5] TECTEG, "Specifications TEG Module TEG1-1263-4.3," ed: TECTEG.
- [6] C. Goupil, W. Seifert, K. Zabrocki, E. Müller, and G. J. Snyder, "Thermodynamics of Thermoelectric Phenomena and Applications," *Entropy*, vol. 13, pp. 1481-1517, 2011.
- [7] G. Min and D.M.Rowe, "Recent Concepts In Thermoelectric Power Generation," presented at the 21st International Conference on Thermoelectronics, 2002.
- [8] D. M. Rowe, "Thermoelectrics, an environmentally-friendly source of electrical power," *Renewable Energy*, vol. 16, pp. 1251-1256, // 1999.
- [9] R. Heinberg. (2011). *Rising Cost of Fossil Fuels and the Coming Energy Crunch*.
- [10] V. Andrei, K. Bethke, and K. Rademann, "Thermoelectricity in the context of renewable energy sources: joining forces instead of competing," *Energy Environ. Sci.*, vol. 9, pp. 1528-1532, 2016.
- [11] Q. R. Ltd. (2011). *Quiet Revolution*. Available: <https://www.quietrevolution.com/>
- [12] T. C. (2010). *Outlook for winf energy in Singapore: sunny, with some clouds*. Available: <http://www.eco-business.com/>
- [13] S. B. Riffat and X. Ma, "Thermoelectrics: A review of present and potential applications," *Applied Thermal Engineering*, vol. 23, pp. 913-935, // 2003.
- [14] T. Jinushi, M. Okahara, Z. Ishijima, H. Shikata, and M. Kambe, "Development of the high performance thermoelectric modules for high temperature heat sources," vol. 534-536, ed, 2007, pp. 1521-1524.
- [15] S. A. Omer and D. G. Infield, "Design and thermal analysis of a two stage solar concentrator for combined heat and thermoelectric power generation," *Energy Conversion and Management*, vol. 41, pp. 737-756, // 2000.
- [16] C. B. Vining. (2009) An inconvenient truth about thermoelectrics. *Nature Materials*. 83.
- [17] K. T. Zorbas, E. Hatzikraniotis, and K. M. Paraskevopoulos, "Power and Efficiency Calculation in Commercial TEG and plication in wasted heat recovery in Automobile."

- [18] L. D. Landau and E. M. Lifshitz, *Electrodynamics of Continuous Media*. Oxford, UK: Butterworth-Heinemann, 1984.
- [19] E. E. Antonova and D. C. Looman, "Finite Element for Thermoelectric Device Analysis in ANSYS," Clemson, SC, USA, 2005.
- [20] T. Reuters. (2015). *Web of Science*. Available: <https://apps.webofknowledge.com/>
- [21] M. K. Yadav and B. Sanyal, "First principles study of thermoelectric properties of Li-based half-Heusler alloys," *Journal of Alloys and Compounds*, vol. 622, pp. 388-393, 2015.
- [22] W. He, G. Zhang, X. Zhang, J. Ji, G. Li, and X. Zhao, "Recent development and application of thermoelectric generator and cooler," *Applied Energy*, vol. 143, pp. 1-25, 2015.
- [23] M. Yasukawa, T. Kono, K. Ueda, H. Yanagi, and H. Hosono, "High-temperature thermoelectric properties of La-doped BaSnO₃ ceramics," *Materials Science and Engineering: B*, vol. 173, pp. 29-32, 2010.
- [24] H. Pang, Y.-Y. Piao, Y.-Q. Tan, G.-Y. Jiang, J.-H. Wang, and Z.-M. Li, "Thermoelectric behaviour of segregated conductive polymer composites with hybrid fillers of carbon nanotube and bismuth telluride," *Materials Letters*, vol. 107, pp. 150-153, 2013.
- [25] X. F. Zheng, C. X. Liu, Y. Y. Yan, and Q. Wang, "A review of thermoelectrics research – Recent developments and potentials for sustainable and renewable energy applications," *Renewable and Sustainable Energy Reviews*, vol. 32, pp. 486-503, 2014.
- [26] L. E. Bell, "Accelerating the commercialization of promising new thermoelectric materials," presented at the Materials Science and Technology Conference and Exhibition, MS and T'08, 2008.
- [27] L. E. Bell, "Addressing the Challenges of Commercializing New Thermoelectric Materials," *Journal of Electronic Materials*, vol. 38, pp. 1344-1349, 2009.
- [28] D. Narducci, "Do we really need high thermoelectric figures of merit? A critical appraisal to the power conversion efficiency of thermoelectric materials," *Applied Physics Letters*, vol. 99, p. 102104, 2011.
- [29] D. M. Rowe, G. Min, and A. K. V Kuznetsov, "Effects of A Limit To The Figure of Merit On Thermoelectric Generation," 2000.
- [30] D. H. Zervos, "Thermoelectric Energy Harvesting 2014-2024: Devices, Applications, Opportunities," IDTechEx April 2015.
- [31] S. B. Inayat, K. R. Rader, and M. M. Hussain, "Nano-materials enabled thermoelectricity from window glasses," *Scientific Reports*, vol. 2, // 2012.
- [32] S. B. Inayat and M. M. Hussain, "Power generation from thermoelectric system-embedded Plexiglas for green building technology," *Applied Nanoscience*, vol. 3, pp. 335-342, 2012.
- [33] W. Wang, V. Cionca, N. Wang, M. Hayes, B. O'Flynn, and C. O'Mathuna, "Thermoelectric Energy Harvesting for Building Energy Management Wireless Sensor Networks," *International Journal of Distributed Sensor Networks*, vol. 2013, pp. 1-14, 2013.
- [34] E. Takanose and H. Tamakoshi., "The development of thermoelectric generator for passenger car.," presented at the 12th International Conference on Thermoelectrics. Yokohama, Yokohama, Japan, 1993.

- [35] J. C. Bass, N. B. Elsner, and F. A. Leavitt, "Performance of the 1 kW thermoelectric generator for diesel engines," presented at the AIP Conf. Proc., Kansas City, Missouri (USA), 1994.
- [36] C. J. Richter, M. A. Karri, B. T. Helenbrook, and E. F. Thacher, "Testing of an automobile exhaust thermoelectric generator in a light truck," *Proceedings of the Institution of Mechanical Engineers, Part D: Journal of Automobile Engineering*, vol. 221, pp. 95-107, 2007.
- [37] M. A. Karri, E. F. Thacher, and B. T. Helenbrook, "Exhaust energy conversion by thermoelectric generator: Two case studies," *Energy Conversion and Management*, vol. 52, pp. 1596-1611, 2011.
- [38] K.M.Saqr, M.K.Mansour, and M.N.Musa, "Thermal design of automobile exhaust based thermoelectric generators:Objectives and Challenges," *International Journal Of Automotive Technology*, vol. 9, pp. 155-160, 2008.
- [39] N. A. a. S. Administration, "Multi-Mission Radioisotope Thermoelectric Generator (MMRTG)," October 2013 2013.
- [40] NASA. *Interstellar Voyager*. Available: <http://www.jpl.nasa.gov/interstellary Voyager/>
- [41] I. Y. Nuwayhid, D. M. Rowe, and G. Min, "Low cost stove-top thermoelectric generator for regions with unreliable electricity supply," *Renewable Energy*, vol. 28, pp. 205-222, 2003.
- [42] A. Killander and J. C.Bass, "A Stove Top Generator For Cold Areas," presented at the IEEE 15th International Conference on Thermoelectric, Pasadena, CA, USA, 1996.
- [43] J. D'Angelo and T. Hogan, "Long Term Thermoelectric Module Testing System," *Rev Sci Instrum*, vol. 80, p. 105102, Oct 2009.
- [44] H. Takazawa, H. Obara, Y. Okada, K. Kobayashi, T. Onishi, and T. Kajikawa, "Efficiency Measurement of Thermoelectric Modules Operating in the Temperature Difference of Up to 550K," presented at the International Conference on Thermoelectric, 2006.
- [45] L.I.Anatychukl and M.V.Havrylyuk, "Procedure and Equipment for Measuring Parameters of Thermoelectric Generator Modules," *Journal of ELECTRONIC MATERIALS*, vol. 40, 2011.
- [46] J. Vizquez, R. Palacios, M. A. Sanz-Bobi, and A. Arenas, "Test bench for measuring the electrical properties of commercial thermoelectric modules," presented at the Thermoelectrics, 2003 Twenty-Second International Conference on - ICT, 2003.
- [47] A. Y. Faraji and A. Akbarzadeh, "Design of a Compact, Portable Test System for Thermoelectric Power Generator Modules," *Journal of Electronic Materials*, vol. 42, pp. 1535-1541, 2012.
- [48] C.-T. Hsu, G.-Y. Huang, H.-S. Chu, B. Yu, and D.-J. Yao, "An effective Seebeck coefficient obtained by experimental results of a thermoelectric generator module," *Applied Energy*, vol. 88, pp. 5173-5179, 2011.

- [49] E. Sandoz-Rosado and R. J. Stevens, "Experimental Characterization of Thermoelectric Modules and Comparison with Theoretical Models for Power Generation," *Journal of Electronic Materials*, vol. 38, pp. 1239-1244, 2009.
- [50] B. J. Huang;, C. J. Chin;, and C. L. Duang;, "A Design Method of Thermoelectric Cooler," *International Journal of Refrigeration*, vol. 23, pp. 208-218, 2000.
- [51] S. Lineykin and S. Ben-Yaakov, "Modeling and Analysis of Thermoelectric Modules," *IEEE Transactions on Industry Applications*, vol. 43, pp. 505-512, 2007.
- [52] Z. Luo, "A Simple Method to Estimate the Physical Characteristics of a Thermoelectric Cooler from Vendor Datasheets," *Journal of Electronics Cooling and Thermal Control*, pp. 1-14, 2008.
- [53] F. L. Tan and S. C. Fok, "Methodology on sizing and selecting thermoelectric cooler from different TEC manufacturers in cooling system design," *Energy Conversion and Management*, vol. 49, pp. 1715-1723, 2008.
- [54] R. Ahiska, S. Dislitas, and G. Omer, "A new method and computer-controlled system for measuring the time constant of real thermoelectric modules," *Energy Conversion and Management*, vol. 53, pp. 314-321, 2012.
- [55] B. Ciylan and S. Yılmaz, "Design of a thermoelectric module test system using a novel test method," *International Journal of Thermal Sciences*, vol. 46, pp. 717-725, 2007.
- [56] Y. Islamoglu, "Modeling of Thermal Performance of a Cooling Tower Using An Artificial Neural Network," *Heat Transfer Engineering*, vol. 26, pp. 73-76, 2005.
- [57] Al-Ajmi, R. M., Abou-Ziyan, H. Z., Mahmoud, and M. A., "Performance Evaluation of 14 Neural Network Architectures Used for Predicting Heat Transfer Characteristics of Engine Oils," *International Journal for Computational Methods in Engineering Science and Mechanics*, vol. 13, pp. 60-75, 2012.
- [58] I. Eryilmaz, S. Inanli, B. Gumusel, S. Toprak, and C. Camci, "Application of Artificial Neural Network For The Heat Transfer Investigation Around A High-Pressure Gas Turbine Rotor Blade," *Proceeding of ASME Turbo Expo*, June 2011 2011.
- [59] K.Jambunathan, S.L.Hartle, S.Ashforth-Frost, and V.N.Fontama, "Evaluating Convective Heat Transfer Coefficients Using Neural Networks," *Heat Mass Transfer*, vol. 39, pp. 2329-2332, 1996.
- [60] G. N. Xie, Q. W. Wang, M. Zeng, and L. Q. Luo, "Heat transfer analysis for shell-and-tube heat exchangers with experimental data by artificial neural networks approach," *Applied Thermal Engineering*, vol. 27, pp. 1096-1104, 2007.
- [61] M. R. J. Nasr and A. H. Khalaj, "Heat Transfer Coefficient and Friction Factor Prediction of Corrugated Tubes Combined With Twisted Tape Inserts Using Artificial Neural Network," *Heat Transfer Engineering*, vol. 31, pp. 59-69, 2010.
- [62] S. S. Sablani, "A Neural Network Approach for Non- Iterative Calculation of Heat Transfer Coefficient In Fluid-Particle Systems," *Chemical Engineering and Processing*, vol. 40, pp. 363-369, 2001.

- [63] Y. Islamoglu, "A New Approach For The Prediction of The Heat Transfer Rate of The Wire-on-Tube Type Heat Exchanger Use of An Artificial Neural Network Model," *Applied Thermal Engineering*, vol. 23, pp. 243-249, 2003.
- [64] P. A. G. Lanza and J. M. Zamarréño, "Prediction of hourly energy consumption in buildings based on a feedback artificial neural network," *Energy and Buildings*, vol. 37, pp. 595-601, 2005.
- [65] R.-M. n. Ricardo, D. n.-G. a. H. c. Martín, H.-L. p. J. Manuel, and P.-V. Arturo, "Use of Artificial Neural Networks for Prediction of Convective Heat Transfer in Evaporative Units," *Ingeniería Investigación y Tecnología*, vol. XV, pp. 93-101, July 2012.
- [66] I. The MathWorks. (2017). *Neuron Model*. Available: <https://www.mathworks.com/help/nnet/ug/neuron-model.html>
- [67] Hagan, Demuth, Beale, and D. Jesus, *Neural Network Design*, 2nd ed. US: IGCtesting, 2016.
- [68] C. Stergiou and D. Siganos. *Neural Network*. Available: https://www.doc.ic.ac.uk/~nd/surprise_96/journal/vol4/cs11/report.html
- [69] D. T. Pham and S. Sagiroglu, "Training multilayered perceptrons for pattern recognition: a comparative study of four training algorithms," *International Journal of Machine Tools & Manufacture*, vol. 41, pp. 419-430, 2000.
- [70] K. A. Gernoth and J. W. Clark, "A Modified Backpropagation Algorithm for Training Neural Networks On Data With Error Bars," *Computer Physics Communications*, vol. 88, pp. 1-22, 1995.
- [71] A. Gosavi, "Neural Network and Reinforcement Learning," ed: Department of Engineering Management and Systems Engineering
Missouri University of Science and Technology Rolla.
- [72] R. Romero-Méndez, P. Lara-Vázquez, F. Oviedo-Tolentino, H. M. Durán-García, F. G. Pérez-Gutiérrez, and A. Pacheco-Vega, "Use of Artificial Neural Networks for Prediction of the Convective Heat Transfer Coefficient in Evaporative Mini-Tubes," *Ingeniería, Investigación y Tecnología*, vol. 17, pp. 23-34, 2016.
- [73] F. P. Incropera, *Fundamentals of Heat and Mass Transfer*: John Wiley & Sons, 2006.
- [74] I. Mert and H. T. Arat, "Prediction of Heat Transfer Coefficients By ANN For Aluminum and Steel Material," *International Journal of Scientific Knowledge*, vol. 5, 2014.
- [75] H. Versteeg and W. Malalasekera, *An Introduction to Computational Fluid Dynamics: The Finite Volume Method*. United States: Longman Scientific & Technical, 1995.
- [76] J. H. L. IV and J. H. L. V, *A Heat Transfer Textbook*. Cambridge, Massachusetts, USA: Phlogiston Press, 2008.
- [77] F. Kreith, R. M. Manglik, and M. S. Bohn, *Principles of Heat Transfer*. United State: Cengage Learning, 2008.
- [78] T. E. Toolbox. (2016). *Air Properties*. Available: http://www.engineeringtoolbox.com/air-properties-d_156.html

- [79] H.-Y. Li, S.-M. Chao, and G.-L. Tsai, "Thermal performance measurement of heat sinks with confined impinging jet by infrared thermography," *International Journal of Heat and Mass Transfer*, vol. 48, pp. 5386-5394, 2005.
- [80] J. G. Maveety and H. H. Jung, "Design of an Optimal Pin-Fin Heat Sink With Air Impingement," *International Communications in Heat and Mass Transfer*, vol. 27, pp. 229-240, 2000.
- [81] W. A. Khan, J. R. Culham, and M. M. Yovanovich, "Modeling of Cylindrical Pin-Fin Heat Sinks for Electronic Packaging," *IEEE Transactions on Components and Packaging Technologies*, vol. 31, pp. 536-545, 2008.
- [82] T. E. Toolbox. *Air Properties*. Available: http://www.engineeringtoolbox.com/air-properties-d_156.html
- [83] Y. Cheng. (2013). *Boundary Layer App*. Available: <https://www.mathworks.com/matlabcentral/fileexchange/40680-boundary-layer-app/content/tdma.m>
- [84] A. Azadeh, A. Maghsoudi, and S. Sohrabkhani, "An integrated artificial neural networks approach for predicting global radiation," *Energy Conversion and Management*, vol. 50, pp. 1497-1505, 2009.
- [85] Wikipedia. (2017). *Beaufort Scale*. Available: https://en.wikipedia.org/wiki/Beaufort_scale
- [86] A. Blum, *Neural Networks in C++: An Object-Oriented Framework for Building Connectionist Systems* vol. 1. The University of Michigan: John Wiley & Sons, 1992.
- [87] M. J. A. Berry and G. S. Linoff, *Data Mining Techniques: For Marketing, Sales, and Customer Support*: Wiley, 2004.
- [88] W. S. Group. (2016). *Neuroshell 2*. Available: <http://www.wardsystems.com/manuals/neuroshell2/>
- [89] R. vilela-Mendes, I. I. a. o. Interdisciplinar, UL, R. CMAF Ligeiro, and I.-I. d. N. Tecnologias, "Detecting and quantifying ambiguity: A neural network approach," *IET Signal Processing*, 2015.
- [90] F. J. C. P. Soelro, H. F. C. Velho, P. O. Soares, and A. J. S. Neto, "Using Neural Networks To Obtain Initial Estimates For The Solution of Inverse Heat Transfer Problems," *Inverse Problems, Design and Optimization Symposium*, 2004.
- [91] L. V. Kamble, D. R. Pangavhane, and T. P. Singh, "Artificial Neural Network Based Prediction of Heat Transfer From Horizontal Tube Bundles Immersed in Gas-Solid Fluidized Bed of Large Particles," *Journal of Heat Transfer*, vol. 137, p. 012901, 2015.
- [92] G. D. Garson, "Interpreting neural-network connection weights," *AI Expert*, vol. 6, pp. 46-51, 1991.
- [93] M. Gevrey, I. Dimopoulos, and S. Lek, "Review and comparison of methods to study the contribution of variables in artificial neural network models," *Ecological Modelling*, pp. 249-264, 2003.

- [94] I. Mudawar, "Two-Phase Microchannel Heat Sinks: Theory, Applications and Limitations," *Journal of Electronic Packaging*, vol. 133, Dec 2011.